ABSTRACT

NONUNIFORM SAW GRATING RESONATOR AND FILTERS

DOKHEE CHOI

The properties of the uniform and tapered surface acoustic wave reflective grating, the Fabry - Perot resonator and the Fabry - Perot resonator filter are investigated by means of the matrix analysis of the equivalent transmission line model. Network elements are given for the grooved surface. From these the transmission characteristics and equivalent curcuits of reflectors and SAW Fabry - Perot resonator filters are calculated. A formal equivalence between transmission line and tapered grating is shown and used to apply the Chebyshev optimization technique borrowed from microwave technology. The modified Bessel taper is found to be the most effective to supress side lobes. Such a taper function is used to evaluate the performance of Fabry - Perot resonator filters.

ACKNOWLEDGEMENTS

The author wishes to express his appreciation and deep sense of gratitude to Dr. Otto Schwelb for his guidance and assistance during the entire preparation of this thesis. The author also wishes to acknowledge the support of the National Science and Engineering Research Council of Canada.

TABLE OF CONTENTS

LIST OF IMPORTANT ABBREVIATIONS AND SYMBOLS

$\bar{A}$	Transmission matrix on wave basis
$A_m(z)$	m-th mode amplitude
$a_i^{\pm}$	Normalized traveling i-th mode amplitude
BW	3dB band width
b	Normalized groove suceptance
b_T	Normalized transducer suceptance
C_{ij}	Coupling coefficient of (i - j)th mode
$c(c_R)$	Relative penetration depth (at resonance)
C_T	Static capacitance of the transducer
E	Edge steepness parameter of a groove
f_o	Bragg frequency
$f_H(f_L)$	Higher(lower) stop bandedge frequency
$F(F_R)$	Normalized frequency (at resoanance)
f_{FP}	F - P resonator resonant frequency
f_R	Grating resonant frequency
$h(h_i)$	Groove depth of a constant(tapered) grating
I	Identity matrix
I_1	Modified Bessel function of 1st kind
k	Propagation constant of SAW
k_L, k_C	Inductive and capacitive coupling constants
k_o	Free space wave number

L_C	Length of resonator
M	Transfer matrix
N	Number of grooves of a grating
N_T	Number of fingers of interdigital transducer
$p(p_i)$	Period of constant (tapered) groove
$Q'(Q)$	Transmission matrix on V - I basis of symmetrical (non symmetrical) groove
Q_{RT}	Q matrix of the entire resonator IDT combination
Q_L	Loaded Q factor
$q(q')$	Integral number of cavity length (optimized)
R	Coupled mode system matrix
R_s	Side lobe suppression ratio
r	Normalized off set parameter
$r_d(r_u)$	Reflection coefficient of the down(up) step of a grating
S	Scattering matrix
t	Magnitude of transmission coefficient
$t_d(t_u)$	Transmission coefficient of a down(up) step of a grating
T_g	Transmission coefficient of a groove
T_N	Chebyshev polynomial of the 1st kind
U_N	Chebyshev polynomial of the 2nd kind
$y(y_i)$	Aspect ratio of a constant(tapered) grating
$\tilde{y}$	Input admittance of a grating at the center of IDT
v_o	Rayleigh velocity
$v_p(v_g)$	Phase(group) velocity

Z_C , Z_I	Wave impedance
$\bar{Z}$ (Z)	Normalized(unnormalized) characteristic impedance of tapered line
z	z coordinate
$\bar{z}(\bar{z}_i)$	Normalized impedance of the mark region of a constant (tapered) grating
z_i	Normalized z coordinate by length L
$\bar{Z}_\pm$	$(Z_I \pm 1/Z_I)$
$\bar{Z}'_\pm$	$(\lvert Z_I \rvert \pm 1/\lvert Z_I \rvert)$
$Z_\pm$	$(\bar{z} \pm 1/\bar{z} - b^2\bar{z})$
$Z_i^\pm$	$(\bar{z}_i \mp 1/\bar{z}_i \pm b^2\bar{z}_i)$
α	Attenuation constant
β, β_i, β	Propagation constant
κ, κ_i, κ_{ij}	Coupling coefficient
δ	Effective characteristic impedance deviation
δ_z	Impedance mismatch in a groove
γ	Complex wave number
ρ, ρ_i	Magnitude of reflection coefficient
$\rho_{max}(\rho_s)$	Magnitude of reflection coefficient at resonance (the first sidelobe)
$\Gamma_C^\pm$	Characteristic reflection coefficient
Γ	Complex reflection coefficient of a transmission line or grating
Γ_g	Reflection coefficient of a groove
$\theta_M(\theta_s)$	Electrical length of the mark(space) region of a grating
λ	Wave length of the operating frequency

ω	Angular frequency
ξ	Deviation parameter of the operating frequency from the Bragg frequency.
τ	Time delay

CHAPTER I

INTRODUCTION

The utilization of Surface Acoustic Wave (SAW) devices which perform signal processing functions in VHF, UHF electronic systems has a history spanning only a decade and has lead to some well established techniques. These include time delay, frequency filtering, multi-channel coupling spectral analysis and signal compression to name only a few.

The fast development of SAW devices is attributed to two factors. Firstly to the fact that the discipline is closely related to the well developed fields of microwaves and optics, and secondly to the demand for miniaturization in the wake of the microelectronics revolution.

Elastic surface wave propagation has first been described by Lord Rayleigh in 1895. Rayleigh waves are especially suited for analog signal processing applications at VHF - UHF frequencies because being on the surface at a substrate they are accessible and can be easily manipulated.

The bulk and surface acoustic wave velocity in piezoelectric crystals is five orders of magnitude slower than the velocity of light. Consequently the SAW wavelength is five orders of magnitude shorter than that of an electromagnetic wave of the same frequency. Since device demensions usually measure 10 to 100 wavelengths SAW components operating in the 30 - 500 MHz frequency range lend themself well to

miniaturization. For this reason many an electronic signal processing device has been redesigned using an elastic wave as the medium to carry the information. SAW device development in the GHz frequency range is dependent on submicron microelectronic technology and is presently still in its infancy.

In addition to their ease of fabrication SAW resonators and filters also have high performance electrical characteristics. Resonator Q values of 4×10^4 are not uncommon. SAW devices also show a high degree of environmental stability making them attractive for use in clocks, NDE transducers, temperature and strain sensors and other extended reliability applications.

The essential component of the SAW resonator and filter is the grating reflector. It comprises a substrate whose surface is polished to within a fraction of the acoustic wavelength used, and approximately perturbed by metalization, grooving, in-diffusion or by ion implantation to exhibit a high reflectivity in a very narrow frequency band. The substrate material is usually piezo-electric ST-X quartz or YZ $LiNbO_3$, although the operation of grooved, in-diffused or ion implanted gratings does not depend on piezoelectricity.

To launch a SAW or to perform trackchanging, coupling, beam compression or hybrid coupling however, a piezoelectric substrate is needed because the interdigital transducer (IDT) commonly used for launching Rayleigh waves, and the multistrip coupler employed to perform the other functions operate on the principle of interdependence between the electric and the elastic fields.

Chronologically first the IDT was developed in the late 1960's. Once collimated surface wave beam generation was well in hand, beam processing configurations could be realized. Among these the first has been the multistrip coupler {41, 42} . This device consists of a large number of metalic strips deposited on the surface of the substrate perpendicular to the SAW beam and is in fact a grating which however operates in the passband region. The same device operated at a frequency where the grating period is an integral number of half wave lengths becomes a narrow band reflector.

It has been suggested that in place of metallic strips, transverse grooves would serve equally well as reflective gratings. Moreover these need not be machined in piezoelectric substrates since piezoelectricity is not required for their operation. The idea of using such a distributed groove reflector was first reported in 1970 {1}. Since its first appearance SAW grooved reflector has been the subject of considerable study for several years {15, 16, 17, 18, 19, 20}.

In this thesis the performance characteristics of uniform and tapered gratings are analyzed including the effect of chirping i.e. variable period length and/or mark to space ratio (aspect ratio). The emphasis is on the analysis and optimization of nonuniform gratings using the methods developed for microwave impedance transformers and combining these with compensation for the effect of energy storage.

There are two main analytic approaches to treat both uniform and nonuniform grating arrays.

In the coupled mode approach the wave amplitudes satisfy

coupled, first order, linear differential equations with constant or variable coefficients depending whether the grating array is uniform or not. Integration of the resultant Riccati equation provides the reflection coefficient of the grating. The local coupling coefficient is an input parameter which must first be evaluated from the given grating geometry.

The network equivalent approach uses the transfer matrix of the individual cell in a scheme where these matrix are numerically multiplied. The reflection coefficient obtains from the transfer matrix of the entire grating which is the product of the unit cell equivalent network matrices. This approach has the advantage of using transfer matrices whose elements are easily related to the geometrical and material parameters, and is the subject of this work.

Chapter II presents fundamental analytical concepts; the coupled mode theory and the matrix analysis of periodic structures. Grating structures operate on the principle of superposing in-phase wavelets reflected at periodically spaced discontinuities. The entire grating can be viewed as a transmission system supporting counter propagating waves. Coupled mode theory then relates the reflected wave amplitude to the forward wave amplitude and predicts the width of the stopband and the attenuation and phase constants as a function of frequency in the vicinity of the stopband. The discussion on the matrix analysis of periodic structures includes an evaluation of three numerical methods to find the product of a large number of transfer matrices. The comparison is based on the error introduced in the

reciprocity condition (unit determinant) and finds one method to be superior to the rest.

Chapter III is devoted to uniform grating arrays. A discussion on the relationship between geometrical and network parameters opens the Chapter. Empirical energy storage parameters are used but a comparison has been attempted with recently published analytical results. Admissible approximations and closed form expressions for the transmission coefficients follow. Numerical results are given for the grating reflection coefficient as a function of various parameters including that of distributed loss. Finally several Fabry-Perot configurations are introduced and their salient features discussed.

In Chapter IV tapered and chirped gratings are investigated extensively. In the first part of this chapter, based on the equivalent circuit and coupled mode theory, the discrete coupling coefficient κ_i is defined and related to the geometric parameters of grooved structures. The effect of weak perturbation of the period, the groove depth and the aspect ratio on the transfer characteristics is treated next. Remaining part of this chapter is devoted to the optimization process of tapered and chirped grating to represent the Chebyshev filter characteristics of ordinary tapered transmission line. Several taper functions are compared and it is found that best sidelobe suppression is obtained in gratings tapered by a modified Bessel functions used by Klopfenstein [39] and Collin [36] for the optimized characteristics waveguide impedance transformers. The other characteristics of the tapered gratings i.e. 3dB band width, roll off slope etc. are found

to be improved also by increasing the number of unit cell over 200.

In Fabry-Perot resonator application the wide band width and large phase excursion of the tapered grating causes several axial modes to appear within the resonator passband. The individual axial resonances have a high Q factor and sidelobe suppression between the modes is good. It appears therefore that such configurations could be used to advantage in comb filters and channel filters.

The Appendix includes a conversion table for the network equivalents of two-ports and listing for the SAW7 computer program.

CHAPTER II

FUNDAMENTAL CONCEPTS

2.1 Coupled Mode Analysis

Modes are the characteristic solutions(or eigen-solutions) of bounded passive isotropic systems characterized by elliptical differential equations such as transmission lines, resonators, etc. Modes and their associated characteristic values (or eigen values) display the following properties:

(1) In a wave guide or resonator with "perfect" boundaries, modes are orthogonal to each other or can be orthogonalized, i.e. no coupling between modes is encountered.

(2) Modes constitute a complete set in terms of which a given distribution can be decomposed.

(3) The characteristic values pertaining to the modes are discrete.

The above properties are a consequence of the nature of the differential operator involved which is of the Sturm-Liouville type and is self-adjoint [2]. Each mode can be thought of as an individual transmission line or resonator with its associated energy storage and power flow.

A system supporting several modes can be modeled by a multi-port network combining the appropriate two-port equivalents of each

mode.

When the boundary conditions are not "perfect", e.g. when the boundary does not coincide with a coordinate surface or when the interface material is not a perfect conductor, the self-adjoint property of the differential operator is distroyed and coupling between modes occurs. In practice conditions are almost perfect and the coupling between modes is usually weak.

Coupled mode theory developed by Pierce{ 3 }exploits this situation and deals with small modal perturbations caused by small coupling constants. This theory has been extensive applications in the fields of directional couplers, parametric amplifiers, electron beam-circuit interactions, space charge waves and cyclotron waves.

The coupled mode formalism has also proved very useful in integrated optics. They include the behavior of grating couplers corrugated waveguide filter, distributed feedback lasers{ 4 }, mode converter and nonlinear optical interactions. Marcuse { 5 } and Yariv { 6 }have developed a coupled mode formalism applicable to a large class of dielectric waveguides including strip-guides and fibers.

To outline briefly coupling mode theory, consider the four-port depicted in Fig. 2.1 comprising two lossless, passive coupled waveguides.

Defining normalized amplitudes $|a_i^{\pm}| = p_i^{\pm}$ is the forward or backward power flow in waveguide i, the transformation between terminal variables (V,I) and (a^+, a^-) is conveniently written in

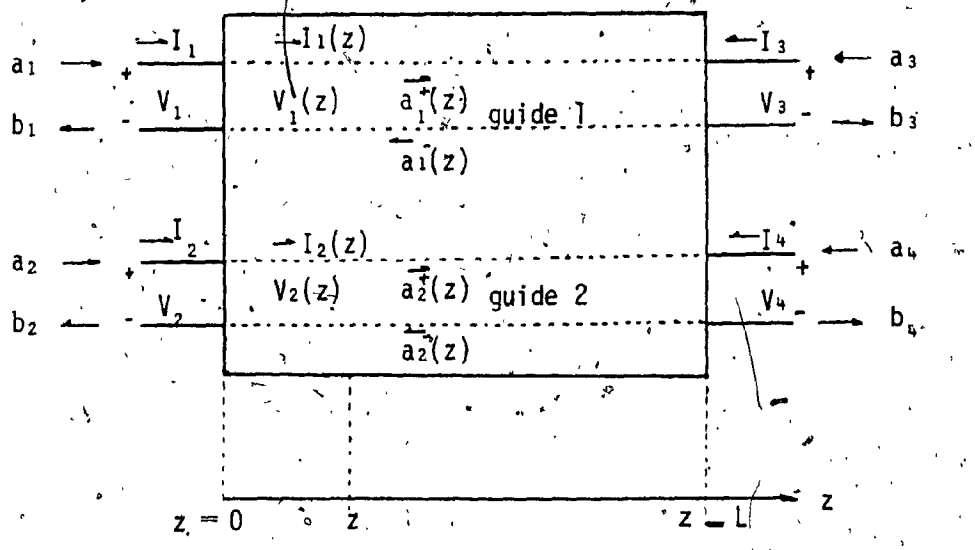

$$a_1 = a_1^+(0) \qquad b_1 = a_1^-(0) \qquad V_1 = V_1(0) \qquad I_1 = I_1(0)$$

$$b_3 = a_1^+(L) \qquad a_3 = a_1^-(L) \qquad V_2 = V_2(0) \qquad I_2 = I_2(0)$$

$$a_2 = a_2^+(0) \qquad b_2 = a_2^-(0) \qquad V_3 = V_1(L) \qquad I_3 = -I_1(L)$$

$$b_4 = a_2^+(L) \qquad a_4 = a_2^-(L) \qquad V_4 = V_2(L) \qquad I_4 = -I_2(L).$$

$$a_1^{\pm}(z) = 1/2^{\frac{1}{2}}\{V_1(z)/Z_1^{\frac{1}{2}} \pm Z_1^{\frac{1}{2}} I_1(z)\}$$

$$a_2^{\pm}(z) = 1/2^{\frac{1}{2}}\{V_2(z)/Z_2^{\frac{1}{2}} \pm Z_2^{\frac{1}{2}} I_2(z)\}$$

Fig. 2.1 A schematic Diagram of the two coupled wave guides. Z_1 Z_2 are characteristic impedances of each guide.

matrix form

$$\bar{X} = T\bar{Y} \text{ or } \bar{Y} = T^{-1}X$$

where $X = (V,I)^T$, $Y = (a^+, a^-)^T$

and $$T = 1/Z^{\frac{1}{2}} \begin{bmatrix} Z & Z \\ 1 & 1 \end{bmatrix}, \quad T^{-1} = 1/2Z^{\frac{1}{2}} \begin{bmatrix} 1 & Z \\ 1 & -Z \end{bmatrix}$$

Then in the coupling region $a_1^{\pm}(z)$ and $a_2^{\pm}(z)$ are the dependent amplitudes of the forward and backward traveling waves in guides 1 and 2 respectively.

The coupled mode equations are

$$d\bar{a}(z)/dz = -j\, C\, \bar{a}(z) \qquad (2.1.1)$$

where $\bar{a}(z) = \{a_1^+(z), a_2^+(z), a_1^-(z), a_2^-(z)\}^T$,

and $$C = \begin{bmatrix} C_{11} & C_{12} & C_{13} & C_{14} \\ C_{21} & C_{22} & C_{23} & C_{24} \\ C_{31} & C_{32} & C_{33} & C_{34} \\ C_{41} & C_{42} & C_{43} & C_{44} \end{bmatrix}$$

C_{ij} $(i \neq j)$ are coupling coefficients giving rise to backward traveling waves and interguide power transfer. The coupling coefficients can be evaluated only when a particular coupled mode system is considered. Let us consider the coupled transmission lines shown in Fig. 2.2.

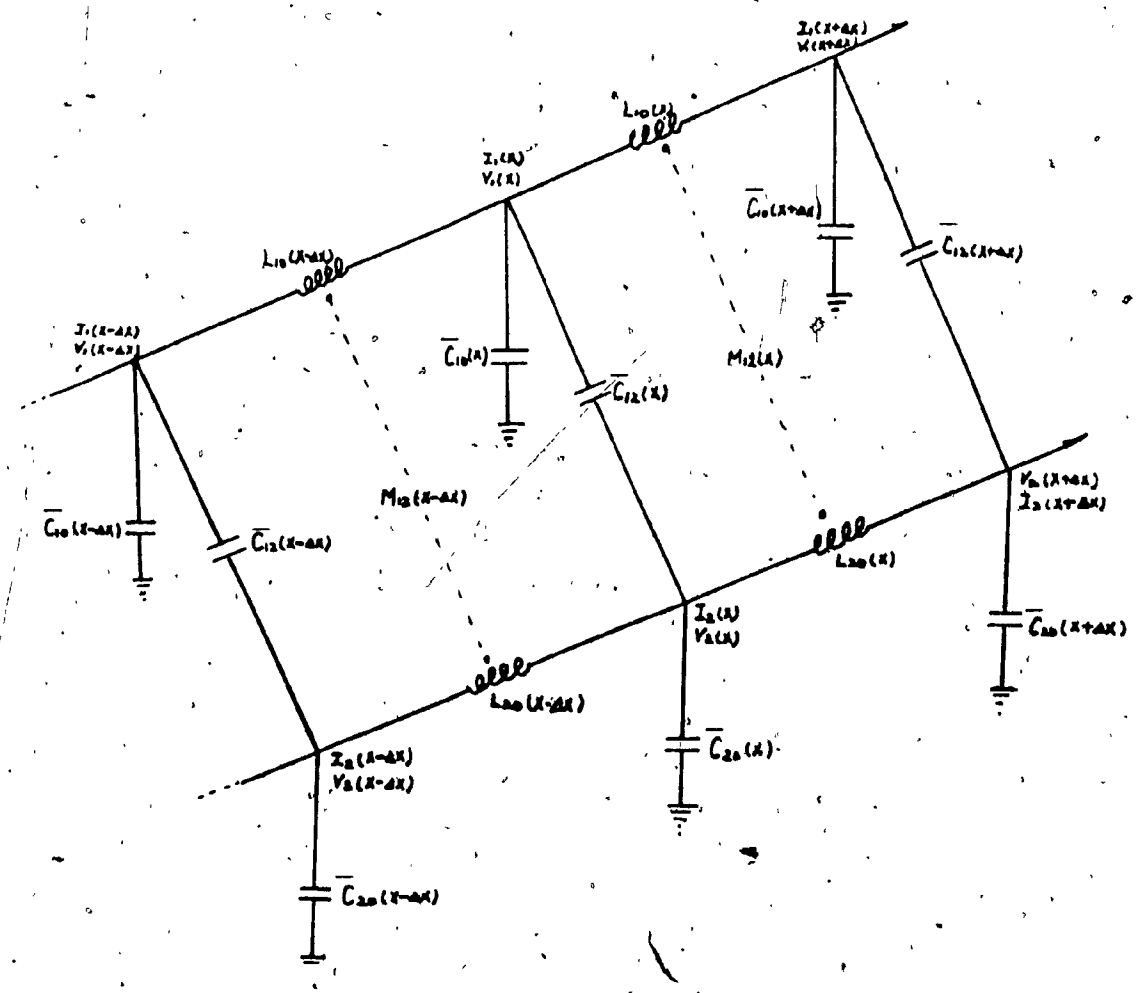

$$L_{11} = L_{10} - M_{12}$$

$$L_{22} = L_{20} - M_{12}$$

$$\bar{C}_{11} = \bar{C}_{10} + \bar{C}_{12}$$

$$\bar{C}_{22} = \bar{C}_{20} + \bar{C}_{12}$$

$$Z_i = \sqrt{\frac{L_{ii}(z)}{\bar{C}_{ii}(z)}} \quad : \text{ characteristic impedance of loaded line } i.$$

Fig. 2.2. Two coupled transmission Lines.

Matric C becomes{ 7}

$$C = \begin{bmatrix} C_{11} & C_{12} & C_{13} & C_{14} \\ C_{12} & C_{22} & C_{14} & C_{24} \\ C_{13} & -C_{14} & -C_{11} & -C_{12} \\ -C_{14} & C_{24} & -C_{12} & C_{22} \end{bmatrix} \qquad (2.1.2)$$

where $C_{11} = \beta_1$

$C_{22} = \beta_2$

$C_{12} = (\beta_1\beta_2)^{\frac{1}{2}} (k_L - k_C)/2$

$C_{13} = jd\{\ln(Z_1)^{\frac{1}{2}}\}/dz$

$C_{24} = jd\{\ln(Z_2)^{\frac{1}{2}}\}/dz$

$C_{14} = -(\beta_1\beta_2)^{\frac{1}{2}}(k_C + k_L)/2$

and $k_L = M_{12}(z)/\{L_{11}(z)L_{22}(z)\}^{\frac{1}{2}}$

$k_C = \bar{C}_{12}(z)/\{\bar{C}_{11}(z)\bar{C}_{22}(z)\}^{\frac{1}{2}}$

are the inductive and capacitive coupling coefficients. Note that nonuniformity, i.e. the nonvanishing coefficients C_{13}, C_{31}, C_{24}, C_{42} are responsible for the coupling between forward and backward traveling waves within one line, whereas the mutual coupling coefficients C_{12}, C_{21}, C_{43}, C_{34}, C_{14}, C_{23}, θ_{32}, and C_{41} cause power to transfer from line 1 to 2 or vice versa.

In the absence of coupling between the guides ($k_C = k_L = 0$) equation (2.1.1) reduces to that of a single nonuniform transmission line;

$$\begin{aligned} da^+/dz + j\beta a^+ + d\{\ln Z(z)^{\frac{1}{2}}\}/dz\, a^- &= 0 \\ da^-/dz - j\beta a^- + d\{\ln Z(z)^{\frac{1}{2}}\}/dz\, a^+ &= 0 \end{aligned} \tag{2.1.3}$$

This equation indicates direct coupling between the forward and backward modes of the nonuniform line.

Let us confine our attention to the uniform transmission line. For this case the C matrix reduces to

$$C = \begin{bmatrix} \beta_1 & C_{12} & 0 & C_{14} \\ C_{12} & \beta_2 & C_{14} & 0 \\ 0 & -C_{14} & -\beta_1 & -C_{12} \\ -C_{14} & 0 & -C_{12} & -\beta_2 \end{bmatrix} \tag{2.1.4}$$

From (2.1.4) it can be seen that there are two distinct mechanisms to cause mutual coupling. First, when $k_L = -k_C$, $C_{14}=0$, there is transfer of power only between the modes traveling in the same direction in the two guides. This is called "Codirectional" coupling and leads to the equation.

$$\begin{aligned} da_1/dz + j\beta_1 a_1 + jC_{12}a_2 &= 0 \\ da_2/dz + j\beta_2 a_2 + jC_{12}a_1 &= 0 \end{aligned} \tag{2.1.5}$$

where the double signs have been omitted for clarity.

On the other hand when $k_L = k_C$, $C_{12} = 0$, leading to "contradirectional" coupling where modes traveling in opposite directions on the two lines are coupled. The coupled mode equations in this case are

$$\begin{aligned} da_1/dz + j\beta_1 a_1 + jC_{14}a_2 &= 0 \\ da_2/dz - j\beta_2 a_2 - jC_{14}a_1 &= 0 \end{aligned} \tag{2.1.6}$$

The coupled mode equations involving a_1^-, a_2^- in (2.1.5) and a_1^-, a_2^+ in (2.1.6) can be obtained by interchanging all signs in the corresponding equations. Equations (2.1.5) and (2.1.6) can be combined and written compactly as

$$d\bar{a}/dz = -jR\bar{a} \tag{2.1.7}$$

where $\bar{a}^T = (a_1, a_2)$ is the complex normalized mode amplitude vector and

$$R = \begin{bmatrix} R_{11} & R_{12} \\ R_{21} & R_{22} \end{bmatrix}$$ is a square matrix

consisting of the propagation constants of the unperturbed modes along the main diagonal and of the mutual coupling coefficients as the off-diagonal entries.

Power conservation constrains the relationship between the coupling coefficients R_{12}, and R_{21}.

For codirectional coupling, power conservation requires that $|a_1(z)|^2 + |a_2(z)|^2 = \text{constant}$.

Substitution of (2.1.7), then results in the condition

$$R_{12} = R_{21}^{*}. \qquad (2.1.8)$$

For the contradirectional case power conservation requires that $|a_1(z)|^2 - |a_2(z)|^2 =$ Constant resulting in the constraint $R_{12} = -R_{21}^{*}$ (2.1.9)

Both cases are shown symbolically in Fig. 2.3.

When R is a constant matrix the system is called uniform. For lossless systems the diagonal elements of R are real and the off-diagonal elements satisfy (2.1.8) or (2.1.9). Thus passive lossless forward (backward) couplers are characterized by a Hermitian (skew Hermitian) R matrix.

The solution of equation (2.1.7) can be obtained by diagonalizing R via its modal matrix S. Thus denoting $\bar{w} = S\bar{a}$, Substitution $\bar{w}$ into (2.1.7) yields

$$d\bar{w}(z)/dz = -jS^{-1}RS\bar{w}(z) \qquad (2.1.10)$$

where $S^{-1}RS = \Lambda_R = \text{diag}\,(k_1, k_2)$ is the diagonal matrix of the eigen values of R. Thus (2.1.7) reduces to the simple decoupled or normal mode equation;

$$d\bar{w}(z)/dz = -j\Lambda_R\bar{w}(z) \qquad (2.1.11)$$

The propagation constants in the codirectional coupler ($R_{12} = R_{21}^{*}$) are

$$k_{1,2} = (R_{11} - R_{22})/2 \pm \{((R_{11} - R_{22})/2)^2 + |R_{12}|^2\}^{\frac{1}{2}} \qquad (2.1.12)$$

which are always real, since R_{11}, R_{22} are real. No growing or decaying waves are allowed and the interaction is characterized by a periodic

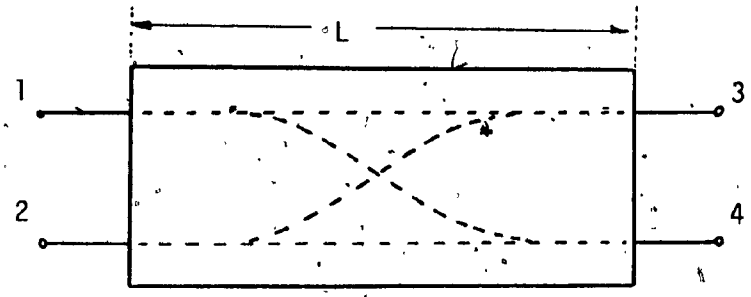

a) Codirectional coupling ($R_{12} = R_{21}^*$)

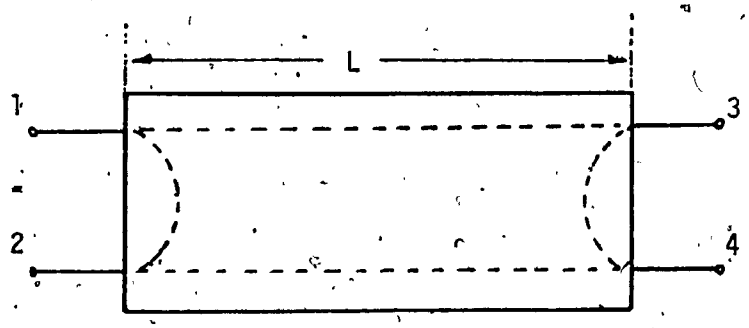

b) Contradirectional coupling ($R_{12} = -R_{21}^*$)

Fig.2.3. Two kinds of passive continuous coupling. L is the coupler length.

power exchange or "beating".

For the contradirectional coupler ($R_{12} = -R_{21}^*$)

$$k_{1,2} = (R_{11} + R_{22})/2 \pm \{((R_{11} - R_{22})/2)^2 - |R_{12}|^2\}^{\frac{1}{2}} \quad (2.1.13)$$

and k_1 and k_2 become complex when the coupling is strong enough to satisfy the condition:

$$|R_{12}|^2 > \left| \frac{R_{11} - R_{22}}{2} \right|^2 \quad (2.1.14)$$

In this case k_1 and k_2 are complex conjugates representing a growing and a decaying wave.

The characteristics of the other cases including active and parametrically coupled systems are tabulated and summarized in a review paper by Barnes {8}. In terms of the eigen values of the R matrix, the complete solution of (2.1.7) is

$$\begin{aligned} a_1(z) &= A_{11}e^{-jk_1z} + A_{12}e^{-jk_2z} \\ a_2(z) &= A_{21}e^{-jk_1z} + A_{22}e^{-jk_2z} \end{aligned} \quad (2.1.15)$$

The amplitude coefficients are obtained from the initial conditions.

The foregoing has shown that the salient characteristics of coupled modes are determined by the coupling coefficient R_{12}. In what follows we give a brief outline for obtaining this coupling coefficient from the geometrical and/or material parameters of a system governed by the wave equation.

Consider a perturbation due to a mechanical corrugation of the

interface of thin film dielectric waveguide shown in Fig. 2.4. The wave function $\psi(x,z)$ in the perturbed region is a solution of

$$\{\nabla^2 + k^2(x)\}\,\psi(x,z) = -k_o^2\,\delta(x,z)\,\psi(x,z) \qquad (2.1.16)$$

where k is the wave number in the unperturbed guide and k_o is free space wave number, $\delta(x,z)$ is the perturbation function, a dimensionless quantity muchless than unity. Due to property (2) (page 7) the solution for the perturbed guide can be decomposed in terms of the eigenmodes of the unperturbed guide $\psi_m(x)$:

$$\psi(x,z) = \sum_{-\infty}^{\infty} A_m(z)\psi_m(x)e^{-j\beta_m z} \qquad (2.1.17)$$

Substitution of (2.1.17) into (2.1.16) yields

$$\{\nabla^2 + k^2(x)\}\{A_m(z)\psi_m(x)e^{-j\beta_m z}\} = k_o^2\delta(x,z)\sum_m A_m(z)\psi_m(x)e^{-j\beta_m z} \qquad (2.1.18)$$

By multiplying both sides of (2.1.18) by $\psi_s^*(x)$, integrating over the entire cross section ($-\infty<x<+\infty$), and assuming that

$$|d^2A_m(z)/dz^2| << \beta_m|dA_m(z)/dz|$$

on the basis that any amplitude variation along the waveguide will be adiabatic compared to the wavelength (weak coupling approximation) we obtain

$$dA_s^-/dz\; e^{j\beta_s z} - dA_s^+/dz\; e^{-j\beta_s z} = -j\frac{\omega\varepsilon_o\mu}{4}\sum_m\{A_m\int_{-\infty}^{\infty}\delta(x,z)\psi_m(x)\psi_s(x)\,dx\,e^{-j\beta_m z}\} \qquad (2.1.19)$$

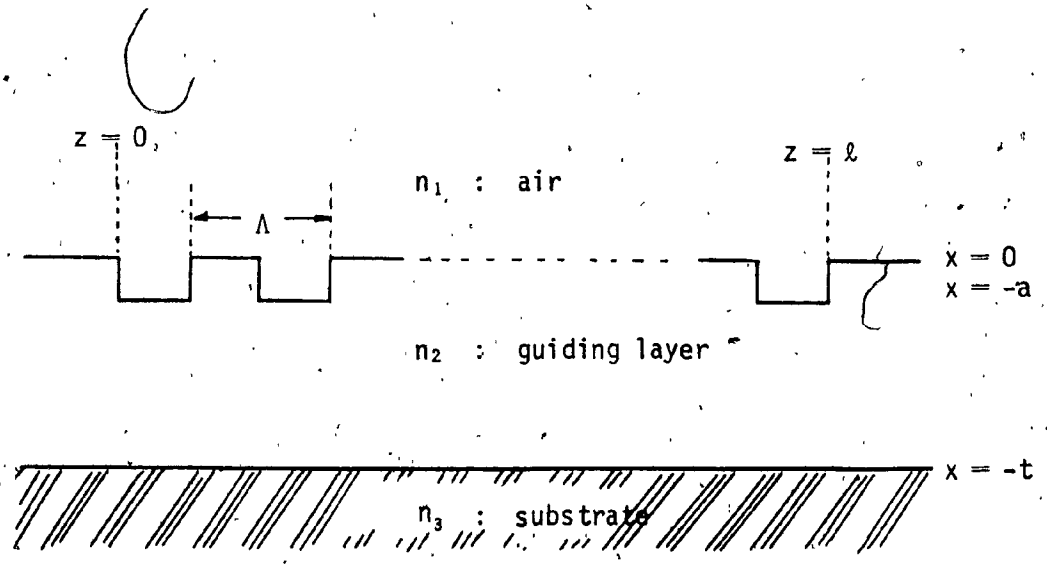

Fig. 2.4 One dimensional corrugated periodic dielectric waveguide.

If the perturbation is periodic in the z direction $\delta(x,z)$ can be expanded in a Fourier series

$$\delta(x,z) = \delta(x)\sum_q a_q e^{j(2\pi q/\Lambda)z} \qquad (2.1.20)$$

Assuming the perturbation period Λ to be related to the wavelength according to

$$\ell \frac{\pi}{\Lambda} = \beta_s, \qquad \ell \text{ ; integer} \qquad (2.1.21)$$

the right side of (2.1.19) will contains a term ($q=\ell$, $m=s$) proportional to

$$A_s^+ \exp\{j(2\ell\pi/\Lambda - \beta_s)z\}$$

Since $(2\pi\ell/\Lambda - \beta_s) \simeq \beta_s$, this term is phase matched to the source term $A_s^- \exp(j\beta_s z)$ on the left side of (2.1.19). Thus one has

$$dA_s^-/dz = \frac{-j\omega\epsilon_0}{4} A_s^+ \int_{-\infty}^{\infty} \delta(x)\{\psi_s(x)\}^2 dx a_\ell e^{j(2\ell\pi/-2\beta_s)z} \qquad (2.1.22)$$

A corresponding relation applies between dA_s^+/dz and A_s^-.

Denoting

$$\kappa = \frac{j\omega\epsilon_0 a_\ell}{4} \int_{-\infty}^{\infty} \delta(x)\{\psi_s(x)\}^2 dx$$

and $$\Delta\beta = \beta_s - \ell\pi/\Lambda \equiv \beta_s - \beta_0$$

these expressions take the form

$$dA_s^-/dz = \kappa A_s^+ e^{-2j\Delta\beta z}$$
$$dA_s^+/dz = \kappa^* A_s^- e^{2j\Delta\beta z} \qquad (2.1.23)$$

The system (2.1.23) finally results in the coupled mode equations

$$d\bar{\psi}/dz = -jR\bar{\psi} \qquad (2.1.24)$$

where $\bar{\psi}^T = (\psi_1, \psi_2) = \{A_s^+ \exp(-j\beta_1 z), A_s^- \exp(-j\beta_2 z)\}$

and $\beta_1 = \beta_s, \quad \beta_2 = -\beta_s$

which is identical to the general coupled mode equation (2.1.7).

The solution of (2.1.24) satisfying the boundary condition

$$\psi_2(\ell) = 0$$

is

$$\psi_1(z) = \psi_1(0) \frac{e^{-j\beta_0 z}}{-\Delta\beta\sinh(s\ell)+js\cosh(s\ell)} \{\Delta\beta\sinh(s(z-\ell))+js\cosh(s(z-\ell))\}$$

$$\psi_2(z) = \psi_1(0) \frac{j\kappa e^{j\beta_0 z}}{-\Delta\beta\sinh(s\ell)+js\cosh(s\ell)} \sinh\{s(z-\ell)\} \qquad (2.1.25)$$

where $s = \{\kappa^2 - (\Delta\beta)^2\}^{\frac{1}{2}}$.

Under phase matching condition ($\Delta\beta = 0$)

$$|\psi_1(z)| = \psi_1(0) \frac{\cosh\{\kappa(z-\ell)\}}{\cosh(\kappa\ell)}$$

$$|\psi_2(z)| = \psi_1(0) \frac{\sinh\{\kappa(z-\ell)\}}{\cosh(\kappa\ell)} \qquad (2.1.26)$$

These distributions are illustrated in Fig. 2.5. For large arguments of the cosh and sinh functions in (2.1.26), the incident mode amplitude

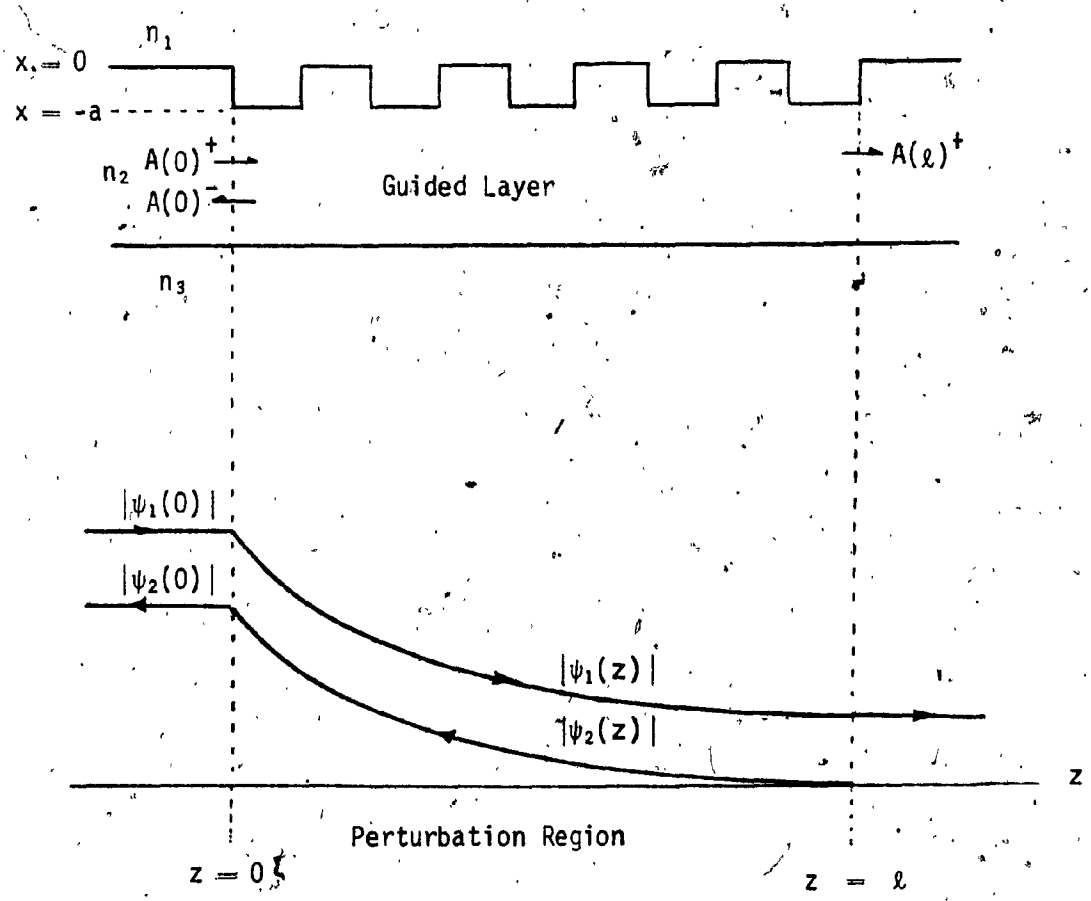

Fig. 2 . 5 Corrugated structure and Mode amplitude distributions in the perturbed region when phase matching condition satisfied (after{6}).

drops off exponentially along the perturbation region.

The expression for κ_o, determined above indicates that for a periodically perturbed grating structure in the weak coupling approximation the system matrix is constant. If the perturbation is not periodic the coupling coefficient will generally be a function of z.

In some applications it is the wavenumber of the coupled waveguides which is made to depend on the axial coordinate. In the linearly tapered coupler e.g. $\beta_1(z) = \beta_o(1+\gamma z)$ and $\beta_2(z) = \beta_o(1-\gamma z)$ but κ is a constant, Smith [9] showed that in this case the exact solution of (2.1.14) can be expressed in terms of parabolic cylinder functions:

$$\psi_1(\xi) = \nu^{\frac{1}{2}}\, e^{j\beta_o z}/2^{\frac{1}{2}}\{\cos\lambda E(a_1,\xi)+j\sin\lambda \tilde{E}(a_1,\xi)\}$$
$$\psi_2(\xi) = \nu^{\frac{1}{2}}\, e^{j\beta_o z}/2^{\frac{1}{2}}\{\cos\lambda E(a_2,\xi)-j\sin\lambda E(a_2,\xi)\} \qquad (2.1.27.)$$

where $\xi = (\gamma\beta_o)^{\frac{1}{2}} z$

$$\cos\lambda = \exp(-\pi\nu)$$

$$\sin\lambda = \{1-\exp(-2\pi\nu)\}^{\frac{1}{2}}$$

$$a_{1,2} = -\nu \pm \tfrac{1}{2}j$$

$$\nu = \kappa^2/2\gamma\beta_o$$

and $E(a,\xi)$, $\tilde{E}(a,\xi)$ are two independent complex solutions of the parabolic cylinder differential equation.

For the most general case where all elements of the system

matrix R are z dependent, Chen and Ishimaru[10] developed a transformation which reduces the coupled mode equations to a pair of Riccati differential equations. Thus they have shown that

$$\text{if} \quad \bar{a}(z)/dz = -jR(z)\bar{a}(z), \tag{2.1.28}$$

$$\text{where} \quad \bar{a}^T(z) \triangleq \{a_1(z), a_2(z)\}$$

$$R(z) = \begin{bmatrix} R_{11}(z) & R_{12}(z) \\ R_{21}(z) & R_{22}(z) \end{bmatrix}$$

$$\text{then} \quad a_1(z) = (-C_1 j \int_0^z R_{12} e^{-j\theta}\, dz + C_2) \exp(-j\psi)$$

$$a_2(z) = \{C_1(-jh_o \int_0^z R_{12}\exp(-j\theta)dz + \exp(-j\theta)) + C_2 h_o\}\exp(-j\psi) \tag{2.1.29}$$

$$\text{where} \quad \theta = \int_0^z (R_{22} - R_{11} - 2R_{12}h_o)\, dz$$

$$\psi = \int_0^z (R_{11} + R_{12}h_o)\, dz$$

and C_1, C_2 are constants of integration and h_o is a transform parameter which is a particular solution of the generalized Riccati differential equation

$$h_o' + j(R_{11} - R_{22})h_o + jR_{12}h_o^2 = jR_{21}.$$

In the case of uniform coupling where all elements of R are constant

$$R = \begin{bmatrix} \beta_1 & jC_{12} \\ jC_{21} & \beta_2 \end{bmatrix}, \qquad h_o = -\frac{\beta b}{C_{12}} \tan \beta_b z + j\frac{\beta d}{C_{12}}$$

and (2.1.29) reduces to

$$\bar{a}(z) = M(z)\bar{a}(0) \qquad (2.1.30)$$

where $M(z) = e^{-\beta_a z}\begin{bmatrix} \cos\beta_b z - j\beta_d/\beta_b \sin\beta_b z, & C_{12}/\beta_b \sin\beta_b z \\ C_{21}/\beta_b \sin\beta_b z, & \cos\beta_b z + \beta_d/\beta_b \sin\beta_b z \end{bmatrix}$

is the transfer matrix

and $\beta_a = (\beta_1 + \beta_2)/2$, $\beta_d = (\beta_1 - \beta_2)/2$, $\beta_b = (\beta_d^2 - C_{12}C_{21})^{\frac{1}{2}}$

Some other special cases where (2.1.29) can be reduced to simple integral form are given below with the solutions.

Case I) $R_{11}(z) = R_{22}(z)$

$R_{12}(z) = R_{21}(z)$

In this case, the particular solution h_o of Riccati equation and the system transfer matrix M(z) are

$$h_o(z) = j\cot\theta$$

and $$M(z) = \exp(-j\int_o^z R_{11}(z)dz)\begin{bmatrix} \cos\theta & -j\sin\theta \\ -j\sin\theta & \cos\theta \end{bmatrix} \qquad (2.1.31)$$

where $\theta = \int_o^z R_{12}(z)dz$

Case II) $R_{11}(z) = -\{\beta(z) + \mu_1 n(z)\}$

$R_{22}(z) = -\{\beta(z) - \mu_2 n(z)\}$

and $R_{12}(z) = R_{21}(z) = -\mu_3 n(z)$

where μ_1, μ_2 and μ_3 are constants.

this case results in h_o and the system transfer matrix

$$h_o = j\alpha\tan\theta - \nu/2$$

$$M(z) = \exp(j\psi)\begin{bmatrix} \cos\theta + j\nu\sin\theta/(2\alpha), & j\sin\theta/\alpha \\ j\{\alpha - \nu^2/(4\alpha)\}\sin\theta, & \cos\theta - j\nu\sin\theta/(2\alpha) \end{bmatrix} \quad (2.1.32)$$

where $\psi = \int_0^z \beta dz + \{(\mu_1 - \mu_2)/2\}\int_0^z \eta dz$

$$\nu = (\mu_1 + \mu_2)/\mu_3$$

$$\alpha = \{1 + (\nu/2)^2\}^{\frac{1}{2}}$$

$$\theta = \mu_3\alpha\int^z \eta dz$$

Case III) $R_{11}(z) = -\{\beta(z) + \mu_1 n(z)\}$

$R_{22}(z) = -\{\beta(z) - \mu_2 n(z)\}$

and $R_{21}(z) = -R_{12}(z) = -\mu_3 n(z)$.

Then $h_o = -j\alpha'\tan\theta' + \nu/2$

$$M(z) = \exp(j\psi)\begin{bmatrix} \cos\theta' + j\nu\sin\theta'/2\alpha, & -j\sin\theta'/\alpha' \\ -j\{\alpha' - \nu^2/4\alpha'\}\sin\theta', & \cos\theta' - j\nu/2\alpha'\sin\theta' \end{bmatrix}$$

(2.1.33)

where

$$\alpha' = \{(\nu/2)^2 - 1\}^{\frac{1}{2}}$$

$$\theta' = \mu_3\alpha\int \eta dz$$

ψ, ν are the same as before.

In the general case (2.1.29.) must be solved numerically. The difficulty lies in providing the particular solution (h_*) for this quadrature, since h_* is itself a numerical solution to (2.1.28.).

2.2 Matrix Analysis of Periodic Structures

Periodic structures play an important role in microwave passive and active devices specially such as filters and coupling components. The interest in this type arises from two basic properties common to all periodic structures, namely,

(1) Passband - stopband characteristics

(2) Support of waves with phase and group velocities much less than the velocity of light.

Basically above feature can be deduced from Floquet's theorem which expresses the fact that, in any infinite periodic line, the field distribution must be periodic.

Since the physical boundaries are periodic the most general function that can satisfy this requirement can be expressed as

$$f(x,y,z) = \sum_n E_n(x,y)e^{-j2n\pi z/L}e^{-\gamma z} \qquad (2.2.1)$$

where $f(x,y,z)$ is a periodic function and the n-th term on the right of equation is called the n-th space harmonics.

If there are no loss, then $\gamma = j\beta$ and the phase constant for the n-th space harmonics can be written as

$$\beta_n = \beta_0 + 2\pi n/L \qquad (2.2.2)$$

Therefore phase and group velocities can be obtained as

$$v_p = \omega/\beta_n = \omega/(\beta_0 + 2\pi n/L) \qquad (2.2.3)$$

and

$$v_g = d\omega/d\beta_n = d\omega/d\beta_0 \qquad (2.2.4)$$

Thus v_p decreases as n increase while v_g is the same for all space harmonics. A typical $\omega - \beta$ diagram is given in Fig. 2.6.a.

The circuit analysis of a periodic structure involves constructing an equivalent network for a single basic section of the structure first. Usually equivalent network consists of transmission line with a loading impedance.

Consider an equivalent circuit whose parameters for each section are known as depicted in Fig. 2.7. The Q matrix of the unit cell will be

$$Q = \begin{bmatrix} A & B \\ C & D \end{bmatrix} = \begin{bmatrix} \cos\theta - b\sin\theta/2, & j(b\cos\theta/2 - \sin\theta - b/2) \\ j(b\cos\theta/2 + \sin\theta + b/2), & \cos\theta - b\sin\theta/2 \end{bmatrix} \qquad (2.2.5)$$

and A matrix is

$$A = \begin{bmatrix} A_{11} & A_{12} \\ A_{21} & A_{22} \end{bmatrix} = \begin{bmatrix} (1 + jb/2)e^{j\theta} & jb/2 \\ -jb/2 & (1 - jb/2)e^{-j\theta} \end{bmatrix} \qquad (2.2.6)$$

Then the determinants of (2.2.5) and (2.2.6) are unity ($\Delta Q = \Delta A = 1$), which is the reciprocal condition of the transfer matrix.

The relationship between n and n + 1 section is

$$\begin{bmatrix} a_n \\ b_n \end{bmatrix} = A \begin{bmatrix} b_{n+1} \\ a_{n+1} \end{bmatrix} \qquad (2.2.7)$$

for A matrix. If this structure is capable of supporting a propagating wave, from Floquet's theorem

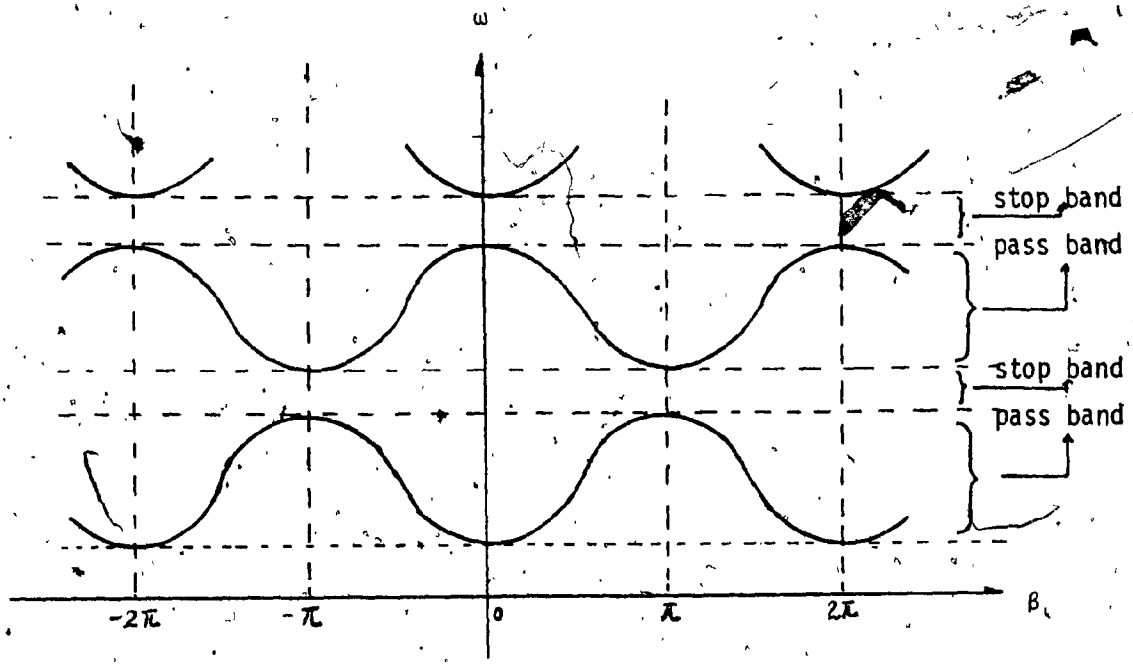

a) Brillouin(ω - β) diagram

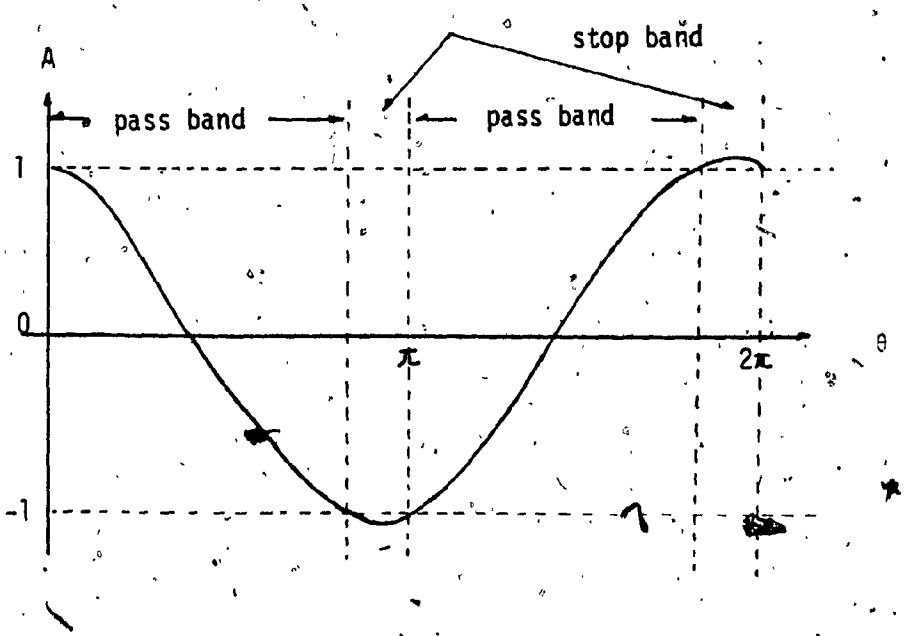

b) A - θ diagram

Fig. 2.6. Periodic structure characteristics

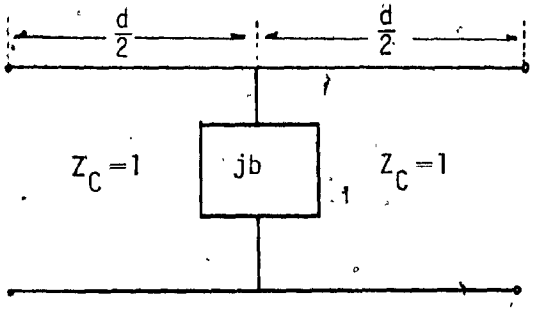

a) A basic unit cell

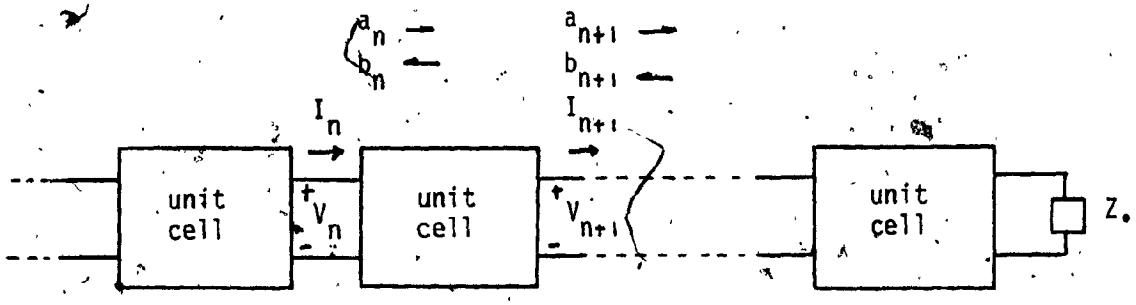

b) Cascaded connection of basic unit cell network.

Fig. 2.7 An equivalent network with capacitive loading periodic structure.

$$a_{n+1} = e^{-\gamma d} b_n$$
$$b_{n+1} = e^{-\gamma d} a_n \qquad (2.2.8)$$

After substituting (2.2.8) into (2.2.7), we can have following dispersion relation

$$\cosh\gamma d = (A_{11} + A_{22})/2 = (A + D)/2 = \cos\theta - b\sin\theta/2 \qquad (2.2.9)$$

where $\gamma = \alpha + j\beta$

when $|\cos\theta - b\sin\theta/2| < 1$, then $\gamma = j\beta$ and (2.2.9) will become

$$\cos\beta d = \cos\theta - b\sin\theta/2 \qquad (2.2.10)$$

when the right hand side of equation (2.2.10) is greater than unity or smaller than -1, then $\gamma = \alpha$ or $\pi/d + \alpha$ respectively.

So
$$\pm\cosh\alpha d = \cos\theta - b\sin\theta/2 \qquad (2.2.11)$$

where +(-) corresponds to the case of $\gamma = \alpha(\pi/d + \alpha)$.

Thus there exist frequency bands for which wave propagation can take place separated by frequency bands in which the wave is attenuated. From (2.2.9) the condition of band edge frequency is

$$|(A + D)/2| = |(A_{11} + A_{22})/2| = 1 \qquad (2.2.12)$$

The relation between $\cosh\gamma d$ and θ is shown in figure (2.6.b.). Due to small perturbation effect of b usually the stopband is much smaller than the passband.

Another parameters of importance in connection with periodic

structure are the characteristic impedance $\bar{Z}_C$ for V - I basis and the characteristic reflection coefficient $\bar{\Gamma}_C$ for wave basis. By employing Q matrix for analyzing this periodic structure we can show that the ratio of voltage and current at the n or n+1 th port will be

$$\bar{Z}_C^{\pm} = V_n/I_n = V_{n+1}/I_{n+1} = 2B\{(D - A) \pm ((A + D)^2 - 4)^{\frac{1}{2}}\}^{-1} \quad (2.2.13)$$

where +(-) signs refer to propagation in the + (-) z direction. Because $\bar{Z}_C$ is independent to n-th reference plane it is called iteractive impedance. For bilaterally symmetric network A = D. So $\bar{Z}_C$ can be reduced as $\bar{Z}_C^{\pm} = \pm(C/D)^{\frac{1}{2}}$. (2.2.14)

On the other hand the ratio of a_n and b_n is called the characteristic reflection coefficient $\bar{\Gamma}_C$. Thus from (2.2. 7) and (2.2.8.) $\bar{\Gamma}_C^{\pm}$ will be

$$\bar{\Gamma}_C^{\pm} = 2A_{21}\{(A_{11} - A_{22}) \pm ((A_{11} + A_{22})^2 - 4)^{\frac{1}{2}}\}^{-1} \quad (2.2.15)$$

Note that (2.2.15) is identical form with (2.2.13). From (2.2.13) and (2.2.15) the following relation between $\bar{\Gamma}_C^{\pm}$ and $\bar{Z}_C^{\pm}$ can be derived by making use of conversion table (Appendix II)

$$\bar{\Gamma}_C^{\pm} = (Z_C^{\pm} - 1)(Z_C^{\pm} + 1)^{-1} \quad (2.2.16)$$

Next let us concern about the group velocity of the propagating wave for the periodic structure. If the scattering matrix for a periodic unit cell is known such as

$$S = \begin{bmatrix} S_{11} & S_{12} \\ S_{21} & S_{22} \end{bmatrix}$$

The transmission coefficient T which is defined as the complex ratio of incident wave and transmitted wave in the unit cell is related to the element of S as

$$T = S_{12} = |S_{12}|e^{j\phi} \tag{2.2.17}$$

The phase term ϕ in (2.2.17) represents phase lag between two conjecutive reference planes n and n+1. Then the derivative of S_{12} with respect to ω is

$$dS_{12}/d\omega = e^{j\phi}d(|S_{12}|)/d\omega + j|S_{12}|e^{j\phi}d\phi/d\omega \tag{2.2.18}$$

After deviding each side of (2.2.18) by S_{12}

$$S_{12}^{-1}dS_{12}/d\omega = |S_{12}|^{-1}d|S_{12}|/d\omega + jd\phi/d\omega \tag{2.2.19}$$

Therefore we have the following relationship

$$d\phi/d\omega = Im\{S_{12}^{-1}dS_{12}/d\omega\} \tag{2.2.20}$$

Usually left term is defined time delay $-\tau$ which is the duration for wave propagation in unit cell. Then group velocity $v_g = \ell/\tau$ (2.2.21) where ℓ is the length of unit cell. Therefore v_g can be obtained from S_{12} directly

$$\begin{aligned} v_g &= \ell/-Im\{S_{12}^{-1}dS_{12}/d\omega\} \\ &= \ell/Im\{A_{11}^{-1}dA_{11}/d\omega\} \end{aligned} \tag{2.2.22}$$

From (2.2.20) and (2.2.21)

$$v_g = \ell/\tau = \ell(d\omega/d\phi) = d\omega/d(\phi/\ell) = d\omega/d\beta \tag{2.2.23}$$

which is identical form with (2.2.4).

A linear two-port as depicted in Fig. 2.8.a is characterized by a matrix relating its input and output terminal parameters. Some of the most common representations are summerized in Table A.1 in Appendix II whereas the interrelations between these representations are tabulated in Table A.2.

For the cascaded network consisting of N identical unit cells as shown in Fig. 2.8.b the entire transfer matrix is obtained by raising the transfer matrix of the unit cell to the N th power. Using the Q matrix as an example, it can be shown{ 11 }that for a reciprocal network ($\Delta Q = 1$)

$$Q_T = Q^N = \begin{bmatrix} A_T & B_T \\ C_T & D_T \end{bmatrix} = QU_{N-1}(\xi) - IU_{N-2}(\xi) \qquad (2.2.24)$$

where $\xi = (A + D)/2$ and $U_n(\xi)$ is the Chebyshev polynomial of the 2nd kind of order N. From the relationship between the Chebyshev polynomials of the first (T_n) and second kind { 12 }

$$\xi U_{N-1}(\xi) = U_N(\xi) - T_N(\xi) = T_N(\xi) + U_{N-2}(\xi) \qquad (2.2.25)$$

The diagonal elements of (2.2.1) are

$$AU_{N-1}(\xi) - U_{N-2}(\xi) = T_N(\xi) + \tfrac{1}{2}(A - D)\, U_{N-1}(\xi)$$

$$\text{and} \quad DU_{N-1}(\xi) - U_{N-2}(\xi) = T_N(\xi) - \tfrac{1}{2}(A - D)U_{N-1}(\xi). \qquad (2.2.26)$$

Thus the diagonal elements of bilaterally symmetric cascaded networks

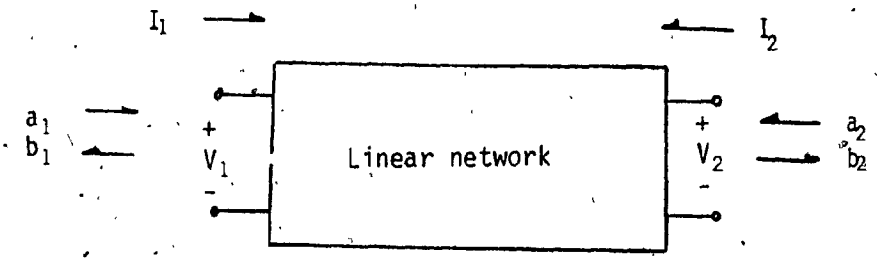

a) A two port network

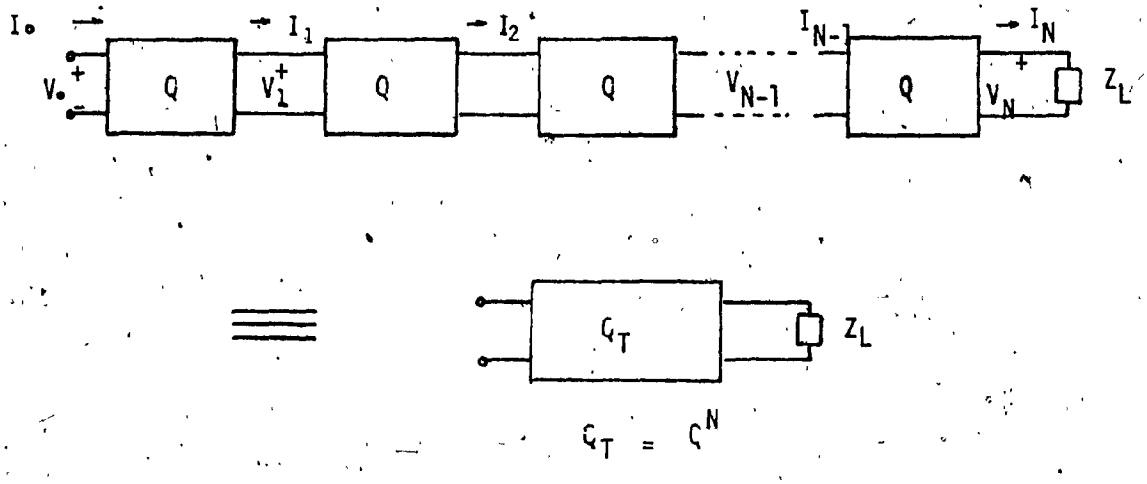

b) A cascaded network

Fig. 2.8. A cascated two port representation

reduce to

$$A_T = D_T = T_N(\xi) \qquad (2.2.27)$$

Proofs of the Chebyshev identify (2.2.24) based on the modal matrix and on Sylvesters theorem are to be found in Appendix I.

For the periodic transmission line, the same results can also be obtained from Z matrix representation without resorting to the Chebyshev identity { 13 }. For nonperiodic (taper or chirped) transmission lines where the characteristic impedance is a function of the length coordinate a general closed form solution cannot be found. Here it becomes necessary to multiply directly the Q(or A) matrices of each section;

$$Q_T = \prod_i^N Q_i \qquad (2.2.28)$$

In this case an iterative process is available to find Q_T[45]. One decomposes the Q matrix of the i-th section according to

$$\begin{bmatrix} \cos\theta & jZ_i\sin\theta \\ j\sin\theta/Z_i & \cos\theta \end{bmatrix} = \cos\theta(I + jR_i\tan\theta) \qquad (2.2.29)$$

where I : unit matrix, $R_i = \begin{bmatrix} 0 & Z_i \\ 1/Z_i & 0 \end{bmatrix}$

The resultant Q matrix of the entire structure is then obtained as

$$Q_T = \cos^N\theta \prod^N (I + jR_i\tan\theta)$$

$$= \cos^N\theta\{I - t^2\sum^{{}_NC_2}\prod R_i + t^4\sum^{{}_NC_4}\prod R_i - t^6\sum^{{}_NC_6}\prod R_i \cdots\cdots\}$$

$$+ jt\cos^N\theta\{\sum^{{}_NC_1}\prod R_i - t^2\sum^{{}_NC_3}\prod R_i + \cdots\cdots\}. \qquad (2.2.30)$$

where $t = \tan\theta$, I : unit matrix and ${}_NC_i$ is the binomial coefficient. The elements of Q_T are

$$\left.\begin{aligned} A_T &= \cos^N\theta(1 - a_1t^2 + a_2t^4 - a_3t^6 + \cdots\cdots a_{N/2}t^N) \\ B_T &= jt\cos^N\theta(b_1 - b_2t^2 + b_3t^4 - b_4t^6 + \cdots b_{N/2}t^{N-2}) \\ C_T &= jt\cos^N\theta(c_1 - c_2t^2 + c_3t^4 - c_4t^6 + \cdots c_{N/2}t^{N-2}) \\ D_T &= \cos^N\theta(1 - d_1t^2 + d_2t^4 - d_3t^6 + \cdots\cdots d_{N/2}t^N) \end{aligned}\right\} (2.2.31)$$

where

$$a_1 = \sum_1^{N-1} A_j, \qquad a_2 = \sum_1^{N-3} B_j \qquad a_3 = \sum_1^{N-5} C_j, \cdots\cdots$$

$$b_1 = \sum_1^{N} Z_i, \qquad b_2 = \sum_1^{N-2} Z_j\Big(\sum_{j+1}^{N-1} A'_k\Big), \qquad b_3 = \sum_1^{N-4} Z_j\Big(\sum_{j+1}^{N-3} B'_k\Big), \cdots$$

$$c_1 = \sum_1^{N} Z_i^{-1}, \qquad c_2 = \sum_1^{N-2} Z_j^{-1}\Big(\sum_{j+1}^{N-1} A_k\Big), \qquad c_3 = \sum_1^{N-4} Z_j^{-1}\Big(\sum_{j+1}^{N-3} B_k\Big), \cdots$$

$$d_1 = \sum_1^{N-1} A'_j, \qquad d^2 = \sum_1^{N-3} B'_j, \qquad d_3 = \sum_1^{N-5} C'_j, \cdots\cdots$$

and

$$A_j = Z_j\Big(\sum_{j+1}^{N} Z_i^{-1}\Big), \qquad B_j = \sum_{k=j+2}^{N-1} Z_j\Big(\sum_{j+1}^{k-1} Z_i^{-1}\Big)A_k, \qquad C_j = \sum_{k=j+2}^{N-3} Z_j\Big(\sum_{j+1}^{k-1} Z_i^{-1}\Big)B_k$$

$$A'_j = Z_j^{-1}\Big(\sum_{j+1}^{N} Z_i\Big), \qquad B'_j = \sum_{k=j+2}^{N-1} Z_j^{-1}\Big(\sum_{j+1}^{k-1} Z_i\Big)A'_k, \qquad C'_j = \sum_{k=j+2}^{N-3} Z_j^{-1}\Big(\sum_{j+1}^{k-1} Z_i\Big)B'_k.$$

This scheme can be called iterative method.

A comparison of the numerical efficiency of the above methods follows. The direct multiplication, Chebyshev and iterative methods are

compared to establish their relative accuracy and their demand on computer resources. Before going into details of Analysis, the analytic method to determine the accuracy of matrix multiplication of the periodic network yields some useful conclusions. Firstly in the passband calculation i.e. when the first element of Q matrix is expressed by $\cos N\theta$, the results will be correct to the computer precesion type declaration. Secondly in the stopband where the first element of transfer matrix is expressed by hyperbolic form the accuracy deteriorates with proportion to the argument of hyperbolic function and the number of unit cells independently. Therefore, first comparison of three methods are made in the passband and shown in table 2.1. The arguments start from 1.2 and increase by 0.04 radian.

From this comparison it is clear that the direct and Chebyshev methods are superior to the iterative method. Further the execution time for the iterative method is found to be almost eight times more than the other methods. The accuracy for the other two methods are examined with reference to mathmatical table { 12}and found to be accurate to the last digit of the table.

In the stopband two methods are compared for different number of unit cells. As seen in (2.2.5) the determinant of reciprocal transfer matrix is always unity. So this determinant serves as the criterion for the relative numerical accuracy of employed methods. For the Chebyshev method,the recursive property of Chebyshev functions is used in the program work.

Table 2.2. shows the first element of transfer matrix with

THETA(RADIAN)	ITERATIVE METHOD	DIRECT METHOD	CHEBYCHEV METHOD
1.20	.814203077667	.814180970526	.814180970526
1.24	-.092788246317	-.092776204597	-.092776204597
1.28	-.692896433657	-.692895821920	-.692895821920
1.32	.998591075558	.998590072440	.998590072440
1.36	-.612548100444	-.612548239496	-.612548239496
1.40	-.197813565601	-.197813574004	-.197813574004
1.44	.871147401127	.871147401031	.871147401032
1.48	-.941026309023	-.941026309029	-.941026309029
1.52	.359044286883	.359044286891	.359044286891
1.56	.471652293549	.471652293561	.471652293562
1.60	-.975629312769	-.975629312795	-.975629312795
1.64	.803775459687	.803775459710	.803775459711
1.68	-.075136090931	-.075136090898	-.075136090898
1.72	-.705551005040	-.705551006686	-.705551006686
1.76	.997493956933	.997493920327	.997493920327
1.80	-.598459713344	-.598460069058	-.598460069058

Table 2.1 Passband comparison (N = 200, Z = 1.015)

COMPARISON OF MATRIX-MULTIPLICATION

NUMBER OF CELLS	DIRECT METHOD		CHEBYSHEV	
10	1.01127110957658	.99999999999981	1.01127110957594	.99999999999854
20	1.04533851412867	.99999999999962	1.04533851412668	.99999999999559
30	1.10297016855566	.99999999999940	1.10297016855122	.99999999999022
40	1.18546521824182	.99999999999921	1.18546521823373	.99999999998195
50	1.29468328467625	.99999999999901	1.29468328466373	.99999999997154
60	1.43308638544802	.99999999999888	1.43308638542794	.99999999995224
70	1.60379443358620	.99999999999879	1.60379443355851	.99999999993192
80	1.81065556732317	.99999999999865	1.81065556728481	.99999999990077
90	2.05833289556992	.99999999999844	2.05833289561951	.99999999986355
100	2.35240961524130	.99999999999804	2.35240961517320	.99999999980042
110	2.69951486789788	.99999999999795	2.69951486780883	.99999999972013
120	3.10747317631424	.99999999999784	3.10747317620007	.99999999961364
130	3.58548032608419	.99999999999767	3.58548082593825	.99999999946505
140	4.14431317040572	.99999999999716	4.14431317021808	.99999999923796
150	4.79656753045447	.99999999999716	4.79656753021300	.99999999890838
160	5.55694716695339	.99999999999602	5.55694716666039	.99999999855106
170	6.44259272432342	.99999999999636	6.44259272396266	.99999999814190
180	7.47346861879581	.99999999999659	7.47346861835631	.99999999759052
190	8.67281308070852	.99999999999727	8.67281303016027	.99999999655302
200	10.06766199576231	.99999999999955	10.06766199509366	.99999999539659

Table 2.2 StopBand comparison ($\alpha = 0.015$, $Z = 1.015$)

the determinant in parallel for the different number of unit cell. Attenuation constant is usually small and 0.015 is used for the numerical work. As can be expected error propagates almost linearly with increase of the number of unit cells. From this Table 2.2. it is clear that direct method yields remarkably accurate numerical results. Therefore this method will be employed for the following work.

CHAPTER III

SAW PROPAGATION IN UNIFORM GRATINGS

3.1 Introduction

Referring to Fig. 3.0, a unit amplitude acoustic surface wave (Rayleigh wave) is seen entering the grating from the left. The grating scatters the surface wave; the transmitted fraction whose complex amplitude is T emerges at the output edge of the grating, while the reflected portion with complex amplitude Γ appears at the input edge.

Very strong reflection is experienced when the phase shift along one period is an integral multiple of π, i.e. when $\lambda = 2d/n$ where λ is the wavelength and n is an integer. The fundamental or π mode resonance occurs for n = 1. The frequency of this fundamental resonance is called the Bragg frequency whose value is $f_o = v_o/2d$ where v_o is the velocity of the surface wave.

The actual resonance frequency of the grating (f_R), i.e. the frequency where $|\Gamma|$ is maximum can be fractionally more or less than f_o depending whether the grating increase or decrease the velocity of the surface wave.

Gratings are fabricated either by etching grooves into the substrate or by overlaying metal or dielectric strips. The geometric discontinuity, the mechanical loading of the strips and the piezoelectric shorting in case of metallic overlays on piezoelectric sub-

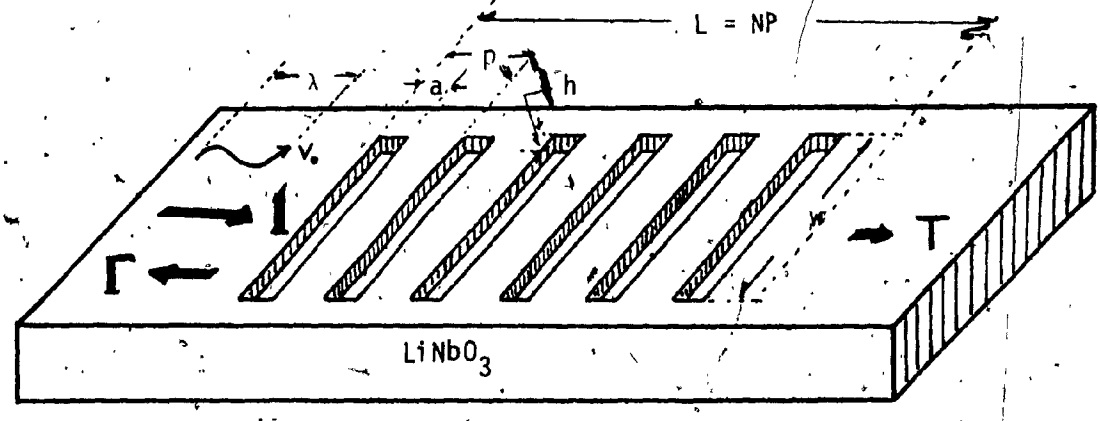

Fig. 3.0. Three dimensional grooved array

(p : period, N : number of unit cells, h : height of grooves
w : groove width)

strates will determine the actual velocity of the SAW in the grating.

In this work we shall deal exclusively with the properties of grooved gratings which are found to slow down the SAW velocity. Hence maximum reflection is seen to occur for $f_R/f_o = 1$. Moreover only the vicinity of the practically significant fundamental resonance will be analyzed.

In practical gratings the surface perturbation is weak; the grooves (h) are shallow compared to their width (w) or to the wavelength (λ) and if overlays are used the free surface wave velocity or impedance is only slightly modified by them. As a consequence the stopband is narrow and the methods of coupled mode theory can be used to advantage.

In Sec. 3.2 the equivalent circuit of a grating fabricated by applying periodic perturbation to the substrate surface will be presented and several analytic expressions for frequency response characteristics of a grating will follow. Next section will be devoted to the approximation analysis of the grating properties obtained by matrix representation. The small reflection theory and the other approximation method will be applied in the passband and near the Bragg frequency separately.

Section 3.4 will deal with energy storage effect of discontinuities of the grating. It was found that the second harmonic response of the reflection coefficient is affected by the energy storage parameter b which depends on the edge-steepness E heavily.

The last section presents properties of SAW Fabry-Perot resonator

and filter characteristics consisting of reflective gratings. The insertion loss of the F-P resonator and the acoustically coupled filter will be obtained and optimum design of resonator is discussed.

3.2 Circuit Model of the Reflective Array

The Surface Acoustic Wave (SAW) reflectors are usually made of one dimensional periodic structure with surface perturbation. The most widely used substrates for SAW devices are the simple crystal piezoelectrics such as $LiNbO_3$, Quartz, $Bi_{12}GeO_{20}$ and $LiTaO_3$ { 14 } Fig. 3.1. showes three tipes of a distributed reflector, each consisting of a periodic array of typically several hundred reflecting elements. The practical fabrication methods of grooves or the other types are seen in the literatures {14, 44}.

The main features of SAW reflection and transmission near the center frequency of shallow-groove arrays are well predicted by an approximate transmission line model described in the papers{ 15, 16, 17}. The basic component of the model is the equivalent network for each step discontinuities shown in Fig. 3.2.b. The SAW on either side of the step are identical except for a relative displacement of height h. Therefore they are represented by identical transmission lines, with the wave number equal to that of the Rayleigh wave and coupled together by an ideal transformer that represents the mismatch in the Rayleigh-wave field distributions on the two sides of the step.

An equivalent representation results when the transformer is absorbed into one of the line impedances as in Fig. 3.2.b. Then the two different characteristic impedances in the second model and the transformer turn ratio n are related to the reflection coefficient per down step r_d as

$$r_d = (Z_1 - Z_0)(Z_1 + Z_0)^{-1} = (n^2 - 1)(n^2 + 1)^{-1} \quad (3.2.1)$$

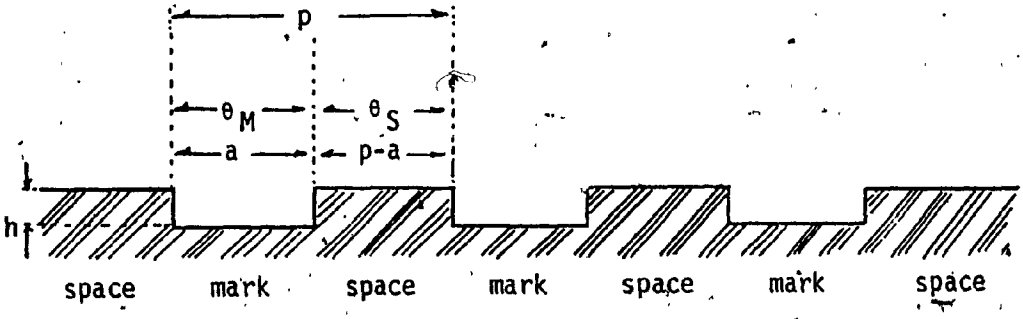

a) Grooves.

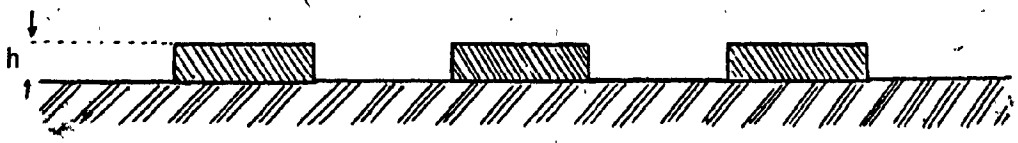

b) Field - shorting and/or massloading strips.

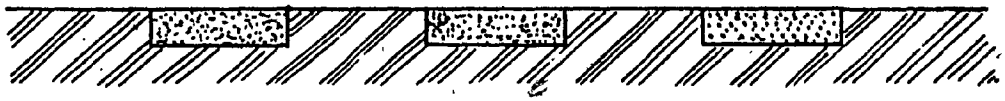

c) Ion - implanted or metal - diffused strips.

$\theta_M = ka, \qquad \theta_S = k_o(p - a), \qquad k_o = \omega/v_o = 2\pi/\lambda, \qquad h/\lambda << 1$

Fig. 3.1 Surface - wave grating reflectors.

where Z_0, Z_1 are SAW characteristic impedances in the space and mark region respectively and n is the transformer turn ratio.

In addition to small reflections at the discontinuities of a groove, a step discontinuity also generates evanescent waves which represent elastic energy storage. This energy storage is modeled by a shunt susceptance jB [15]. This small second-order effect causing grating phase shift and strong second-harmonic reflection was first discovered by experiment [15]. Several workers have since treated the energy storage effect of a step discontinuity, these shall be discussed in the following section in some detail.

A characterization of the equivalent network thus requires the determination of two parameters, namely the impedance mismatch Z_1/Z_0 and the normalized susceptance $b = B/Y_0$. Usually experimental determination from measurement is employed due to the difficulties in theoretical derivation of these step parameters. By employing the relative parameters for Z_1, and B, they can be written as

$$\bar{z} = Z_1/Z_0 = 1 + \delta_z = 1 + C_1 h/\lambda \qquad (3.2.2)$$

$$b = B/Y_0 = C_2(h/\lambda)^2$$

where C_1 and C_2 are constants.

The value of C_1 for shallow grooves has been obtained analytically by several authors [18,19,20]. Their results are in good agreement with measured value. The linear and quadratic features of δ_z and b against h/λ are confirmed experimentally [15]. Equivalent network models with and without energy storage b are shown in Fig. 3.2.

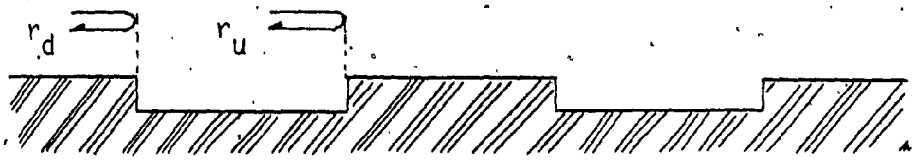

a) Geometry of groove .

$r_d(r_u)$: a reflection coefficient of down (up) step.

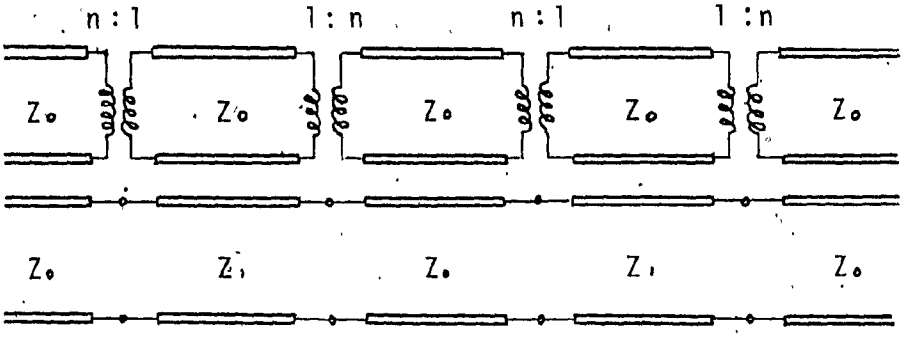

b) Equivalent network without energy storage .

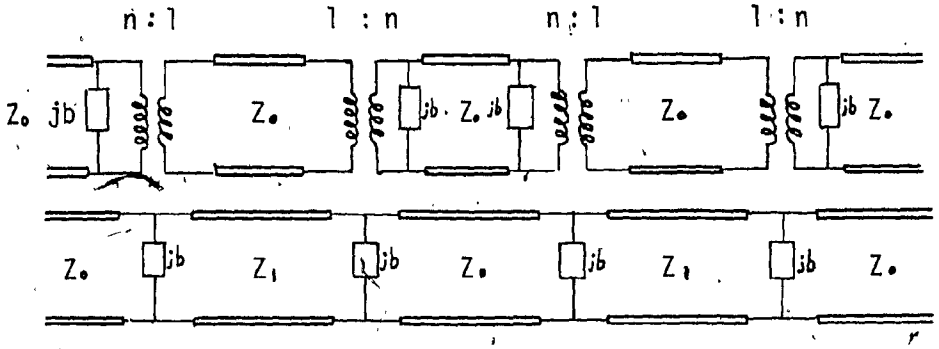

c) Equivalent network with energy storage .

Fig. 3.2 Equivalent networks for SAW in the periodic structure.

To include losses due to mode conversion or lossy substrate it would be more appropriate to represent this source of loss by introducing a complex $b = b_r - jb_i$ parameter{ 17 }. These circuit parameters and typical values of the other related values are tabulated in Table 3.1.

Once the parameters of the equivalent network are defined, the transfer matrix (Q_N or A_N) of an N unit cell gratings is obtained by raising to the N-th power the Q and A matrices of the unit cell respectively {15, 16, 17} . The transfer matrix for the unit cell chosen as non symmetrical way shown in Fig. 3.3. is obtained by the chain rule developed in Chapter 2. Hence we have

$$Q = \begin{bmatrix} A & \bar{B} \\ \bar{C} & D \end{bmatrix} \qquad (3.2.3)$$

where

$$A = \cos\theta_M\cos\theta_S - b\bar{z}\sin\theta_M\cos\theta_S - \bar{z}\sin\theta_M\sin\theta_S$$

$$-j\bar{B} = \sin\theta_S\cos\theta_M + \bar{z}\sin\theta_M(\cos\theta_S - b\sin\theta_S)$$

$$-jC = \cos\theta_S(b\cos\theta_M + \sin\theta_M/\bar{z}) + (b\cos\theta_S + \sin\theta_S)(\cos\theta_M - b\bar{z}\sin\theta_M)$$

$$D = -(b\cos\theta_M + \sin\theta_M/\bar{z})\sin\theta_S + (\cos\theta_S - b\sin\theta_S)(\cos\theta_M - b\bar{z}\sin\theta_M)$$

and $\theta_S = k_\bullet(p - a) = kp(1 - y) = \pi F(1 - y)$

$\theta_M = k_\bullet a = k_\bullet py = \pi Fy$

$F = f/f_\bullet$ $f_\bullet$: Bragg freq., $b = b_r - jb_i$, $y = a/p$.

	YZ LiNbO	ST-X Quartz	Remarks
C_1	0.66~0.75	0.5~0.56	{15, 16, 19 20, 21}
C_2	42.	29.	
δ_z	0.01~0.02		$\delta_z = C_1 \frac{h}{\lambda}$
b_r	0.005~0.01		$b_r = C_2(\frac{h}{\lambda})$
$-b_i$	$\sim 10^{-3}$		$b = b_r - jb_i$
p, λ	$\sim 10^{-4}$ cm		$2p = \lambda$
v_o	3×10^5 cm/sec		{22, 23, 24}
f	$10^7 \sim 10^9$ Hz		
$\frac{h}{\lambda}$	$\sim 10^{-2}$		

Table 3.1 Equivalent circuit parameters for grating reflectors. { } refers to reference.

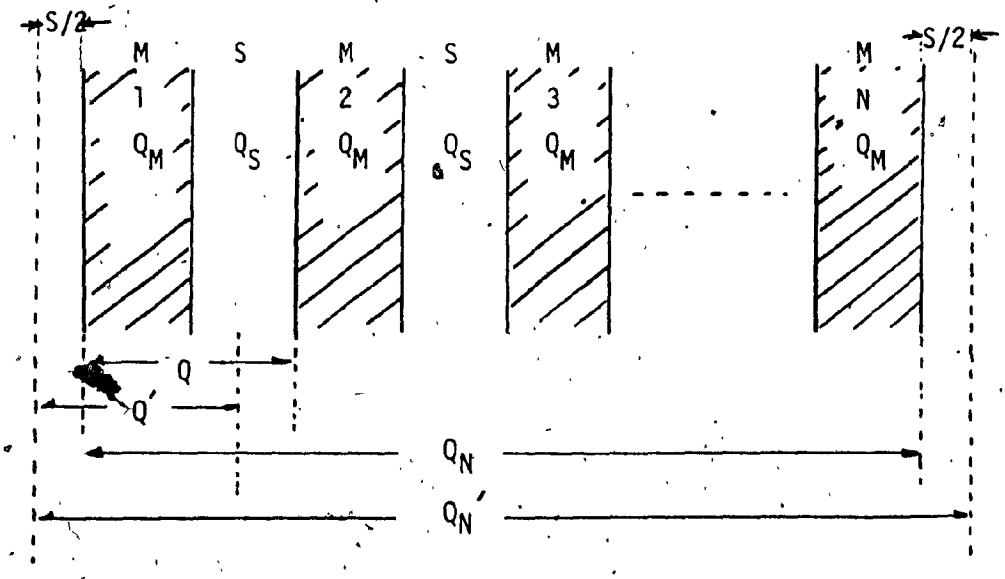

$Q = Q_M Q_S$: Non symmetrical unit cell.

$Q' = Q_{S/2} Q_M Q_{S/2}$: Symetrical unit cell.

$Q_N = Q^{N-1} Q_M$

$Q_N' = (Q')^N$

} Symmetric total Q matrix.

$Q_N' = Q_{S/2} Q_N Q_{S/2}$

where $Q_{S/2} = 1/2^{\frac{1}{2}} \begin{bmatrix} 1 & j \\ j & 1 \end{bmatrix}$

Fig. 3.3. Reference planes for choosing symmetrical unit cell and non symmetrical unit cell.

And elements of A matrix for the same unit cell are:

$$\left.\begin{aligned} A_{11} &= e^{j\theta}S\{(1 + jb)\cos\theta_M - (b\bar{z} - jZ_+)\sin\theta_M\} \\ A_{12} &= je^{-j\theta}S(b\cos\theta_M - Z_-\sin\theta_M) \\ A_{21} &= -je^{j\theta}S(b\cos\theta_M - Z_-\sin\theta_M) \\ A_{22} &= e^{-j\theta}S\{(1 - jb)\cos\theta_M - (b\bar{z} + jZ_+)\sin\theta_M\} \end{aligned}\right\} \quad (3.2.4)$$

where $Z_\pm = \frac{1}{2}(\bar{z} \pm 1/\bar{z} - b^2\bar{z})$.

For a lossless case b is real. Then above elements satisfy the lossless and reciprocal conditions i.e. $A_{11} = A_{22}^*$, $A_{12} = A_{21}^*$. The traces of Q and Q′ in Fig. 3.3 are identical [25] because the different representations of unit cell are related by similarity transformation of the same structure.

The symmetrically chosen Q′ matrix [17] is equivalent to the transmission line of the same length according to the relationship

$$Q' = \begin{bmatrix} A' & \bar{B}' \\ \bar{C}' & D' \end{bmatrix} = \begin{bmatrix} \cos kp & jZ_I \sin kp \\ j\sin kp/Z_I & \cos kp \end{bmatrix} \quad (3.2.5)$$

where k is the propagation constant of the equivalent transmission line and Z_I is its normalized wave impedance. After raising the n-th power of Q′ we obtain Q_N' for the entire grating

$$Q_N' = \begin{bmatrix} A_N' & B_N' \\ C_N' & D_N' \end{bmatrix} = \begin{bmatrix} \cos Nkp & jZ_I \sin Nkp \\ j\sin Nkp/Z_I & \cos Nkp \end{bmatrix} \quad (3.2.6)$$

Note that "primed" matrix Q_N' is referred to the symmetrically chosen unit cell in Fig. 3.3. Therefore "unprimed" transfer matrix Q_N can be obtained directly from (3.2.6) by pre and post-multiplication of $Q_{s/2}^{-1}$ to Q_N' and results in

$$Q_N = \begin{bmatrix} \bar{Z}_+ \sin Nkp & j(\bar{Z}_- \sin Nkp - \cos Nkp) \\ -j(\bar{Z}_- \sin Nkp + \cos Nkp), & \bar{Z}_+ \sin Nkp \end{bmatrix} \quad (3.2.7)$$

The other matrices are obtained from Q_N by making use of conversion Table 2.2 in Appendix II. They are

$$S_N = \begin{bmatrix} S_{N11} & S_{N12} \\ S_{N21} & S_{N22} \end{bmatrix} = \{\cos Nkp + j\bar{Z}_+ \sin Nkp\}^{-1} \begin{bmatrix} \bar{Z}_- \sin Nkp & j \\ j & -\bar{Z}_- \sin Nkp \end{bmatrix} \quad (3.2.8)$$

and

$$A_N = \begin{bmatrix} A_{N11} & A_{N12} \\ A_{N21} & A_{N22} \end{bmatrix} = \begin{bmatrix} \bar{Z}_+ \sin Nkp - j\cos Nkp, & -j\bar{Z}_- \sin Nkp \\ j\bar{Z}_- \sin Nkp, & \bar{Z}_+ \sin Nkp + j\cos Nkp \end{bmatrix} \quad (3.2.9)$$

where $\bar{Z}_\pm = \frac{1}{2}(Z_I \pm 1/Z_I)$.

Reflection coefficient (Γ) and transmission coefficient (T) of the gratings at the input port are obtained from the elements of scattering matrix S_N when output port is matched by characteristic impedance of space region. Therefore from (3.2.8)

$$\begin{aligned} \Gamma &= \rho \exp(j\phi) \\ T &= t \exp j(\phi + \pi/2) \end{aligned} \quad (3.2.10)$$

In the passband k and Z_I are real then

$$\rho = (\bar{Z}_- \sin Nkp)(\cos^2 Nkp + \bar{Z}_+^2 \sin^2 Nkp)^{-\frac{1}{2}}$$
$$t = (\cos^2 Nkp + \bar{Z}_+^2 \sin^2 Nkp)^{-\frac{1}{2}} \qquad (3.2.11)$$

In the stopband $k = \pi/p + j\alpha$ and $Z_I = j|Z_I|$, so

$$\rho = (\bar{Z}'_+ \sinh N\alpha p)(\cosh^2 N\alpha p + \bar{Z}'^2_- \sinh^2 N\alpha p)^{-\frac{1}{2}}$$
$$t = (\cosh^2 N\alpha p + \bar{Z}'^2_- \sinh^2 N\alpha p)^{-\frac{1}{2}} \qquad (3.2.12)$$

where $\bar{Z}'_\pm = \frac{1}{2}(|Z_I| \pm 1/|Z_I|)$.

An important additional parameter in reflector and resonator design is the relative penetration depth c [26] which can be interpreted as how much deeply SAW penetrate the grating near the resonant frequency. Recalling the definition of the time delay τ defined in (2.2.20). The relative penetration depth c is related to τ as

$$c = 2\tau f_o \qquad (3.2.13)$$

where f_o is the Bragg frequency. Note that c is twice of the virtual penetration depth of a grating. From (2.2.20) and (3.2.13) c can be rewritten as

$$c = -\pi^{-1} d\phi/dF \qquad (3.2.14)$$

3.3 Approximation Method

The elements of Q matrix for a unit cell given by (3.2.3) will characterize the reflecting phenomena of the grating completely. But before embarking on the exact solution obtained by numerical technique, the study of the effect of various parameters employed to describe the elements of the unit Q matrix will be helpful to understand and design a grating reflector. To this end some approximation will be in order.

The most important characteristics in the reflective array is the reflection coefficient (Γ) given in equation (3.2.10). In the passband from (3.2.11) the magnitude of Γ can be rewritten as

$$\rho = F_N(\theta)(\bar{B} - \bar{C})\{\cos^2 N\theta + (\bar{B} + \bar{C})^2 F_N^2(\theta)\}^{-\frac{1}{2}} \qquad (3.3.1)$$

where $F_N(\theta) = \sin N\theta/\sin\theta$. Therefore the passband reflection coefficient is largely determined by the properties of the $F_N(\theta)$ function.

To derive this functional dependency we apply first the small reflection theory [27] to the analysis of the grating. Referring to Fig. 3.4. the reflection coefficient Γ_g for a single groove consists of a down step separated from an up-step by a distance "a" can be obtained directly as

$$\begin{aligned}\Gamma_g &= r_d + t_d r_u t_u \\ &= -r_o - jb/2 + e^{-jb}(r_o - jb/2)e^{-j2ka} \\ &= -2j\exp(-j\theta)\{r_o \sin\theta + (b/2)\cos\theta\} \qquad (3.3.2)\end{aligned}$$

where $\theta = ka + b/2$ and $k = 2\pi/\lambda$. Then the total reflection

$Y_1/Y_0 = 1 + \delta_y$, $\delta_y/Y_0 = 2r_0$, $B/Y_0 = b$, h/λ_0, δ_y, $b \ll 1$

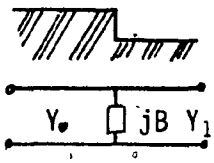

$$\begin{cases} \Gamma_d = \dfrac{Y_0 - Y_1 - jB}{Y_0 + Y_1 + jB} \simeq \dfrac{-\delta_y - jB}{2Y_0} = -r_0 - jb/2 \\ \tau_d = 1 - jb/2 \simeq \exp(-jb/2) \end{cases}$$

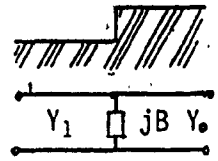

$$\begin{cases} \Gamma_u = \dfrac{Y_1 - Y_0 - jB}{Y_1 + Y_0 + jB} \simeq \dfrac{\delta_y - jB}{2Y_0} = r_0 - jb/2 \\ t_u = 1 - jb/2 \simeq \exp(-jb/2) \end{cases}$$

$\Gamma_d = -\Gamma_u^*$, $t_d = t_u$

a) Single step discontinuity

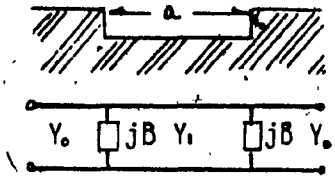

$$\begin{cases} \Gamma_g = r_d + t_d r_u t_u \simeq -2je^{j\theta}(r_0 \sin\theta + b/2\cos\theta) \\ \text{where } \theta = ka + b/2 \\ T_g = t_d e^{-jka} t_u \simeq \exp\{-j(ka + b)\} \end{cases}$$

b) Equivalent network of single groove

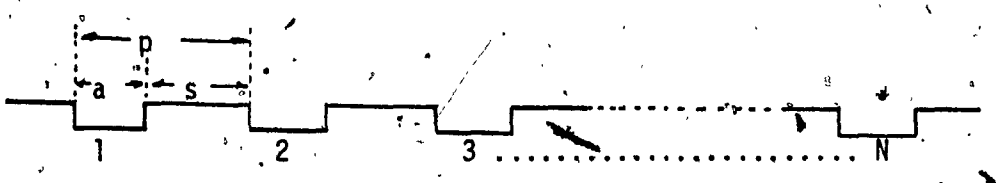

$$\Gamma = \Gamma_g\{1 + T_g^2 e^{-j2ks} + T_g^4 e^{-j4ks} + \ldots\ldots (T_g^2 e^{-j2ks})^{N-1}\}$$

$$= \Gamma_g \exp\{-j(N-1)(kp + b)\} \sin N(kp + b)/\sin(kp + b)$$

c) Equivalent network of grating

Fig. 3.4. Equivalent circuits relevant to a grooved grating

coefficient for an array of N grooves of width "a" separated by "s" can be written as the series

$$\Gamma = \Gamma_g\{1 + T_g^2 e^{-j2ks} + T_g^4 e^{-j4ks} + \ldots\ldots + (T_g^2 e^{-j2ks})^{N-1}\}$$

$$= \Gamma_g \exp\{-j(N-1)\theta'\} \sin N\theta'/\sin\theta' \qquad (3.3.3)$$

where $T_g = \exp\{-j(ka + b)\}$, and $\theta' = ka + b$. Therefore above $F(\theta)$ dependency of Γ is easily understood.

From (3.3.3) the resonant frequency f_R for the maximum reflection coefficient is determined when $\theta' = n\pi$ $n = 1,2,3\ldots$. For π mode i.e. $n = 1$ the relative resonant frequency F_R is

$$F_R = f_R/f_o = 1 - b/\pi. \qquad (3.3.4)$$

(3.3.4) represents frequency shift b/π caused by the energy storage b. At the resonant frequency maximum reflection coefficient for an array can be obtained by applying L'Hospital rule to (3.3.3). Then

$$|\Gamma|_{max} = |N\delta_z| \quad \text{at resonance} \qquad (3.3.5)$$

where $\delta_z = -2r_o$.

Equation (3.3.5) states that $|\Gamma|_{max}$ is due to the coherent addition of equal reflection from N grooves, consistant with the initial assumption that multiple reflections between grooves are neglected. When $N\delta_z$ is large such that $N\delta_z > 1$. We cannot neglect the multiple reflection anymore. In other words the number of grooves and δ_z limit validity of (3.3.3.).

A more improved approximation near the Bragg frequency which will be treated next shows that

$$|\Gamma|_{max} \simeq \tanh N\delta_z \qquad (3.3.6)$$

instead of equation (3.3.5).

For reflector applications the frequencies of interest are usually those near the Bragg frequency defined before in equation (3.2.3.). So it is convenient to define a parameter ξ to measure the deviation of the operating frequency f from the Bragg frequency

$$\xi = \pi(f/f_o - 1) \qquad (3.3.7)$$

In order to make use of symmetric properties of unit cell, let us assume unit cell Q matrix be chosen bilaterally symmetric way shown in Fig. 3. 3. . By introducing above defined normalized frequency and neglecting terms of third order in δ_z, and be i.e. $b^2\delta_z$ or $\xi b\delta_z$ etc. Q'matrix reduces to

$$Q' = \begin{bmatrix} A' & B' \\ C' & D' \end{bmatrix} = \begin{bmatrix} -1 + \frac{1}{2}\{(\xi + b)^2 - \delta^2\}, & -j\{(\xi + b) - \delta\} \\ -j\{(\xi + b) + \delta\}, & -1 + \frac{1}{2}\{(\xi+b)^2 - \delta^2\} \end{bmatrix} \qquad (3.3.8)$$

where $\delta = \delta_z \sin\pi y - b\cos\pi y$.

Let us consider the stopband width first. At the stopband edge frequencies f_L and f_H from the band edge condition (2.2.12) and (3.3.8) we have

$$(\xi + b) = \pm\delta \qquad (3.3.9)$$

where ± represents upper (lower) stopband edge frequency. Therefore

$$(f_H - f_L)/f_o = \Delta f/f_o = z|\delta|/\pi = 2\pi^{-1}|-b\cos\pi y + \delta_z \sin\pi y| \quad (3.3.10)$$

After substituting h/λ into b and δ_z, we obtain relative stopband width functions against h/λ or y. They are drawn in Fig. 3.5 and 3.6 respectively. Note that for every y in Fig. 3.5 there are certain value of h/λ where stopband colapse occurs. As aspect ratio y increases stopband colapse occurs at higher h/λ.

The $\beta(\omega)$ dispersion characteristics, given in terms of the relative frequency variable $\xi + b$ is obtained as follows. Within the first stopband $A' < -1$, $k = \pi/p + j\alpha$ and $A' = -\cosh\alpha p \simeq 1 - \frac{1}{2}(\alpha p)^2$, $\alpha p \ll 1$. Then

$$(\alpha p)^2 = \delta - (\xi + b)^2 \quad (3.3.11)$$

In the passband, adjacent to the first stopband, $A > -1$, $k = \pi/p \pm \Delta\beta$ so $A' = -\cos\Delta\beta p \simeq -1 + \frac{1}{2}(\Delta\beta p)^2$ $\Delta\beta p \ll \pi/2$ and

$$\Delta\beta p = \{(\xi + b)^2 - \delta^2\}^{\frac{1}{2}} \quad (3.3.12)$$

Equations (3.3.11) and (3.3.12) are drawn in Fig. 3.7.

The inner coordinate system is centered at the intersection of the uncoupled forward travelling wave characteristics: $k = k_o/(1 - b/\pi)$ and backward travelling wave characteristics: $k = 2\pi/p - k_o/(1 - b/\pi)$. The solid hyperbola and the dashed circle are the result of coupling between these characteristics.

The approximation introduced in obtaining (3.3.8) also results in simple expressions for transmission equivalent impedance Z_I, reflection coefficient Γ and transmission coefficient T. They are

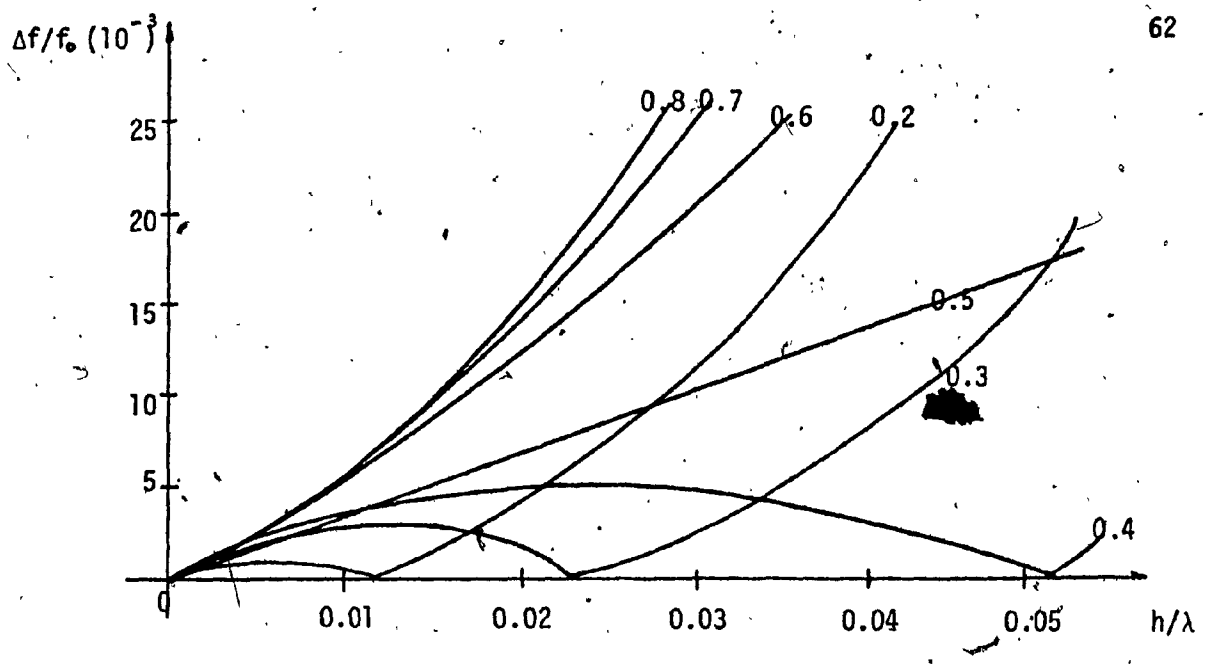

Fig. 3.5. The relative stopband - h/λ functions
Thé parameter is the aspect ratio (y).

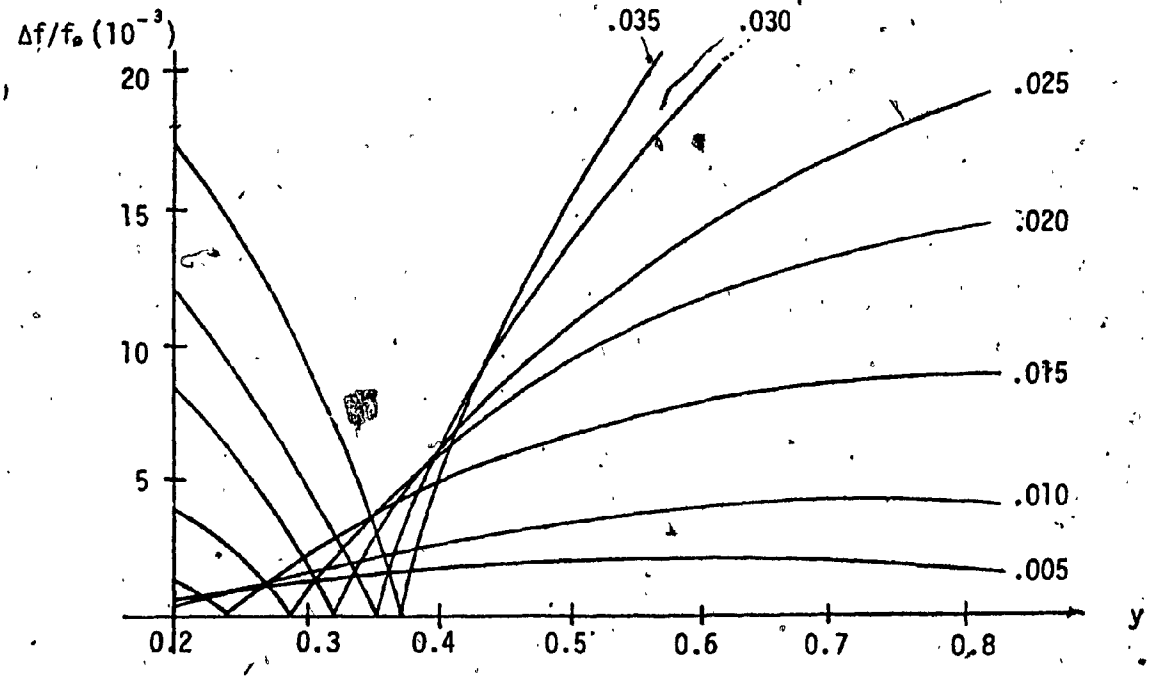

Fig. 3.6. The relative stopband -y functions.
The parameter is groove depth (h/λ).

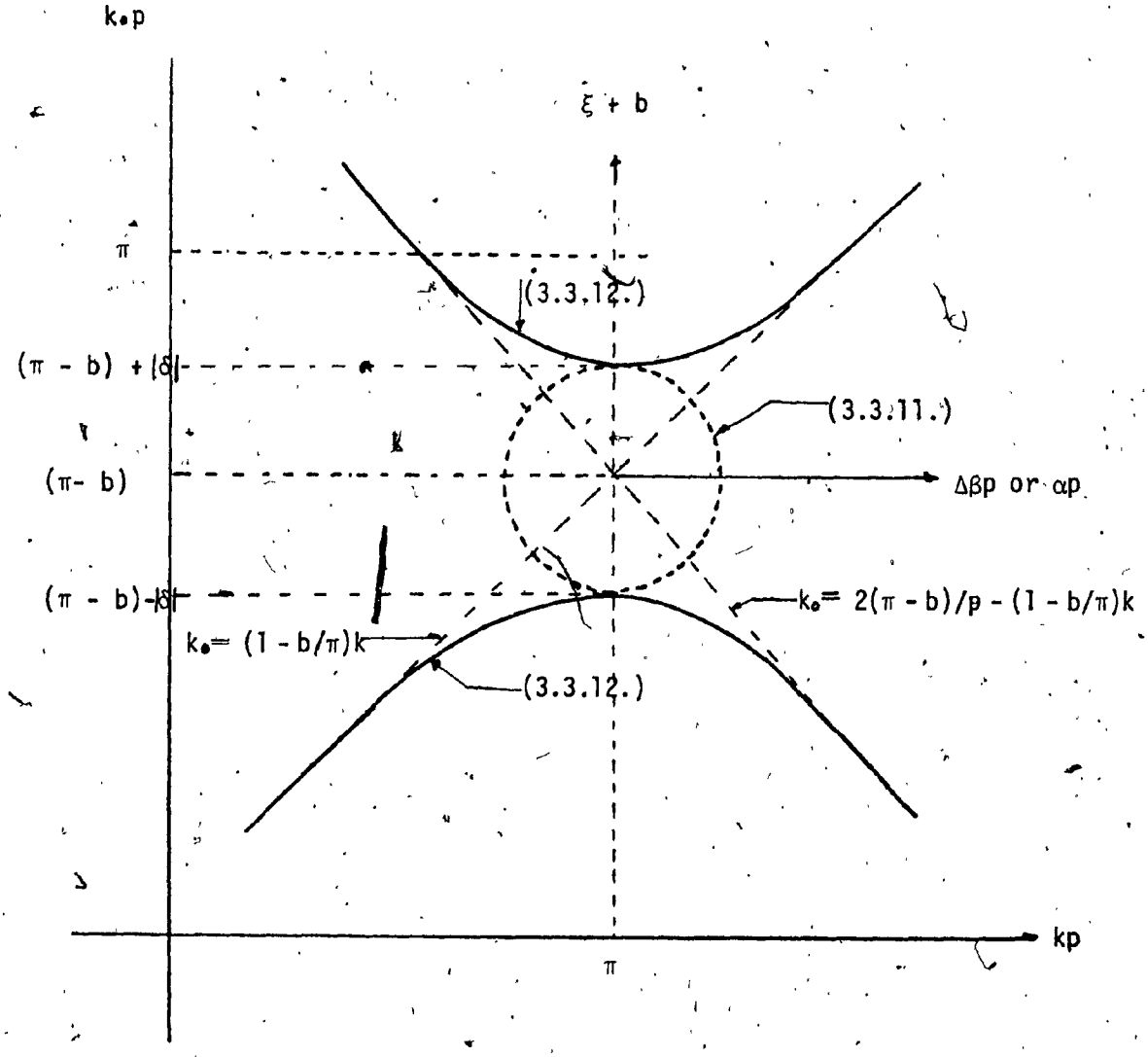

Fig. 3.7 The Brillouin diagram $kp = \pi \pm \{(\xi + b)^2 - \delta^2\}^{\frac{1}{2}}$

$$|Z_I| = \begin{cases} \{((\xi + b) - \delta)/C(\xi + b) + \delta)\}^{\frac{1}{2}} & \text{passband} \\ \{(\delta - (\xi + b))/C(\xi + b) + \delta)\}^{\frac{1}{2}} & \text{stopband} \end{cases}$$

Note Z_I is pure real in passband and pure imaginary in stopband.

$$\Gamma = \rho e^{j\phi} = \delta\,(\sin Nkp/\sin kp)\{\cos Nkp + j(\xi + b)\sin Nkp/\sin kp\}^{-1} \qquad (3.3.13)$$

and

$$T = \pm j\{\cos Nkp + j(\xi + b)\sin Nkp/\sin kp\}^{-1} \qquad (3.3.14)$$

where

$$\rho = \delta\,(\sin Nkp/\sin kp)\{\cos^2 Nkp + (\xi + b)^2(\sin Nkp/\sin kp)^2\}^{-\frac{1}{2}} \qquad (3.3.15)$$

$$\phi = -\tan^{-1}\{(\xi + b)(\tan Nkp/\sin kp)\} = \pi\{(f - f_o)\tanh Nkp/f_o\delta\} \qquad (3.3.16)$$

and $k = \pi/p - j\alpha$ or $k = \beta$ whether operating frequency is in the stopband or in the passband. The last step in ϕ was obtained from the approximation of $\xi + b << 1$ and $\sin kp \sim kp$.

At resonance the approximate values of ρ and ϕ is obtained by setting $\xi + b = 0$, $f = f_R$ $kp = \delta$ and $\sin kp \simeq kp$. Then

$$\left.\begin{aligned} \rho &= \tan N\delta \\ \phi &= 0 \end{aligned}\right\} \text{ at Resonance} \qquad (3.3.17)$$

From the definition of penetration depth in (3.2.11) c can be calculated at resonance and results in

$$c_R = \tanh N\delta\ /\delta \qquad (3.3.18)$$

3.4 Analysis of Energy Storage Effect

This section deals with some detailed analysis of second-order effects that have been observed with SAW gratings. The terminology "second order" refers to the effects that vary quadratically with relative groove depth h/λ. Therefore impedance mismatch term δ_z is usually referred to the first order effect and b is caused by the effect of the second order. The second order effect i.e. the energy storage effect was successfully explained by L_1 and Melngailis {15} in a grooved array using the improved transmission line model which includes "b" to represent the energy storage. Since then the constant C_2 has been determined and used only by experimental method.

However recently several papers {28, 29, 30} have been presented to analyze the second order effect theoretically, but their theories are too involved and even derived results are not consistant with each other. Therefore a brief derivation of the results is presented and the comparison of their results are followed.

Before going on to the second order analysis the results of a first order grating will be summarized as follows: Firstly, to the first order in the grating depth, near the Bragg frequency, the reflection of a SAW incident on the grating is maximum because the reflections from the front and back of each groove add in phase. At second harmonics the latter reflections are out of phase and no reflection is expected. Secondly the first order grating dispersion diagram shows the symmetricity of the curve about the "unperturved" Bragg frequency ω_s. There is no shift in the resonant frequency of the grating to first order. The

major second order effects which were obtained experimentally are:

(1) Resonance frequency shift

(2) Grating phase shift

(3) Strong second-harmonic reflection.

A brief description of second order effect analysis given by H. Shimizu [28] is followed. Fig. 3.8 shows a more realistic groove by the groove depth h, the effective width a, the edge-steepness parameter E and a slope to the groove edge of θ(In this analysis θ is assumed less than 90°).

For the first order analysis the details of the groove edge are relatively unimportant. However in the second order analysis it is found to be important in determining the second order effect. Based on the vector acoustic mode functions and by applying appropriate boundary condition to them the following modified coupled mode equations which include the evanescent bulk waves can be obtained

$$\begin{aligned} da_{\circ}^{+}(z)/dz &= \{\kappa_{\circ\circ}^{++}(z) + \xi^{++}(z)\}a_{\circ}^{+}(z) + \{\kappa_{\circ\circ}^{+-}(z) + \xi^{+-}(z)\}a_{\circ}^{-}(z) \\ da_{\circ}^{-}(z)/dz &= \{\kappa_{\circ\circ}^{-+}(z) + \xi^{-+}(z)\}a_{\circ}^{+}(z) + \{\kappa_{\circ\circ}^{--}(z) + \xi^{--}(z)\}a_{\circ}^{-}(z) \end{aligned} \tag{3.4.1}$$

where $\kappa_{ij}^{mn}(z)$ are coupling coefficients, which are proportial to h and $\xi^{mn}(z)$ is the coefficient of indirect coupling between the contra-directional SAW's via evanescent bulk waves and given by

$$\xi^{mn}(z) = \sum_{i=1}^{2} \int_{\circ}^{\infty} \{\kappa_{\circ i}(z,\gamma)\left(\int_{\circ}^{z} \kappa_{i\circ}^{+m}(z',\gamma)dz'\right) + \kappa_{\circ i}^{m-}(z,\gamma)\left(\int_{a+z}^{z} \kappa_{i\theta}^{-n}(z',\gamma)dz'\right)\}d\gamma$$

Since $\kappa_{ij}^{mn}(z)$ is 1st order of h, $\xi^{mn}(z)$ is quadratic in h.

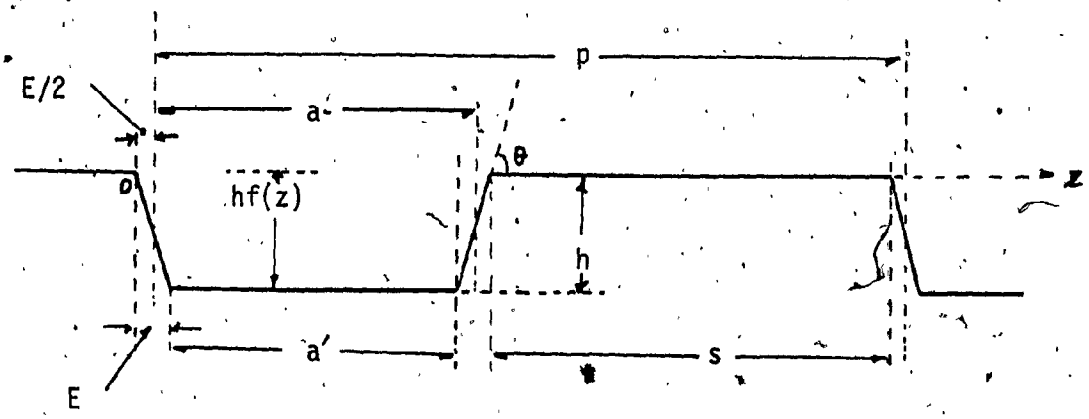

$$f(z) \begin{cases} \frac{z}{E} & ,0 < z < E \\ 1 & ,E \leq z \leq a \\ \frac{1}{E}(a+E-z) & ,a \leq z \leq a+E \end{cases}$$

Fig. 3.8. More realistic grating profile

From above derived coupled equation the reflection coefficient Γ per groove can be obtained and results in

$$\Gamma = a_{\bullet}^{-}(0)/a_{\bullet}^{+}(0) = \Gamma_1 + \Gamma_2 \qquad (3.4.2.)$$

where Γ_1 is the first order reflection coefficient given by

$$\Gamma_1 = \int_{a+E}^{0} \kappa_{oo}^{-+}(z)dz \qquad (3.4.3.)$$

and Γ_2 is the second order reflection coefficient given by

$$\Gamma_2 = \int_{a+E}^{0} \xi^{-+}(z)dz \qquad (3.4.4.)$$

From (3.4.2.), we can easily recognize that the Γ_1 and Γ_2 correspond to $r_{\bullet}$ and b/2 in equation (3.3.2.). Therefore C_1 and C_2 can be related to edge steep parameter E. Although Γ_1 can be easily calculated from the expression $\kappa_{oo}^{-+}(z)$, the calculation of Γ_2 requires the numerical integration. Therefore C_1 calculated from the final results of equation (13) by Shimizu [28] is

$$C_1 = 0.68\sin(2\pi E/\lambda_g)(2\pi E/\lambda_g) \qquad (3.4.5.)$$

where λ_g is the SAW wave length of the Bragg frequency. Above C_1 and C_2 obtained by numerical integration as a function of edge steepness parameter E are shown in Fig. 3.9. As can be expected, δ_z(or C_1) is insensitive to E whereas b(or C_2), is very sensitive to E hear 90°. When h/λ is 0.015 and θ reduces to 3.43 C_1 decrease to zero which results in $\Gamma_1 = 0$. But this triangular perturbation will cause a certain amount of reflection Γ_1' though very small. Therefore it can be seen that the above analysis on C_1 and C_2 are valid only when θ is

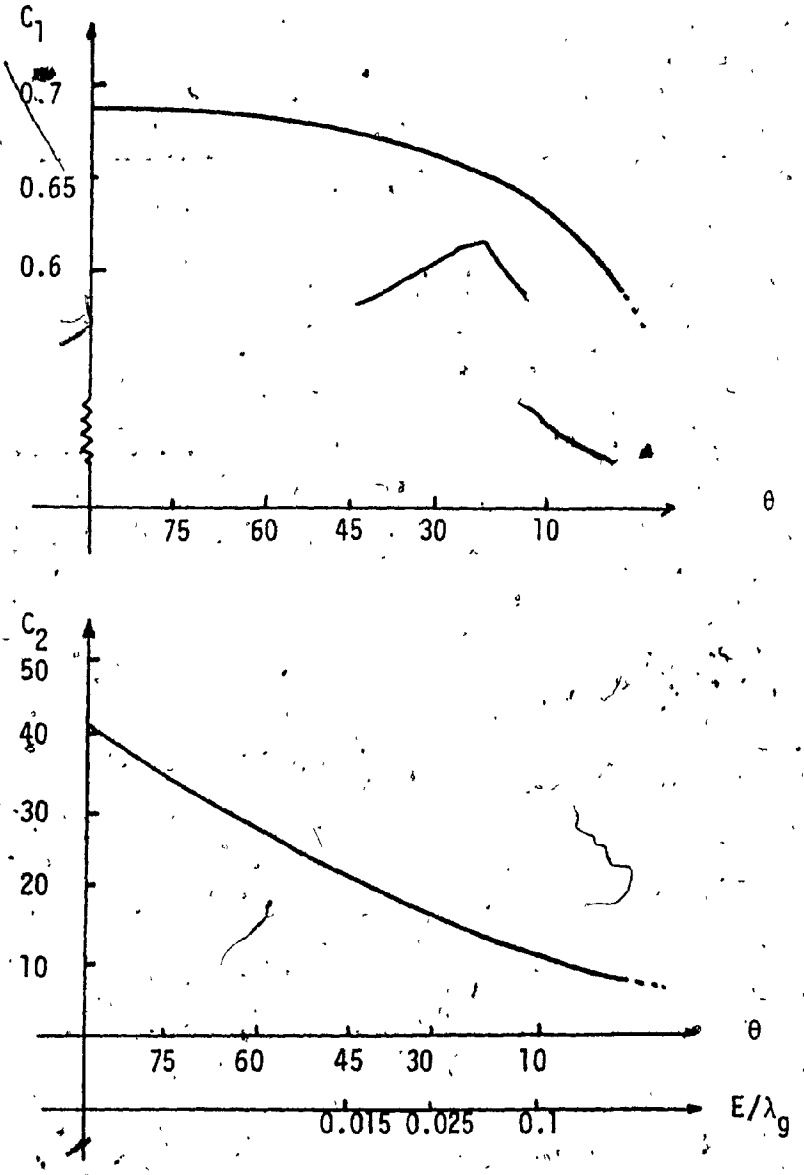

Fig. 3.9. First and second order effects as a function of edge steepness parameter θ and E after [28] when $h/\lambda = 0.015$, $y = 0.5$

moderately large.

Haus and Wright [29] who have dealt with the same subject arrived at somewhat different conclusions. To derive the second order dispersion relation of SAW propagation theoretically, they employed variational principle technique with a proper boundary condition and as a result obtained the upper and lower frequencies of the band gap in closed form to the second order. From the downward shift of the new center frequency of the grating the coefficient C_2 can be derived analytically.

However according to their conclusion as θ increases to 90° C_2 increases indefinitely. The authors explain that this blow-up nature is the result of an almost infinite sum of ever decreasing terms in which truncation or numerical integration should be avoided. Several interesting figures in their paper are redrawn in Fig. 3.10. The dotted line in Fig. 3.10.a represents logarithmic increase as $\theta \rightarrow 90^\circ$. Note that C_2 varies with h/λ also in Fig. 3.10.b, This figure shows that the energy storage b is not exactly quadratic dependent on h/λ. However this conclusion has not verified by their experimental work.

By comparing Fig. 3.9 with Fig. 3.10 discrepancies on the second order coefficient C_2 are clear. Therefore further analytical work and experimental verification are needed to this second order effect and in the remaining part of this thesis empirically obtained values 0.67 and 42. when θ is 90° are employed continuously for C_1 and C_2 .

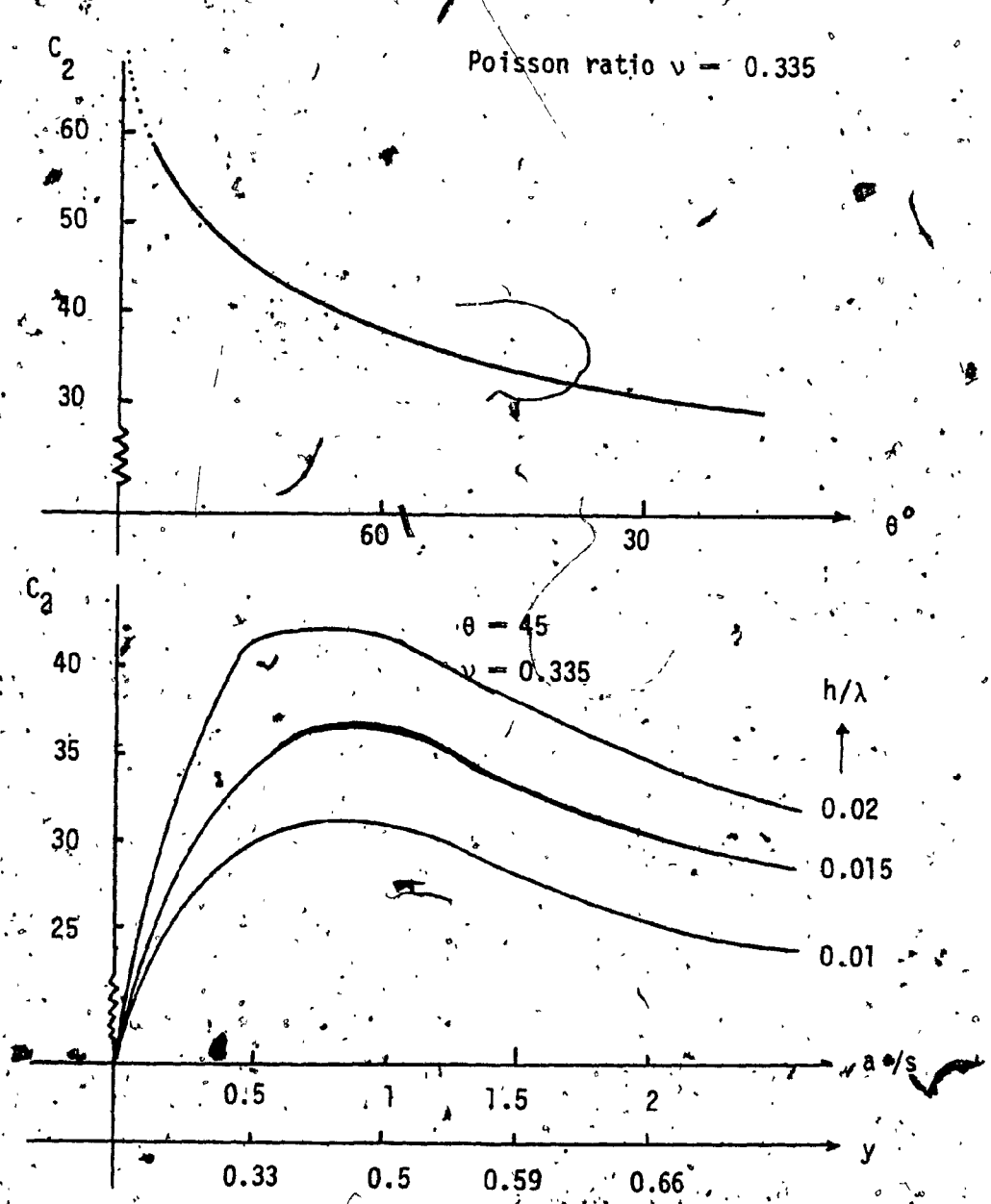

Fig. 3.10. Theoretical dependency of C_2 with θ and y after [29]

3.5 Numerical Results

In the previous section small reflection model and some approximation of matrix elements near Bragg frequency have shown the general properties of the reflective gratings. Now we are seeking exact numerical solution for the fundamental frequency response of the uniform gratings based on the unit cell whose matrix elements are given in (3.2.3.).

Although a unit cell is not bilaterally symmetric the array consisting of N unit cells is chosen symmetrically shown in Fig. 3.3. Some specific values of input parameters which are employed in FORTRAN program "SAW7" are listed in Table 3.2.

The program "SAW7" attached in Appendix III provides us with all the most important characterisitcs of the given array. They include reflection coefficient (Γ), transmission coefficient (T), input impedance (Z_i) standing wave ratio (SWR), penetration depth (c) against normalized frequency F.

Although above characteristics are primary concern for a SAW devices designer, they are analized fully and shown in the several papers already published [15, 16, 17, 19] . The other important characteristics which will be useful in designing gratings are as follows.

Fig. 3.11 shows maximum reflection coefficient against relative groove height h/λ with $b_i = 0$ and 0.0011. In the lossless case note that when h is 1.5% of λ ρ_{max} is almost unity.

Next Fig. 3.12 shows $\rho_{max} - b_i$ lossterm diagram. In practical SAW devices application the lossterm is usually very small (10^{-3}) or

Parameters	Data	Remarks
C_1	0.67	$\delta_z = C_1 h/\lambda$
C_2	42.	$b_r = C_2(h/\lambda)^2$
b_i	0.(0.0011)	$b = b_r - jb_i$
y	0.5	$y = a/p$
h/λ	0.015(0.02)	$h/\lambda \ll 1$
N	200.	number of grooves
q	30.	cavity length ($L_C = qp$)
REC	10^{-6}	
b_T	0.177	IDT suseptance
τ	0.03	$\tau = \omega C_T Z_0$

Table 3.2 Input parameters of Fortran program "SAW7". b_T and τ are discussed in the next section.

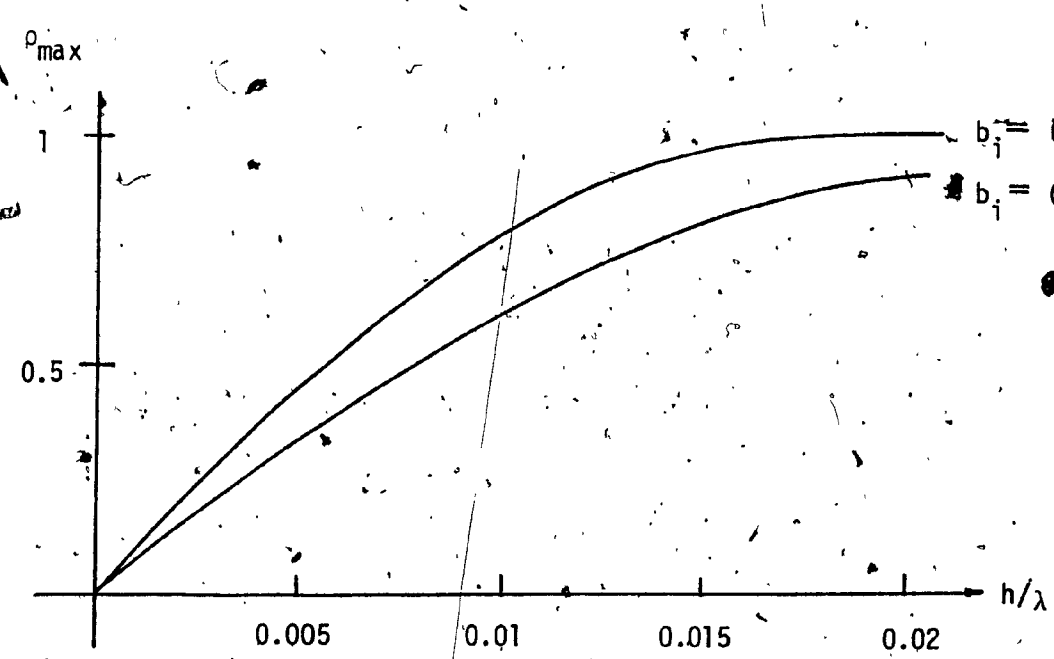

Fig. 3.11. ρ_{max} - h/λ characteristics

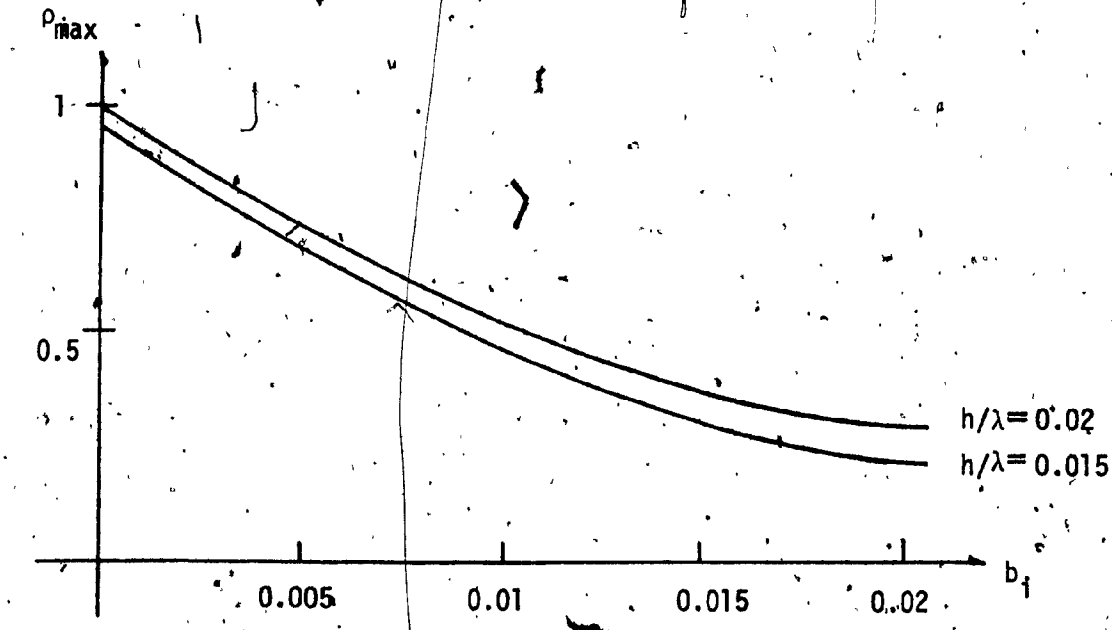

Fig. 3.12 ρ_{max} - b_i characteristics

almost negligible. Therefore this figure shows that ρ_{max} is above .93 when the grating perturbation depth is only 2% of the SAW wavelength λ.

ρ_{max} - number of grooves diagram is shown in Fig. 3.13. This figure indicates that when the number of reflector N is more than 200 the lossless ρ_{max} is at the stage of saturation. Next Fig. 3.14 illustrates the effect of aspect ratio y to ρ_{max} and shows a good agreement with the stopband width - h/λ diagram given in Fig. 3.5. Considering that the stopband width reduces to zero for a special value of aspect ratio y in Fig. 3.5. ρ_{max} will be 0 at this value of y. Therefore Fig. 3.12 indicates indirectly band collapse feature. It was found also that the y value where band collapse occures moves to .5 as h/λ reduces to 0 and vise versa.

Lastly, the second order effect treated in previous section are shown in Fig. 3.15. Based on the Shimizu's analytic results on C_1, C_2, the fundamental ρ_{max} is found to be independent on the edge - steepness parameter E. But as shown in this figure second harmonic ρ_{max} depends on E almost linearly and drops fastly near $\theta = 90°$. By increasing lossterm b_i above 10^{-3} it was found also that C_2 is less dependent on the steepness parameter E.

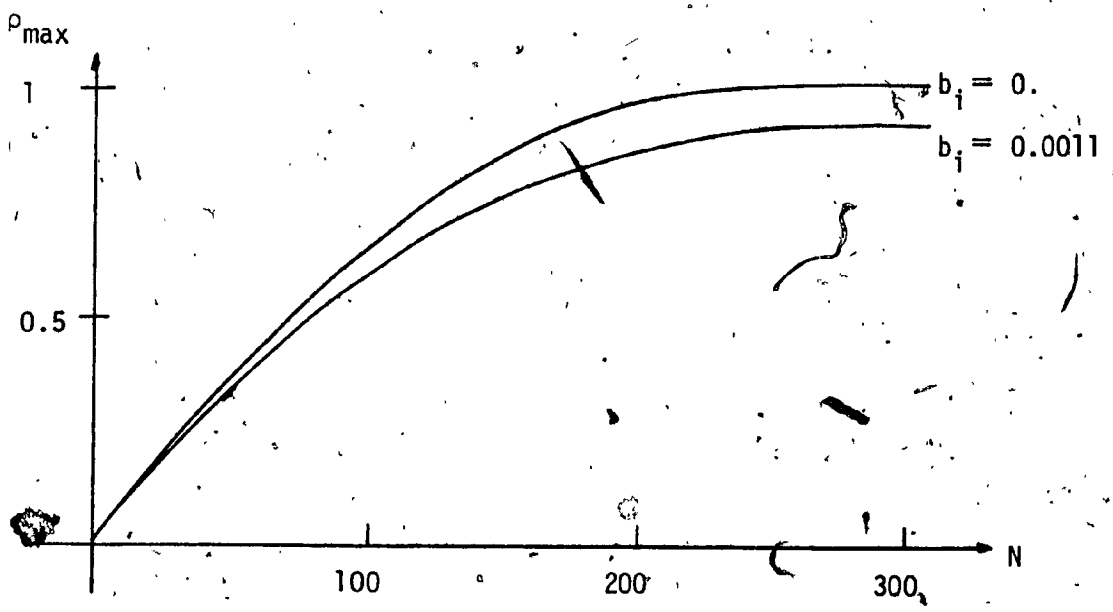

Fig. 3.13. ρ_{max} - number of unit cell (N) characteristics

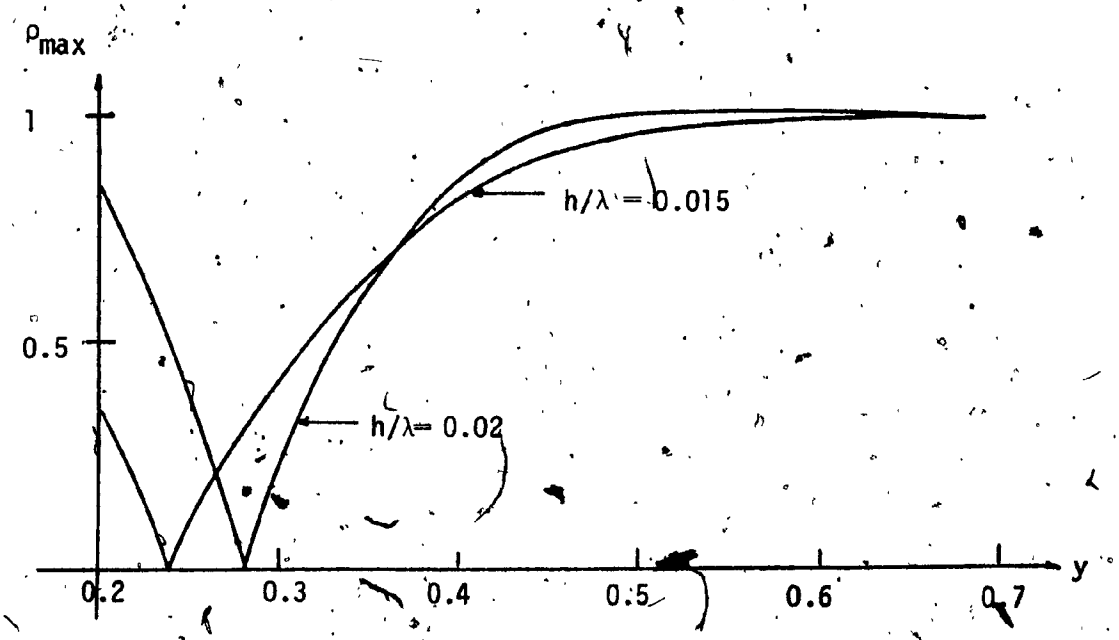

Fig. 3.14 ρ_{max} - y characteristics

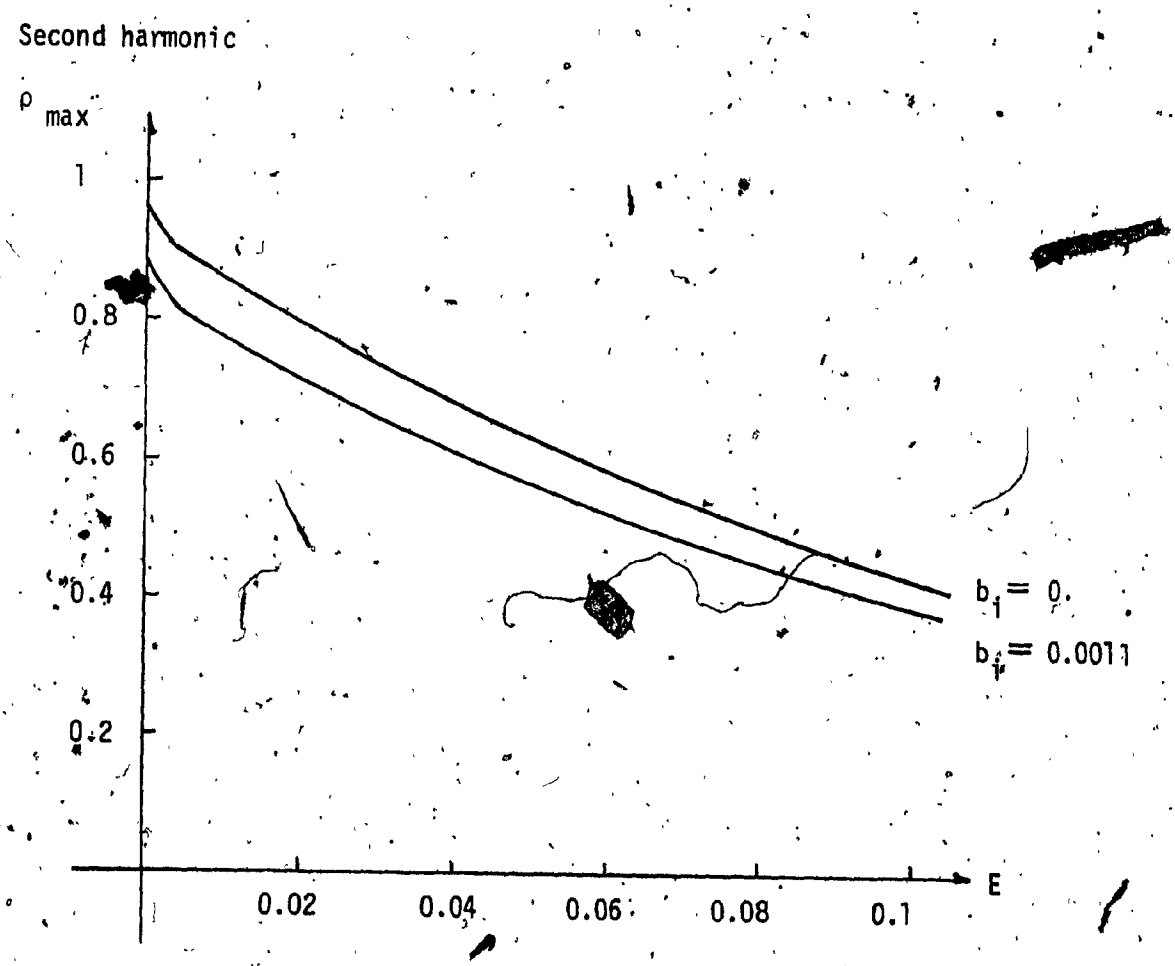

Fig. 3.15. Second harmonic ρ_{max} - the edge steep parameter E characteristics

3.6 The SAW Fabry-Perot Resonator

SAW Fabry-Perot resonator or cavity is obtained when two identical reflective arrays separated by a distance which allows the constructive interference of successive reflections between them.

The schematic diagram of the SAW resonator with reference planes is shown in Fig. 3.16. Coupling a signal into the resonator is accomplished by means of one or more standard interdigital transducers (IDT), which may be variously positioned, as shown in Fig. 3.17.

IDT is a two terminal device which consists of a series of parallel metal electrodes periodically spaced on the surface of a piezoelectric substrate and used as means of generating and detecting surface elastic waves for electronic applications.

When a cavity is formed between two identical grating reflectors. The grating behaves as an imperfect mirror located a distance $\frac{1}{2}cp$ from its terminal plane within the stopband and a standing wave is formed between reflectors. It was found that the cavity resonance condition is satisfied for $f_{FP} \sim f_R$ when the cavity length L_C shown in Fig. 3.16 is some multiple of the grating period p { 23 } . Resonance does not occur exactly at reflector resonance frequency f_R because of small discrepancy between wave velocity in the free surface cavity region and the grating region.

Fig. 3.16 shows the two possible standing wave patterns in a cavity at resonance when the cavity length L_C is an odd number of periods, standing wave is maximum at the center of the cavity and referred to parallel resonance cavity. The reverse is for the series

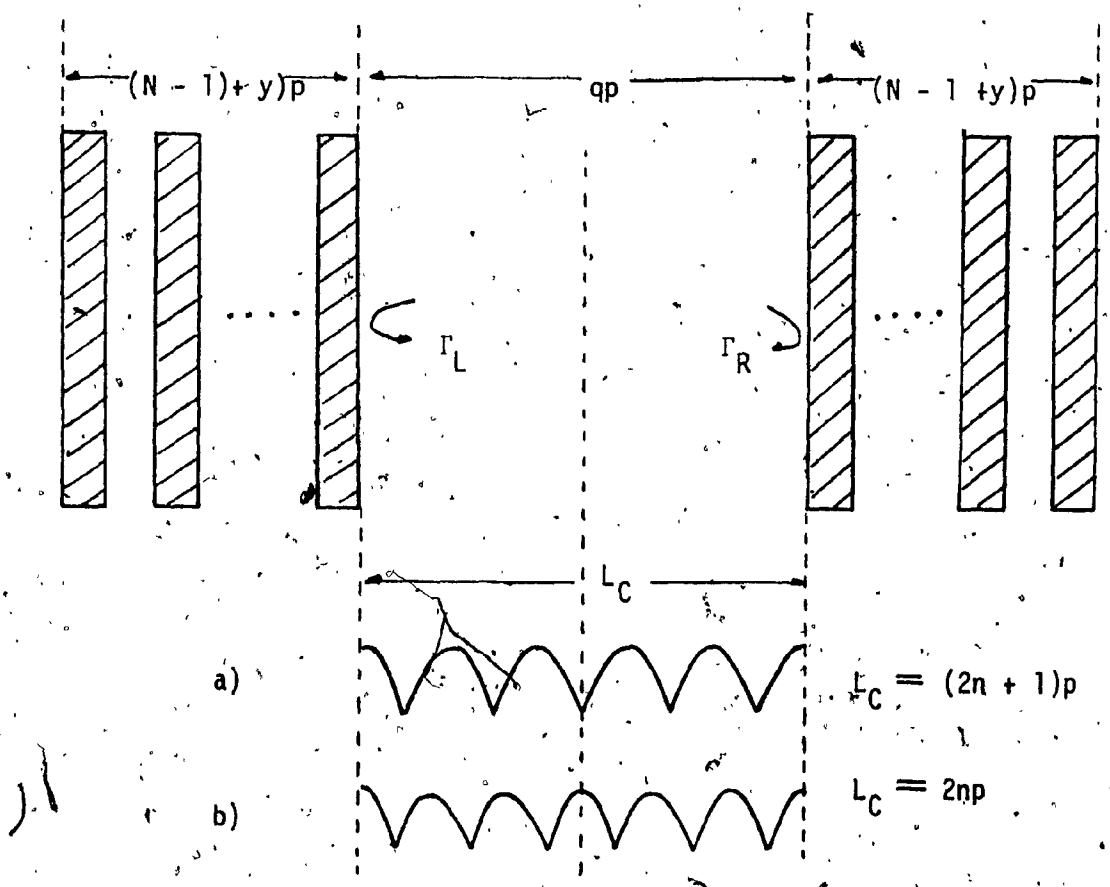

a) Series resonance (odd multiple)

b) Parallel resonance (even multiple)

Fig. 3.16 F - P resonator geometry with reference plane

resonance cavity in which standing wave is minimum at the centerline.

If the reflection coefficient of arrays are written Γ_L and Γ_R shown in Fig. 3.16 for a free resonance to occur in the cavity, Γ_L and Γ_R should satisfy following condition:

$$\Gamma_R \Gamma_L = 1 \qquad (3.6.1.)$$

Recalling $\Gamma_R = \Gamma_L = \rho e^{j\phi}$ given in (3.3.13) above condition can be rewritten by magnitude and phase separately as follows:

$$\left.\begin{aligned} \rho^2 \exp(-2\alpha L_c) &= 1 \\ k_o L_c - \phi &= m\pi \end{aligned}\right\} \qquad (3.6.2.)$$

where $f = f_{FP}$, m : integer number.

They are called gain and phase conditions respectively in Transverse Resonant Condition {31} . Then phase condition above can be used directly for determining cavity resonant frequency f_{FP}.

By assuming f_{FP} is close to f_R and substituting (3.3.16) into (3.6.2). We have

$$f_{FP}/f = \{m + f_R \tanh N\delta /(f\delta)\}\{q + \tanh N\delta /\delta\}^{-1} \qquad (3.6.3.)$$

where $q = L_c/p$. When $f_{FP} = f_R$, the value of cavity length becomes

$$q' = m/(1 - b/\pi) \qquad (3.6.4.)$$

Conversely when condition (3.6.4.) is met f_{FP} coincides with f_R. This requirement is necessary for obtaining high Q resonator characteristics. Therefore the increased length of resonator q' is called

"optimized resonator length".

If the cavity length is not optimized, then

$$f_{FP}/f_R = 1 + mb/\pi\{\tanh N\delta/\delta + m\}^{-1} \qquad (3.6.5.)$$

indicating that the cavity resonance frequency is located above the grating resonance frequency.

A deviation in relative cavity length from the q' given in (3.6.4.) to q causes a fractional shift in the resonance frequency:

$$(f_{FP} - f_R)/f_R = (1 - q'/q)\{1 + \tanh N\delta/(\delta q)\}^{-1} \qquad (3.6.6.)$$

The spacing between consecutive resonance. The socalled free spectral range is

$$\Delta f_{FP}/f_o = (L_C/p + \tanh N\delta/\delta)^{-1} \qquad (3.6.7.)$$

At resonance the second term of the denominator (3.6.7.) can be recognized as the relative penetration depth c_R. Therefore free spectral range is

$$\Delta f_{FP} = f_o/(q + c_R) = 2pf_o/(2L_C + 2c_R) = v_o/2\ell \qquad (3.6.8.)$$

where v_o : velocity of SAW

ℓ : $L_C + c_R$: virtual length of resonator

$2p$: λ

which is identical form of typical definition of Δf_{FP} given in equation (4.1.10.) { 32 }.

Next let us consider the transmission characteristics of the entire F-P resonator in which IDT's are placed externally to the

cavity shown in Fig. 3.17.b. Provided that an array is matched to the characteristic impedance Z_o at the input and output ports S matrix of an array is

$$S_A = \begin{bmatrix} \Gamma_A & T_A \\ T_A & \Gamma_A \end{bmatrix} \qquad (3.6.8.)$$

where $\Gamma_A = \rho e^{j\phi}$: reflection coefficient of an array

$T_A = te^{j(\phi + \pi/2)}$: transmission coefficient of an array

and A matrix is

$$A_A = T_A^{-1} \begin{bmatrix} 1 & -\Gamma_A \\ \Gamma_A & e^{2j\phi} \end{bmatrix} \qquad (3.6.9.)$$

where last element of A_A is obtained from the lossless and reciprocal condition of scattering matrix.

Therefore the entire resonator A matrix (A_R) can be obtained by cascading two A matrices of the grating array with simple transmission line A matrix;

$$A_R = \begin{bmatrix} A_{R11} & A_{R12} \\ A_{R21} & A_{R22} \end{bmatrix} = T_A^{-2} \begin{bmatrix} e^{j\theta} - \Gamma_A^2 e^{-j\theta} & -\Gamma_A e^{j\theta} + \Gamma_A e^{-j(\theta - 2\phi)} \\ \Gamma_A e^{j\theta} - \Gamma_A e^{-j(\theta - 2\phi)} & -\Gamma_A^2 e^{j\theta} + e^{-j(\theta - 4\phi)} \end{bmatrix} \qquad (3.6.10.)$$

$$S_R = \begin{bmatrix} S_{R11} & S_{R12} \\ S_{R21} & S_{R22} \end{bmatrix} = (e^{-j\theta} - T_A^2 e^{j\theta})^{-1} \begin{bmatrix} \Gamma_A\{e^{j\theta} - e^{-j(\theta - 2\phi)}\} & T_A^2 \\ T_A^2 & \Gamma_A\{e^{j\theta} - e^{-j(\theta - 2\phi)}\} \end{bmatrix} \qquad (3.6.11)$$

N_T : Number of fingers in the transducer

$\vec{y}$: input admittance at the center of IDT by looking to one array

C_o : Static capacitante between IDT fingers

Since the standing wave maxima in Fig. 3.16 represent the location of peak SAW electric potential, effective coupling between transducer and F-P cavity requires the transducer fingers to line up with the standing wave maxima at resonance. Therefore the length ℓ which is the distance between the center of IDT and the center of the cavity should be properly determined.

As an example let us consider the F-P resonator with IDTs located inside between arrays shown in Fig. 3.17.c. If N_T is odd and the cavity is parallel resonant circuit (q is even) shown in Fig. 3.20 the length of ℓ should be even integral number of p for strong coupling. By employing the normalized offset parameter $r = 2\ell/p$ {17} and the optimization length given in 3.6.4. we have following pair of parities for maximum coupling between input and output ports when q : even, N_T : odd. Then

$$r : \text{even} \longrightarrow r' = r/(1 - b/\pi) \qquad (3.6.20.)$$

From the Fig. 3.20

$$L_\ell = \tfrac{1}{2}(q - r)p \longrightarrow L'_\ell = \tfrac{1}{2}(q' - r')p \qquad (3.6.21.)$$

where "primed" notation stands for optimized values.

The other several combinations of parities for the maximum

coupling of IDT and resonator are tabulated in several papers{ 16, 17 }. Note that parity set of m { 17 }is different from our case because of different definition of the array length.

Once the position of IDT is determined according to parities of q, N_T, the calculation of the transfer matrix Q_{R-T} of the entire IDT - Resonator combination is straight forward and results in

$$Q_{R\,T} = Q_T Q_r \tilde{Q}_T \qquad (3.6.22.)$$

where Q_T : Q matrix of IDT-Array combination

Q_r : Q matrix of the space between centers of IDT

$$= \begin{bmatrix} \cos\theta & j\sin\theta \\ j\sin\theta & \cos\theta \end{bmatrix}, \quad \theta = k_0 pr' = F\pi r'.$$

After multiplication we have

$$Q_{R\,T} = \begin{bmatrix} Q_{11} & Q_{12} \\ Q_{21} & Q_{22} \end{bmatrix} \qquad (3.6.23.)$$

where

$$Q_{11} = -\cos\theta\{1 + j2\overset{+}{y}\tau/b_T^2\} - j\sin\theta\{\overset{+}{y} + j\tau(1 + \overset{+}{y}^2)/b_T^2\}$$

$$Q_{12} = -\cos\theta\{2\overset{+}{y}/b_T^2\} - j\sin\theta\{(1 + \overset{+}{y})^2/b_T^2\}$$

$$Q_{21} = -\cos\theta\{-2\tau^2\overset{+}{y}/b_T^2 + j2\tau\} - j\sin\theta\{b_T^2 + j2\tau\overset{+}{y} - \tau^2(1 + \overset{+}{y}^2)/b_T^2\}$$

$$Q_{22} = Q_{11}$$

And S matrix is

$$S = \frac{1}{DEN}\begin{bmatrix} S'_{11} & 2 \\ 2 & S'_{22} \end{bmatrix} \qquad (3.6.24.)$$

where

$$DEN = -\cos\theta 2(x^2 + \overleftarrow{y}x^2/b_T^2) - j\sin\theta\{2\overleftarrow{y}x + b_T^2 + (1 + \overleftarrow{y}^2)x^2/b_T^2\}$$

$$S'_{11} = S'_{22} = -\cos\theta 2\{\overleftarrow{y}(1+\tau^2)/b_T^2 - j\tau\} - j\sin\theta\{(1+\overleftarrow{y}^2)(1+\tau^2)/b_T^2 - b_T^2 - 2j\tau\overleftarrow{y}\}$$

and $x = 1 + j\tau$.

Therefore insertion loss of the resonator with transducer pair is

$$T = S_{21} = 2/DEN = [-\cos\theta(x^2 + \overleftarrow{y}x^2/b_T^2) - j\sin\theta\{\overleftarrow{y}x + b_T^2/2 + (1+\overleftarrow{y})x^2/2b_T^2\}]^{-1} \qquad (3.6.25.)$$

If $\tau = 0$ ($C_T = 0$) and $\theta = (2n+1)\pi$ S matrix reduces to

$$S = (1 + \overleftarrow{y}/b_T^2)^{-1}\begin{bmatrix} \overleftarrow{y}/b_T^2 & 1 \\ 1 & \overleftarrow{y}/b_T^2 \end{bmatrix} \qquad (3.6.26.)$$

and

$$A = \begin{bmatrix} 1 + \overleftarrow{y}/b_T^2 & -\overleftarrow{y}/b_T^2 \\ \overleftarrow{y}/b_T^2 & 1 - \overleftarrow{y}/b_T^2 \end{bmatrix} \qquad (3.6.27.)$$

which is identical form to (4.4.6.)[17].

Turning to filter with a grating coupler shown in Fig. 3.19.b, the length between center of IDT and the edge of the grating coupler should be $\theta = n\pi$ $n = 1, 2, \ldots$ for maximum coupling.

Therefore if grating coupler is assumed to be identical to the resonator gratings the overall Q matrix Q_{RT} for grating coupled filter can be obtained directly as

$$Q_{RT} = Q_T Q_S Q_A Q_S \tilde{Q}_T \qquad (3.6.28.)$$

where Q_T : Q matrix of IDT - grating combination.

Q_A : Q matrix of grating coupler.

Q_S : Q matrix of transmission line with length θ.

$\tilde{Q}_T$: Q_T^{-1}

If θ is chosen for maximum coupling (3.6.28.) reduces to the following simple form

$$Q_{RT} = Q_T Q_A \tilde{Q}_T \qquad (3.6.29.)$$

and the insertion loss for the grating filter near the Bragg frequency is

$$|S_{RT}|_{21} = |DEN|^{-1} \qquad (3.6.30.)$$

where

$$DEN = -(\xi + b)\sinh(N\alpha p)/\alpha p\{1 + \overleftarrow{y}(1 - \tau^2)/b_T^2 + j\tau(1 + 2\overleftarrow{y}/b_T^2)\}$$

$$+ \cosh N\alpha p\{-\tau(\overleftarrow{y} + (\overleftarrow{y}^2 - 1)/b_T^2) + j(\overleftarrow{y} + \tfrac{1}{2}(\overleftarrow{y}^2 + 1)(1 - \tau^2)/b_T^2)\}$$

$$+ \delta\sin(N\alpha p)/\alpha p\{-\tau(\overleftarrow{y} + (\overleftarrow{y}^2 - 1)/b_T^2) + j(\overleftarrow{y} + \tfrac{1}{2}(\overleftarrow{y} - 1)(1 - \tau^2)/b_T^2)\}.$$

The complete insertion loss spectrum for resonator filters given in (3.6.25.) and (3.6.30.) are shown in Fig. 3.21. The parameters including b_T and τ to obtain their figures are given in Table 3.2. The position of IDT are properly chosen to obtain optimized filter

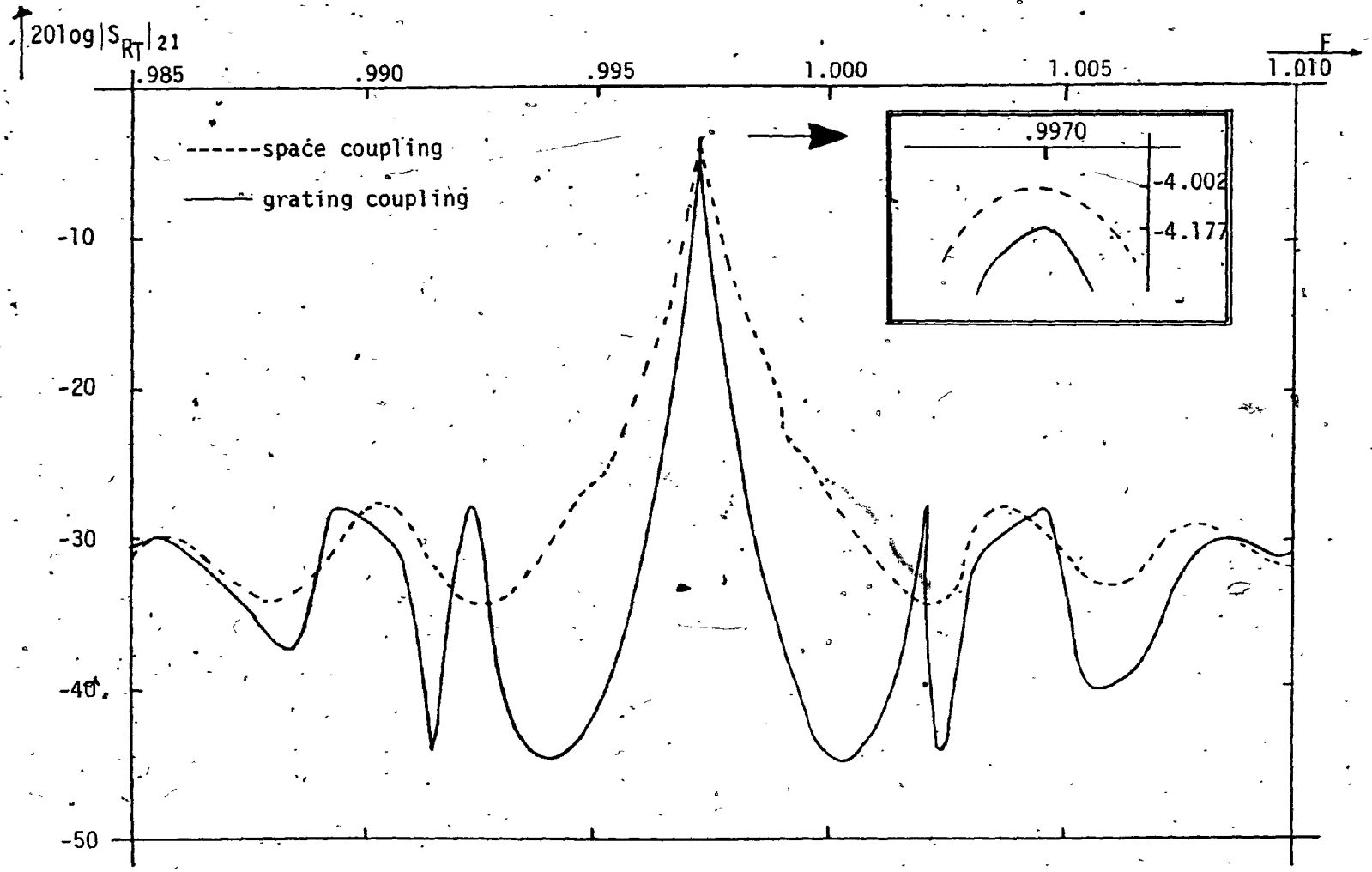

Fig. 3.21 Insertion loss characteristics of space and grating coupler resonator filters

characteristics.

Recently Cross and Schmidt have reported similar analysis on the periodic grooved resonator and filters {34} . Although our method of analysis is different from that employed in their analysis insertion loss characteristics of (3.6.25,) are found to be virtually identical to theirs. This figure shows that the optimized resonator length and the position of IDT's are chosen properly indicating that all the cardinal frequencies (grating, resonator and filter resonant frequencies) are coincided at the same frequency F_R.

CHAPTER IV

SAW PROPAGATION IN NONUNIFORM GRATINGS

4.1 Introduction

The reflection characteristic of uniformly distributed array and SAW Fabry-Perot resonator transmission characteristic which are constructed with the arrays are studied in the last chapter. Uniform grating have fixed transmission and reflection characteristics determined by the depth, the periocity and the internal structure of the unit cell.

By introducing additional nonuniformity in the grating the above characteristics can be improved or modified with respect to sidelobe suppression, roll-off and phase or time delay.

There are three types of nonuniformities considered in this chapter. That which affects the periodicity (p-chirping) will reduce the maximum obtainable reflection coefficient and generally broaden the stopband. Nonuniformity of the aspect ratio (y-chirping) has little effect on the maximal reflection coefficient and can either broaden or reduce the bandwidth. Finally a nonuniform coupling coefficient (tapering) can effectively reduce the sidelobes of the array characteristics.

By applying these uniformities in combination a wide variety of transmission and delay characteristics can be obtained.

The nonuniformities of the structure are represented by some perturvation in the coupling strength which can be called "tapering" and small variation of periedicity or aspect ratio which can be referred "chirping". Therefore some terminology and definition needed to the nonuniformity of our array are in order.

In the grooved structure, the unit cell is characterized by three geometric parameters; the groove depth (h), the period (p) and the aspect ratio (y). On nonuniform gratings these are functions of the axial coordinate z. Typical nonuniformities are shown in Fig. 4.1.

One must bear in mind that the nature of the SAW grating and its ultimate application in a filter structure limits the extent of the allowed uniformity to relatively small perturbations along the array. Since strong reflection at a given frequency is caused by uniform periodicity, narrow band devices tolerate only a small perturbation.

The origin of the coordinate system is taken to coincide with the edge of the first groove. Sometimes it is advantageous to use normalized length coordinate $z_i = z/L$ instead of z itself.

The three types of nonuniformities considered are

$$\left.\begin{aligned} &\text{a)}\ h(z_i) = h\, f(z_i) \\ &\text{b)}\ p(z_i) = p\, g(z_i) \\ &\text{c)}\ y(z_i) = y\, t(z_i) \end{aligned}\right\} \qquad (4.1.1)$$

h, p are constants with a dimension of length and y is a dimensionless constant. f(z) is the taperfunction and g(z), t(z) are chirping functions.

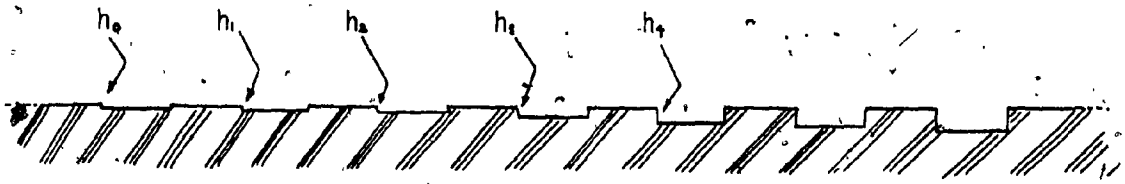

$h_i = haz_i$ p,y : constant

a) Tapered grooves (nonuniform groove depth)

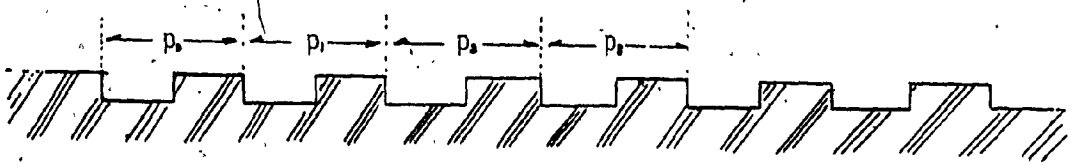

$P_i = P(1 + bz_i)$ $b \ll 1$, h, y : constant

b) p-chirped grooves (nonuniform periodicity)

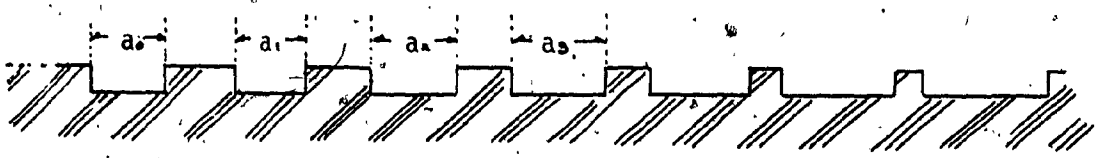

$Y_i = Y(1 + cz_i)$ p, h : constant

c) y-chirped grooves (nonuniform aspect ratio)

Fig. 4 . 1 Linearly varying nonuniform groove structures.

One must note that (4.1.1) represent discrete functions, i.e. for a tapered grating the groove depth of the i-th groove is $h_i = h\ f_i$

$i = 1,2....N.$

The relationship between the elements of the R matrix introduced in Section 2.1 and the tapering and chirping functions can easily be obtained from a discretized version of (2.1.7). To this end one introduces the transfer matrix of the grating which extends from $z = 0$ to $z = z_i$

$$\bar{u}(z_i) = M(z_i)\ \bar{u}(o) \qquad (4.1.2)$$

where $\bar{u}^T(z_i) = \{a(z_i), b(z_i)\}$ as indicated on Fig. 4.2.

In order to relate $M(z_i)$ and system matrix R assume discrete transfer matrix $M(z_i)$ are known in the coupling region $0 \le z_i \le 1$. In discrete form (2.1.7) can be written as a difference equations expressing the transfer characteristics of the i-th unit cell.

Thus $$\{\bar{u}(z_{i+1}) - \bar{u}(z_i)\}/p_i = -jR_i\bar{u}(z_i) \qquad (4.1.3)$$

where $p_i = z_{i+1} - z_i$.

Note that Equation (4.1.3) redefines the R matrix to express the properties (propagation constants and coupling coefficients) of the i-th unit cell as if it were a short uniform backward wave coupler.

By substituting (4.1.2) into (4.1.3) we get

$$\{(M(z_{i+1}) - M(z_i))/p_i + jRM(z_i)\}\bar{u}(0) = 0 \qquad (4.1.4)$$

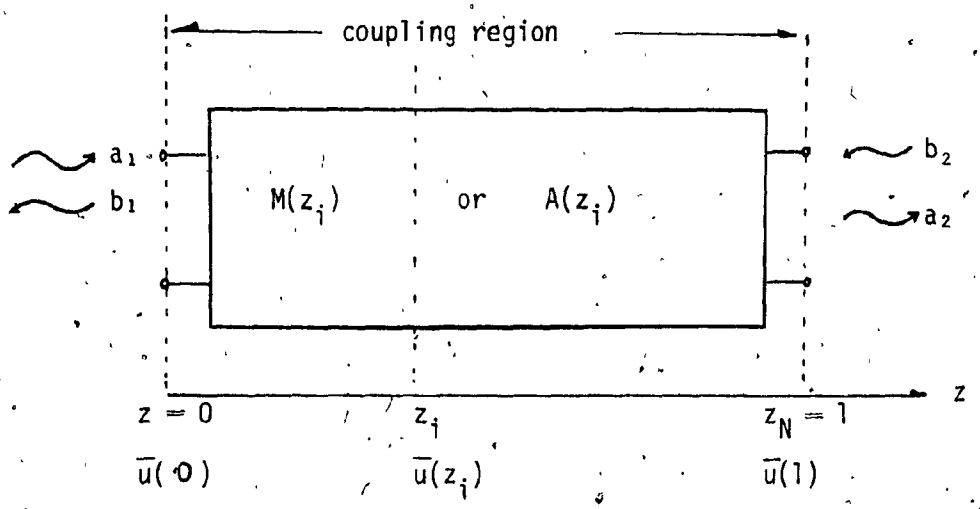

$0 \le z_i \le 1 \qquad i = 1, 2, 3, \ldots\ldots\ldots\ldots N$

$$\left.\begin{aligned} \bar{u}(z_i) &= M(z_i)\bar{u}(0) \\ \bar{u}(0) &= A(z_i)\bar{u}(z_i) \end{aligned}\right\} \qquad M(z_i) = A^{-1}(z_i)$$

The difference equation for coupled groove structure is

$$\{\bar{u}(z_{i+1}) - \bar{u}(z_i)\}/p_i = -jR\bar{u}(z_i)$$

Fig. 4.2 Schematic Diagram for descrete coupling structure.

Since this expression can not depend on the excitation $\bar{u}(0)$, therefore

$$\{M(z_{i+1}) - M(z_i)\}/p_i + jRM(z_i) = 0 \qquad (4.1.5)$$

After substituting $A(z_i)$ for $M(z_i)$ and simplification, we find that

$$R_i = j(A_i^{-1} - I)/p_i \qquad (4.1.6)$$

where A_i is A matrix of the i-th unit cell for our groove structure and I is unit matrix. Substitution of the elements of A_i given in (3.2.4) results in the R_i matrix elements

$$\begin{aligned}
R_{11} &= p^{-1}\{(b\cos\theta_M + Z_+\sin\theta_M)e^{-j\theta}S + j((\cos\theta_M b\bar{z}\sin\theta_M)e^{-j\theta}S - 1)\} \\
R_{12} &= -p^{-1}\, e^{j\theta}S\,(b\cos\theta_M - Z_-\sin\theta_M) \\
R_{21} &= p^{-1}\, e^{-j\theta}S(b\cos\theta_M - Z_-\sin\theta_M) \\
R_{22} &= p^{-1}\{-(b\cos\theta_M + Z_+\sin\theta_M)e^{j\theta}S + j((\cos\theta_M - b\bar{z}\sin\theta_M)e^{j\theta}S - 1)\}
\end{aligned} \qquad (4.1.7)$$

and the subscript i has been dropped for sake of brevity.

In a lossless and reciprocal system the elements of R_i satisfy the following general backward discrete coupling conditions

$$\begin{aligned}
R_{11_i} &= -R_{22_i} \\
R_{12_i} &= -R_{21_i}^*
\end{aligned} \qquad (4.1.8)$$

The first of these is noble, arising from the discrete definition of R_i given (4.1.3)

Note that for a continuous contradirectional coupler R_{11} and R_{22} are both real. In the $p_i \to 0$ limit the diagonal elements of our discrete R_i matrix satisfy this condition. The second condition of

(4.1.8) is in accordance with the requirement of energy conservation in a contradirectional coupler.

Coupling coefficient R_{12} is generally complex quantity such as $R_{12} = \kappa e^{j\phi}$. Therefore magnitude κ and phase ϕ are related to system parameters $\bar{z}$, b, θ_M and θ_S as follows

$$\kappa = (-\bar{Z}\sin\theta_M + b\cos\theta_M)/p_i$$
$$\phi = \theta_S + \pi \tag{4.1.9}$$

Neglecting second order quantities such as δ_z^2, $b\delta_z$ one has

$$\kappa = C_1(h/p\lambda)\sin(\pi Fy) - C_2(h/\lambda p)^2\cos(\pi Fy)$$
$$\phi = \pi F(1 - y) + \pi \tag{4.1.10}$$

Grating reflectors operate near the Bragg frequency. Hence F = 1. With this approximation and assuming y = 0.5

$$\kappa = C_1(h/p\lambda)$$
$$\phi = 3\pi/2 \tag{4.1.11}$$

Therefore it can be concluded that the magnitude of coupling coefficient depends on h, p, and y and phase ϕ depends on y only from (4.1.9).

If a bilaterally symmetric unit cell is chosen{17} , $\phi = 0$ and the coupling coefficient is real. From (4.1.9) it can be seen that for constant h, p and y, κ and ϕ are constants. For tapered

and/or chirped gratings κ and ϕ depend on the axial coordinate.

This chapter starts with the analysis of the perturbation effects for the grating by employing harmonic and linear functions for the grating perturbation. And the conclusion of this analysis necessitates a different approach to formulate the perturbation function for obtaining improved frequency response of the grating.

Section 4.3. deals with a general theory of the tapered transmission line which includes Chebyshev taper characteristics and the inverse transform of the optimized reflection coefficient.

Based on this general theory the optimization process for the tapered grating is followed in section 4.4. The formal equivalence between tapered transmission line and the tapered gratings is shown and the relation of discrete coupling constant κ and system perturbation parameter is obtained.

In the last section the optimumly tapered gratings are employed to form a F-P resonator, with and without interdigital transducer and grating filters. The insertionloss characteristics of them are shown and several numerical results are compared with those of constant grating filter.

4.2 Transmission Properties of Weakly Modulated Periodic Gratings

In the practical design process of the groove structure it is important to determine the tolerance limits for the system parameters, i.e. groove depth h, period p and aspect ratio y.

Therefore we shall consider two types of perturbations harmonic and linear. In the former case the perturbed parameter $S_i(z)$ which can stand for any one of the three geometric parameters p, h or y is assumed be of the form

$$S(z_i) = 1 + a \sin(\omega z_i + \phi) \qquad (4.2.1)$$

whereas in latter case

$$S(z) = 1 + a'(z_i - 0.5) \qquad (4.2.2).$$

Due to weakness of the perturbation considered, constants in (4.2.1), (4.2.2) are chosen relatively small values, such as 0.05. For convenience sake, ω and ϕ in (4.2.1) are chosen as $\omega = 5\pi$ and $\phi = 0$. The full array length experiences five periodic perturbation in the former case.

Some useful quantities which characterize the frequency response when the perturbation is small are summarized in Table 4.1.

In order to compare the frequency response new quantities are defined as follows

* ρ_{max} : Maximum reflection coefficient at resonance.
* ρ_s : Maximum reflection coefficient at the first sidelobe
* ΔF : $|F(\text{at } \rho = 0.9\rho_{max}) - F(\text{at } \rho = 0.1\rho_{max})|$

* BW : 3dB bandwidth
* DF : $\Delta F/BW$
* R_s : ρ_s/ρ_{max}

where DF and R_s are the dimensionless quantities which are measure of the roll-off slope of the reflection coefficient Γ at edge of the mainlobe and sidelobe suppression respectively. The last term of left column c_R is the relative penetration depth at resonance.

The first noticiable fact from the Table 4.1 is that reflection characteristics are immune to the small perturbations with h and/or y. But even 5% periodic perturbation (p) changes ρ considerably.

From the Table 4.1 several comments are in order as follows:

(1) Resonance frequency

The resonant frequency is invariant to the small perturbation of h, p or y even to 10% harmonic perturbations

(2) ρ_{max} and bandwidth

The variation of p or y reduces ρ_{max} almost proportionally to the degree of perturbation while the variation of h makes ρ_{max} to be almost invariant. Note that even 5% perturbation of p changes ρ_{max} to the extent of losing the meaning of reflector. 10% y perturbation cause a small reduction of the bandwidth also.

The sensitivity of the reflection coifficient to the perturbation of the variables h, p and y is of practical interest for design and manufacturing SAW devices and they are fully discussed in the previous paper { 17 }.

	Constant (h, p, y)	h	p	y
F_R	0.9970 0.9970	0.9970 0.9970	0.9970 -	0.9970 -
ρ_{max}	0.9640	0.9640 0.9640	0.4323 0.6622	0.9636 0.9432
BW	0.0080	0.0080 0.0080	0.0050 0.0055	0.0080 0.0072
ΔF	0.0022	0.0022 0.0022	0.0030 0.0032	0.0022 0.0027
DF	0.2750	0.2750 0.2750	0.6000 0.5818	0.2750 0.3750
ρ_s	0.3938	0.3935 0.3933	0.1182 0.1590	0.3840 0.3161
R_s	0.4084	0.4081 0.4080	0.2734 0.2402	0.3985 0.3553
c_R	96	95 94	182 166	95 99

Table 4.1 The effect of the perturbation of grating parameters h, p and y. In the constant grating $h/\lambda=0.015$, $y = 0.5$. Top figure and bottom figure represent 5%, 10% perturbation according to equation (4. 2. 1.) respectively.

From the Table 4.2{17} $d\rho/dy$ at resonance is obtained as 0.415. Note that independent variable y is constant y in our case. Therefore 10% perturbation of y causes the change of ρ_{max} by 0.0415 while our axial coordinate harmonic perturbation of the same amount causes a reduction of ρ_{max} by 0.0208. In other words 10% axial y chirping of grating is equivalent to 5% change of constant aspect ratio y. Since the charge of ρ_{max} with respect to y is not linear as shown in Table 4.2{17} the effect of y chirping in our case is more smaller than that of constant y variation.

3) Roll-off slope and penetration depth

p or y varations generally degrade the roll-off slope sharpness which is almost invariant in case of h perturbation. Note that even 5% perturbation of p deteriates role-off slope considerably. A slight decrease of the penetration depth with h variation indicates some possibilities to improve frequency response by changing h.

From above discussion the following conclusion can be derived. Firstly the general feature of reflection coefficient is invarient to maximum 5% perturbation in p and y while p variation by same amount degrades the performance of ρ_{max} severely indicating that the period length is the most critical geometric parameter in high performance grooved gratings. Even 10% harmonic h perturbation can be tolerable perturbation for a given specifications of gratings.

Secondly the increase of y perturbation up to 10% degrades the general performance of gratings except sidelobe suppression aspect (R_s). But it can be understood that roll-off slope and sidelobe suppression are two contrary requirement which are properly chosen by trade off. Numerical results when the perturbation is increased beyond 10% have shown that even h perturbation degrades reflection performance severely.

A good band rejection filter is characterized by low sidelobe levels and sharp roll-off slope. In this sense it was found that the other trial tapering and chirping functions i.e. quadratic, linear, and polynormial form, or the combination of them do not meet above criteria.

Therefore in order to design improved band rejection filter by employing nonuniform grating, we have to resort to different approach for this requirement. Before going into the problem directly we need some knowledge of the tapered transmission line characteristics which is treated in the following section.

4.3 Review of the Theory of the General Nonuniform Transmission Line

Consider the impedance matching transformer consisting of n quarterwave sections depicted in Fig. 4.3.a. Assuming symmetrical construction ($\rho_0 = \rho_N$, $\rho_1 = \rho_{N-1}$, etc.) and small reflections at discontinuities, the total reflection coefficient referred at the input port is

$$\Gamma = \rho_0 + \rho_1 e^{-j2\theta} + \rho_2 e^{-j4\theta} + \ldots + \rho_N e^{-j2N\theta}$$

$$= 2e^{-JN\theta}\{\rho_0 \cos N\theta + \rho_1 \cos(N-1)\theta + \ldots \rho_{N/2}\} \quad (4.3.1)$$

where θ is electrical length of each section and local reflection coefficient $\rho_i = (Z_{i+1} - Z_i)(Z_{i+1} + Z_i)^{-1}$. At center frequency $\theta = \pi/2$.

There are two classical methods to optimize the ρ_i parameters. The binomial method ensures the smoothest possible $\Gamma = \Gamma(\theta)$ function centered at $\theta = \pi/2$, whereas the Chebyshev method results in constant ripple $\Gamma = \Gamma(\theta)$ function and minimum sidelobe levels. The advantage of the former is the smoothness of the Γ function whereas the latter provides steeper skirt characteristics and usually requires less sections to satisfy a given specification in the passband.

In what follows we shall restrict our attention to the Chebyshev case where summation of the cosine series with appropriately chosen ρ_i coefficients results in the expression [35]

$$\Gamma = e^{-jN\theta}\{(Z_L - Z_C)T_N(\sec\theta_m \cos\theta)\}\{(Z_L + Z_C)T_N(\sec\theta_m)\}^{-1} \quad (4.3.2)$$

for the input reflection coefficient of the impedance transformer.

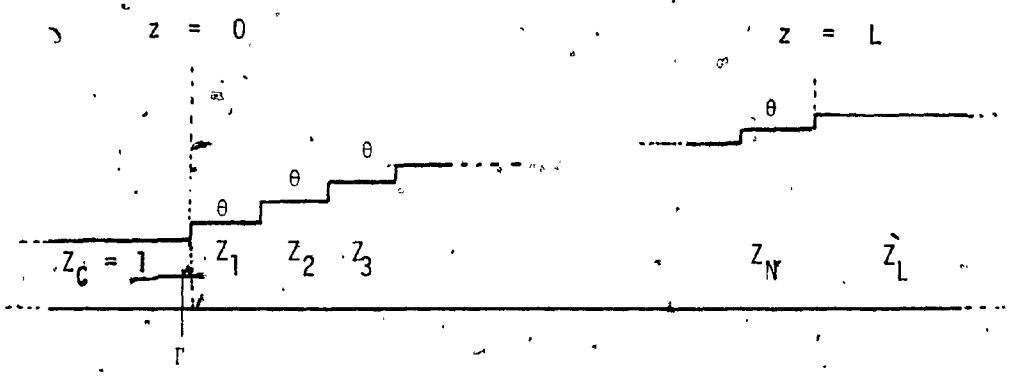

$$\rho_i = (Z_{i+1} - Z_i)/(Z_{i+1} + Z_i)$$

$$\Gamma = \sum_k \rho_k e^{-j2k\theta}$$

a) A multisection quarterwave transformer

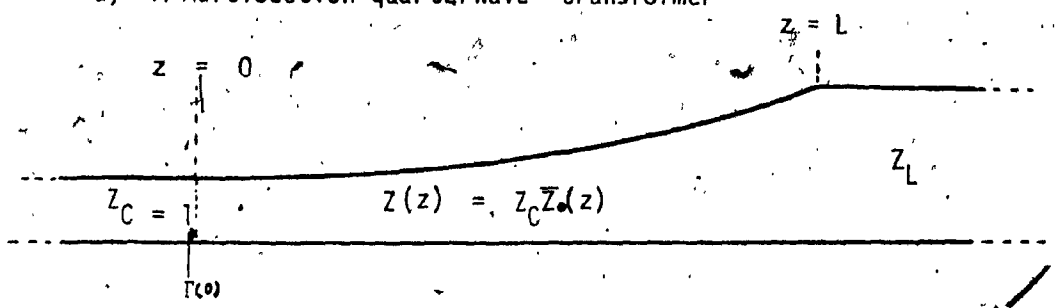

$$d\rho(z) = \{\bar{Z}_o(z + dz) - \bar{Z}_o(z)\}\{\bar{Z}_o(z + dz) + \bar{Z}_o(z)\}^{-1}$$

$$= d\bar{Z}_o(z)/\{2\bar{Z}_o(z)\} = 1/2\, d\{\ln \bar{Z}_o(z)\}$$

$$= d(\ln \bar{Z}_o)dz/2dz$$

$$\Gamma(0) = \frac{1}{2}\int_0^L \frac{d(\ln \bar{Z}_o)}{dz} e^{-j2\beta z} dz$$

b) A tapered transmission line

Fig. 4.3. Reflection coefficients of a quarter wave and tapered line.

In (4.3.2) T_N is the Chebyshev polynomial of the first kind of order N and θ_m is the electrical length of one section at the edge of the passband.

The local reflection coefficients ρ_i are determined by comparing (4.4.1) and (4.4.2). The maximum tolerable reflection at the passband edge is ρ_m as

$$\rho_m = (Z_L - Z_C)(Z_L + Z_C)^{-1} T_N(\sec\theta_m)^{-1} \qquad (4.3.3)$$

If the small reflection assumption is not applicable one can specify that the power reflection be a Chebyshev function. Such a requirement is expressed by

$$P_L = 1 + \{(Z_L - 1)^2 T_N(\sec\theta_m \cos\theta)\}\{4Z_L T_N^2(\sec\theta_m)\}^{-1} \qquad (4.3.4)$$

where the relationship between P_L and Γ is expressed by

$$1 - |\Gamma|^2 = 1/P_L \qquad (4.3.5)$$

and results in

$$\Gamma = e^{-jN\theta} k T_N(\sec\theta_m \cos\theta)\{1 + k^2 T_N^2(\sec\theta_m \cos\theta)\}^{-\frac{1}{2}} \qquad (4.3.6)$$

where $$k = (Z_L - 1)\{2Z_L^{\frac{1}{2}} T_N(\sec\theta_m)\}^{-1}$$

which is passband tolerance on power ratio. The relation of ρ_m and is given by

$$\rho_m = \{k^2/(1 + k^2)\}^{\frac{1}{2}}. \qquad (4.3.7)$$

It is apparent that when the reflection coefficient is small compared

to unify $1/(1 - |\Gamma|^2) \simeq 1 + |\Gamma|$ indicating the validity of (4.3.2).

This Chebyshev n section transformer is usually referred to as optimally designed filter because it produces the smallest side-lobes and because of the property that, for a given passband tolerance maximum tolerated reflection coefficient, the passband is of maximum width, or conversely for a given bandwidth, the passband tolerance is minimum.

The n section transformers described so far make use of discrete discontinuities separated by $\lambda/4$ at the design or center frequency and provides us with a bandpass response. If the total length L of the transformer is kept constant while the number of section is increased each section will reduce in length and in the limit as n approaches infinity, the multisection transformer becomes a tapered transmission line as shown in Fig. (4.3.b).

As n increases the effective section length θ is reduced, the center frequency is increased and the passband is extended. In the limit as $n \to \infty$ the center of the passband increases unbounded and the transformer becomes a highpass filter [36]. In this limit (4.4.2) becomes

$$\Gamma = e^{-j\beta L} k \cos\{L(\beta^2 - \beta_o^2)^{\frac{1}{2}}\} \qquad (4.3.8)$$

where as (4.4.6) reduces to

$$\Gamma = \{e^{-j\beta L} k \cos(L(\beta^2 - \beta_o^2)^{\frac{1}{2}})\}\{1 + k^2 \cos^2(L(\beta^2 - \beta_o^2)^{\frac{1}{2}})\}^{-\frac{1}{2}} \qquad (4.3.9)$$

where $k = (Z_L - 1)\{2Z_L^{\frac{1}{2}}\cosh(\beta_o L)\}^{-1}$ and β_o is the phase constant at the transition frequency.

The nonuniform characteristic impedance of the tapered transmission line obtaines from the system equations

$$\begin{aligned} dV/dz &= -Z(z)I \\ dI/dz &= -Y(z)V \end{aligned} \qquad (4.3.10)$$

where V(z), I(z) are the voltage and current variables, Z(z), Y(z) are the series impedance and the shunt admittance per unit line respectively. Introducing the complex wavenumber and the characteristic impedance functions

$$\begin{aligned} \gamma(z) &= (ZY)^{\frac{1}{2}} \\ \overline{Z}_o(z) &= (Z/Y)^{\frac{1}{2}} \end{aligned}$$

and the local reflection coefficient $\Gamma(z) = (V/I - \overline{Z}_o)(V/I + \overline{Z}_o)^{-1}$ (4.4.7) can be recast into the first order Riccati differential equation { 37 }

$$d\Gamma/dz - 2\gamma\Gamma + \tfrac{1}{2}(1 - \Gamma^2)d(\ln\overline{Z}_o)/dz = 0 \qquad (4.3.11)$$

Let us assume lossless conditions and $|\Gamma|^2 << 1$. Then (4.3.11) becomes

$$d\Gamma/dz - 2j\beta\Gamma = -F(z) \qquad (4.3.12)$$

where $\gamma = j\beta$ and $F(z) = \tfrac{1}{2}d\{\ln\overline{Z}_o(z)\}/dz$. The general solution of

(4.3.12) satisfying the boundary condition $\Gamma(z=L) = 0$ is

$$\Gamma(z) = \int_z^L F(x)\exp\{-2j\int_z^x \beta(\xi)d\xi\}dx \qquad (4.3.13)$$

So that the input reflection coefficient becomes

$$\Gamma(0) = \int_0^L F(x)\exp\{-2j\int_0^x \beta(\xi)d\xi\}dx \qquad (4.3.14)$$

If β is assumed to depend only on the frequency but not on the axial coordinate z, then the interior integration of (4.3.14) is easily resolved and the imput reflection coefficient becomes

$$\Gamma(0) = \int_0^L F(z)\exp(-2j\beta z)dz \qquad (4.3.15)$$

This integral form can be identified as the Fourier transform of F(z){38 }.

Equation (4.3.15) can also be justified by considering an impedance step $d\bar{Z}_o$ at z in Fig.(4.3.a). The differential reflection coefficient produced by this step is

$$d\Gamma(z) = (\bar{Z}_o + d\bar{Z}_o - \bar{Z}_o)/(\bar{Z}_o + d\bar{Z}_o + \bar{Z}_o) \approx \tfrac{1}{2}d\bar{Z}_o/\bar{Z}_o$$

$$= \tfrac{1}{2}d(\ln\bar{Z}_o) = \tfrac{1}{2}\frac{d}{dz}(\ln\bar{Z}_o)dz. \qquad (4.3.16)$$

At the input to the taper this incremental reflection coefficient

$$d\Gamma(0) = e^{-j2\beta z}\tfrac{1}{2}\frac{d}{dz}(\ln Z_o)dz = e^{-j\beta z}F(z)dz \qquad (4.3.17)$$

to the input reflection coefficient. After integration from 0 to L

$$\Gamma(0) = \int_0^L F(z)e^{-j2\beta z}dz$$

which is identical to (4.3.18).

If the limiting form of the input reflection coefficient (4.3.9) is substituted for $\Gamma(0)$, inverse transformation yields {39 }

$$F(z) = \frac{\rho_o}{\cosh A} \frac{A}{L} \frac{I_1\{A(1 - (2z/L - 1))^{\frac{1}{2}}\}}{A\{1 - (2z/L - 1)\}} + \tfrac{1}{2}\{\delta(z/L) + \delta(z/L - 1)\}$$

$$\text{for } 0 \le z \le L \qquad (4.3.18)$$

$$F(z) = 0 \qquad \text{for } z<0,\ L<z.$$

Where I_1 is the modified Bessel function of the first kind, δ is the unit impulse function and $A = \beta_o L$ determineds the maximum magnitude of the reflection coefficient in the passband ($\cosh A = \rho_o / \rho_d$). The first term in (4.3.18) represents the continuous variation of the transformer impedance whereas the impulse functions signify an additional impedance discontinuity of magnitude $\exp\{\rho_o/\cosh A\}$ at each end of the Chebyshev taper.

When A is moderately large and the integral of the first term in (4.3.18) is much larger than unity then the impulse terms can be neglected and

$$F(z) \simeq \frac{\rho_o}{L} \frac{A\, I_1\{A(1 - (2z/L - 1)^2)^{\frac{1}{2}}\}}{\cos(A)\, A\{1 - (2z/L - 1)^2\}^{\frac{1}{2}}} \qquad (4.3.19)$$

This expression will be utilized as a taper function in the next section.

The Riccati differential equation (4.3.11) expresses the functional dependency of the reflection coefficient of a backward coupler and can be obtained directly from the coupled mode equations of this device. Thus, denoting the forward and backward travelling waves by $a_1(z)$ and $a_2(z)$ respectively and the distributed coupling coefficient

by $\kappa(z)$ one has

$$\begin{bmatrix} a_1'(z) \\ a_2'(z) \end{bmatrix} = -j \begin{bmatrix} \beta & \kappa(z) \\ -\kappa(z) & -\beta \end{bmatrix} \cdot \begin{bmatrix} a_1(z) \\ a_2(z) \end{bmatrix} \qquad (4.3.20)$$

Since the reflection coefficient is

$$\rho(z) = ja_2(z)/a_1(z) \qquad (4.3.21)$$

therefore $(\rho/j)' = \{a_2'(z)a_1(z) - a_2(z)a_1'(z)\}/a_1^2(z)$

$$= (\rho/j)d\{\ln(\rho/j)\}/dz \qquad (4.3.22)$$

and by substituting (4.3.20) into (4.3.22) we get

$$\rho'(z) = j2\beta\rho(z) - \kappa(z)(1 - \rho^2(z)) \qquad (4.3.23)$$

which is of the same form as (4.3.11) if one recalls that the coupling coefficient in nonuniform transmission line theory [7] is

$$\kappa(z) = \tfrac{1}{2}d\{\ln(\overline{Z}_o(z))\}/dz \qquad (4.3.24)$$

In ordinary SAW grating couplers κ is a constant, proportional to the relative depth of the grooves. In this case therefore $\overline{Z}_o(z) = Z_C\exp(\kappa z/2)$ is an exponential function.

4.4 Transmission Properties and Characteristics of Optimally Designed Gratings

In the last section it was learned that the inverse transform of the reflection coefficient for the Chebyshev taper is a modified Bessel function, and that the discrete coupling constant κ_i of the gratings given in (4.1.11) is directly related to the inverse transform of the reflection coefficient.

In the previous section it was shown that the periodicity cannot be perturbed significantly without disrupting the desired characteristics of the grating. Consequently a grooved grating incorporating a Chebyshev taper must have a relative groove depth function that is related to the modified Bessel function.

In the optimization process described in this section first those conditions are found which will ensure the input reflection coefficient of the tapered grating to be formally equivalent to that of the Chebyshev transformer, given in equation (4.3.9). These conditions determine the geometric parameters of the i-th unit cell, namely h_i/λ, p_i and y_i.

In this section the following practical assumptions will be made:

(1) Nonuniformities of the transmission line or grating impedance are fractional and therefore the local reflection coefficient is small. Expressed alternatively the taper functions are smooth and gentle. This enables us to use the theory of small reflections.

(2) The relative operating frequency range amounts to a few percent situated near the Bragg frequency.

(3) The geometric perturbation used to fabricate the non-uniform structures is small and consequently powers of second and higher order of the perturbation parameters shall be neglected.

(4) Gratings are envisaged to have a large number of cells; thus justifying an incremental analytic approach, i.e. a transition from discrete to continuous functions.

Referring to Fig. (4.4), for the reflection coefficients of the tapered transmission line (Γ) and the tapered gratings (Γ') one has has

$$\left.\begin{aligned} \Gamma &= \Gamma_0 + \Gamma_1 e^{-j2\theta} + \ldots\ldots + \Gamma_N e^{-j2N\theta} \\ \Gamma' &= \Gamma_0' + \Gamma_1' e^{-j2\theta_1} + \ldots\ldots + \Gamma'_N e^{-j2N\theta_N} \end{aligned}\right\} \qquad (4.4.1)$$

where $\Gamma_i = |\Gamma_i|$, $\Gamma'_i = \rho_i e^{j(\phi_i + \pi/2)}$

and $\theta = kp$, $\theta_i = kp_i + b_i = \pi F_i + b_i$, $F_i = \pi^{-1} kp_i$, $i = 0,1,\ldots\ldots N$.

Our aim is to show the formal equivalence of Γ and Γ' by employing tapering and chirping properly. From the first element of S matrix of the i-th unit cell given in (3.2.4) and by assuming that the unit cell is matched to the characteristic impedance at the output port, we get

$$\Gamma_i' = S_{11_i} = \frac{j(Z_i \sin\theta_{mi} - b_i \cos\theta_{mi})}{(l_i - b_i \bar{z}_i n_i - Z_i \bar{r}_i - b_i m_i) + j(Z_i \bar{n}_i + b_i l_i - b_i \bar{z}_i r_i + m_i)} \qquad (4.4.2)$$

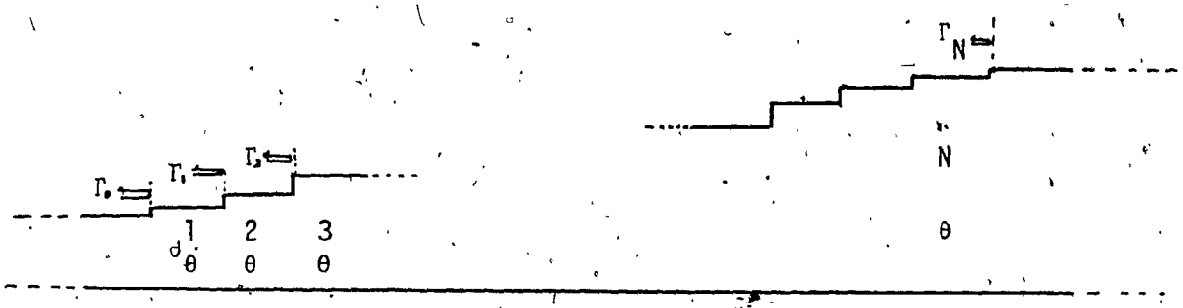

$$\Gamma = \sum_{k=0}^{N} \Gamma_k e^{-2jk\theta}$$

where $\theta = kp$, Γ_k : real

a) N quarter wave transformer

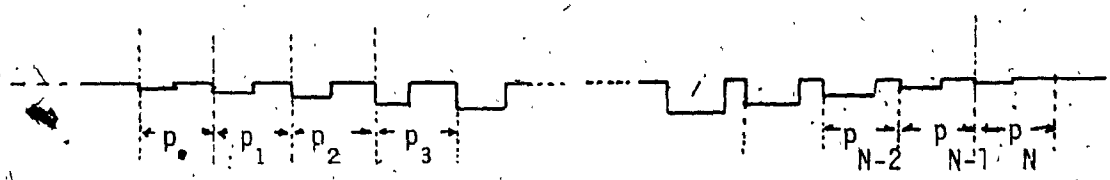

$$\Gamma' = \sum_{k=0}^{N} \Gamma_k' e^{-2jk\theta_k}$$

where $\theta_k = kp_k + b_k$, $\quad \Gamma_k' = |\Gamma_k'| e^{-j\phi_k}$, $\longrightarrow$ $\theta_i = \theta = -\phi_i$

$$\Gamma_i' = S_{11_i} = (A_i + \bar{B}_i - \bar{C}_i - D_i)/(A_i + \bar{B}_i + \bar{C}_i + \bar{D}_i)$$

$$\simeq j(Z_i \pm \sin\theta_i - b\cos\theta_i)e^{-j\theta}$$

b) Tapered grating

Fig. 4.4. Comparison between transmission line and gratings.

Then one obtains

$$\xi_i = -\tan(\pi F_i + b_i) \qquad (4.4.4)$$

Therefore from (4.4.1), (4.4.3) and (4.4.4)

$$-\phi_i = \theta_i = \pi F_i + b_i = kp_i + b_i \qquad (4.4.5)$$

In order to make a constructive reflection at the input plane

Let

$$p_i = p(1 - b_i/\pi) \qquad (4.4.6)$$

then near the Bragg frequency

$$\theta_i = \kappa p - \kappa p b_i/\pi + b_i \simeq \kappa p = \theta \qquad (4.4.7)$$

and

$$\phi_i = -\theta .$$

So with the chirping of $P_i = p(1 - b_i/\pi)$

Γ' can be rewritten as

$$\Gamma' = je^{-j\theta}(\rho_0 + \rho_1 e^{-j2\theta} + \ldots\ldots\rho_N e^{-j2N\theta}) \qquad (4.4.8)$$

where ρ_i : real and $\theta = kp$

The noticeable fact is that from the relation ($\theta_i = -\phi_i$) the constructive condition of θ_i is automatically satisfied by this chirping strategy.

Next let us consider magnitude terms ρ_i in (4.4.8)

From (4.4.3)

$$\rho_i = \frac{|Z_i^+ \sin\theta_{Mi} - b_i \cos\theta_{Mi}|}{\{(1 + b_i^2)\cos^2\theta_{Mi} + 2b_i(Z_i^- - \bar{z}_i)\cos\theta_{Mi}\sin\theta_{Mi} + (Z_i^{-2} + b_i^2\bar{z}_i^2)\sin^2\theta_{Mi}\}^{\frac{1}{2}}} \qquad (4.4.9)$$

where $l_i = \cos\theta_{Si}\cos\theta_{Mi}$

$n_i = \cos\theta_{Si}\sin\theta_{Mi}$

$m_i = \sin\theta_{Si}\cos\theta_{Mi}$

$r_i = \sin\theta_{Si}\sin\theta_{Mi}$

and $Z^{\pm}_i = \frac{1}{2}(\bar{z}_i \mp 1/\bar{z}_i \pm b^2_i\bar{z}_i)$

After substituting l_i, n_i, r_i and m_i to (4.4.2)

$$\Gamma_i' = j\rho_i e^{j\phi_i} \qquad (4.4.3)$$

where $\phi_i = \mathrm{Tan}^{-1}\xi_i$

$$\xi_i = \frac{M_i\sin\{\pi F_i(1 - y_i) + \psi_i\} + N_i\sin\{\pi F_i + \psi_i'\}}{M_i\cos\{\pi F_i(1 - y_i) + \psi_i\} - N_i\cos\{\pi F_i + \psi_i'\}}$$

and $M_i = \{b^2_i(\bar{z} - 1)^2 + (Z_i^- - 1)^2\}^{\frac{1}{2}}$

$N_i = \{b^2_i(\bar{z}_i + 1)^2 + (Z_i^- + 1)^2\}^{\frac{1}{2}}$

$\psi_i = \tan^{-1}\{b_i(\bar{z}_i - 1)(Z_i^- - 1)^{-1}\}$

$\psi_i' = \tan^{-1}\{b_i(\bar{z}_i + 1)(Z_i^- + 1)^{-1}\}$

Usually b_i and δ_{zi} are of the order of 10^{-1} and because F_i is very close to unity for the region of interest, we can simplify ξ_i by neglecting terms of second order in δ_{zi}, b_i and their products.

By employing the same approximation as that for ϕ_i and recalling $\delta_{zi} = C_1 h_i/\lambda$, $b_i = C_2(h_i/\lambda)^2$ it can be shown easily that

$$\rho_i = (h_i/\lambda)\{C_1^2 + C_2^2(h_i/\lambda)^2\}^{\frac{1}{2}} \sin\{\pi F_i y_i - \tan^{-1}(C_2 h_i/C_1\lambda)\} \qquad (4.4.10)$$

To suppress the trignometric term of ρ_i the second chirping can be employed such that

$$y_i = \{y + (\tan^{-1}(C_2 h_i/C_1\lambda))/\pi\}\{1 - b_i/\pi\}^{-1} \qquad (4.4.11)$$

By substituting (4.4.11) into (4.4.10), finally we get

$$\rho_i = \delta_{zi}^2\{1 + (b_i/\delta_{zi})^2\}^{\frac{1}{2}}$$

$$= (h_i/\lambda)\{C_1^2 + C_2^2 h_i/\lambda\}^{\frac{1}{2}} \qquad (4.4.12)$$

provided that the aspect ratio (y) is 0.5 and frequency is near Bragg frequency. From (4.4.12) ρ_i is weakly dependent on frequency. But in practical design λ is usually chosen fixed value of the Bragg frequency. Therefore frequency independancy of ρ_i is justified. Thus we have shown that chirping the periocity according to (4.4.7) and chirping the aspect ratio according to (4.4.11) the input Γ of the tapered grating will be formally equivalent to the Γ of the tapered transmission line.

Therefore the optimization process for Chebyshev gratings can be summarized as follows:

(1) Determine h_i/λ from modified Bessel function.

(2) This gives b_i and δ_{zi}

(3) b_i determines the periodicity chirping function

$$p_i = p(1 - b_i/\pi)$$

(4) Finally the aspect ratio chirping function y_i is computed from (4.4.11).

Referring to (4.1.11) and (4.3.24) the characteristic impedance $\bar{Z}(z)$ of the nonuniform grating is related to $\delta_z(z)$ as

$$\kappa(z) = \delta_z(z)/p(z) = \tfrac{1}{2}d\{\ln\bar{Z}_o(z)\}/dz \qquad (4.4.13)$$

Therefore

$$\bar{Z}_o(z) = Z_C\exp\{\int_o^z(2\delta_z(z)/p(z))dz\} \qquad (4.4.14)$$

We compare several taper functions with that of the Chebyshev taper in order to evaluate their effect on sidelobe suppresion. For this reason we shall choose well known distributions and window functions from the field of digital signal processing.

Referring to taper function given in (4.1.1), they are

(1) $f(z_i) = \dfrac{I_1\{\beta(1 - (2z_i - 1)^2)^{\frac{1}{2}}\}}{\cos\beta\{1 - (2z_i - 1)^2\}^{\frac{1}{2}}}$: modified Bessel

(2) $f(z_i) = \tfrac{1}{2}\{1 + \cos(2\pi z_i + \pi)\}$: raised cosine

(3) $f(z_i) = \{(2\pi)^{\frac{1}{2}}\beta\}^{-1}\exp\{-\tfrac{1}{2}\{(z_i - \tfrac{1}{2})/\beta\}^2\}$: gaussian

(4) $f(z_i) = (\beta/\pi)\{1 + \beta^2(z_i - \tfrac{1}{2})^2\}$: lorentzian

where z_i is normalized length ($0 \le z_i \le 1$) and all taper functions are normalized such that $\int_{-\infty}^{\infty}f(z)dz = 1$. And β is a constant parameter.

The taper functions are illustrated in Fig. 4.5.

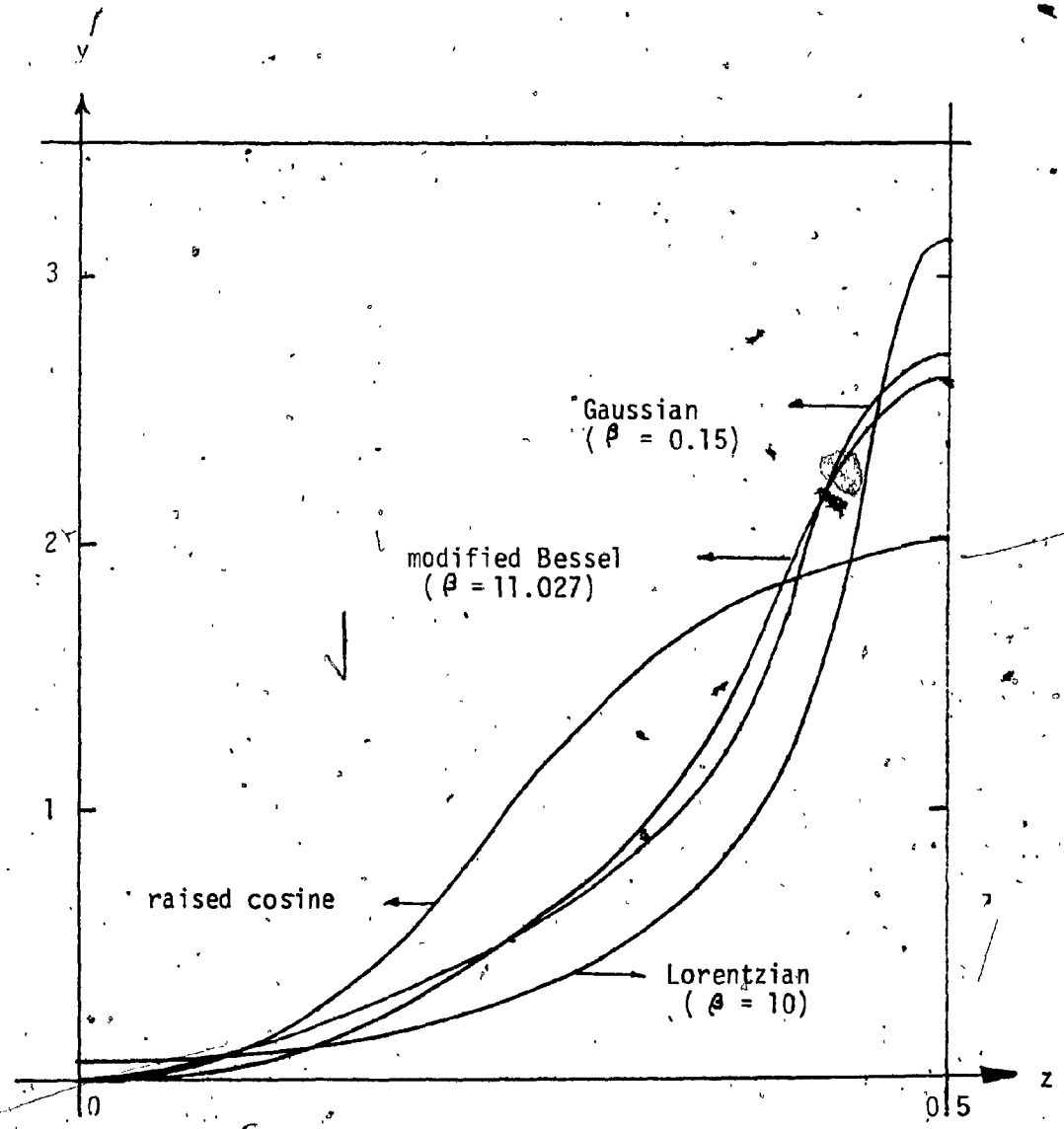

Fig. 4.5. Various taper functions. All functions are symmetric to the y axis at z = 0.5.

Computed grating array reflection coefficients using the taper functions listed above and chirped periodicity but constant aspect ratio ($y = \frac{1}{2}$) are shown in Fig. 4.6.

The computations indicate a sidelobe level variation from -33dB for the raised cosine taper, to -77dB for the modified Bessel function taper. Qualitatively the reflection coefficient sidelobe level is seen to depend on how smoothly the taper terminates at the end of the grating i.e. how large the terminal discontinuity is.

From the table (4.2) it can be seen that there is a trade-off between the roll-off slope and the sidelobe level. The raised cosine profile results in the steepest roll-off and the modified Bessel taper is the most effective in suppressing sidelobes.

The energy storage parameter of the i-th unit cell; b_i causes a phase shift and results in a shift of the resonant frequency. This phase shift is compensated by the chirping function chosen and as a result the resonant frequency of the grating is equal to the Bragg frequency defined by the π resonance of the first unit cell.

As shown in Fig. 4.6 the raised cosine taper and the modified Bessel taper have the most desirable characteristics in the vicinity of the stopband. In order to appreciate the effect of p chirping we compare the reflection coefficient characteristics of the modified Bessel function taper for chirped and constant periodicity. The results, shown in Fig. 4.7. indicate a considerable degradation in the steepness and sidelobe suppression when p is held constant. Also the

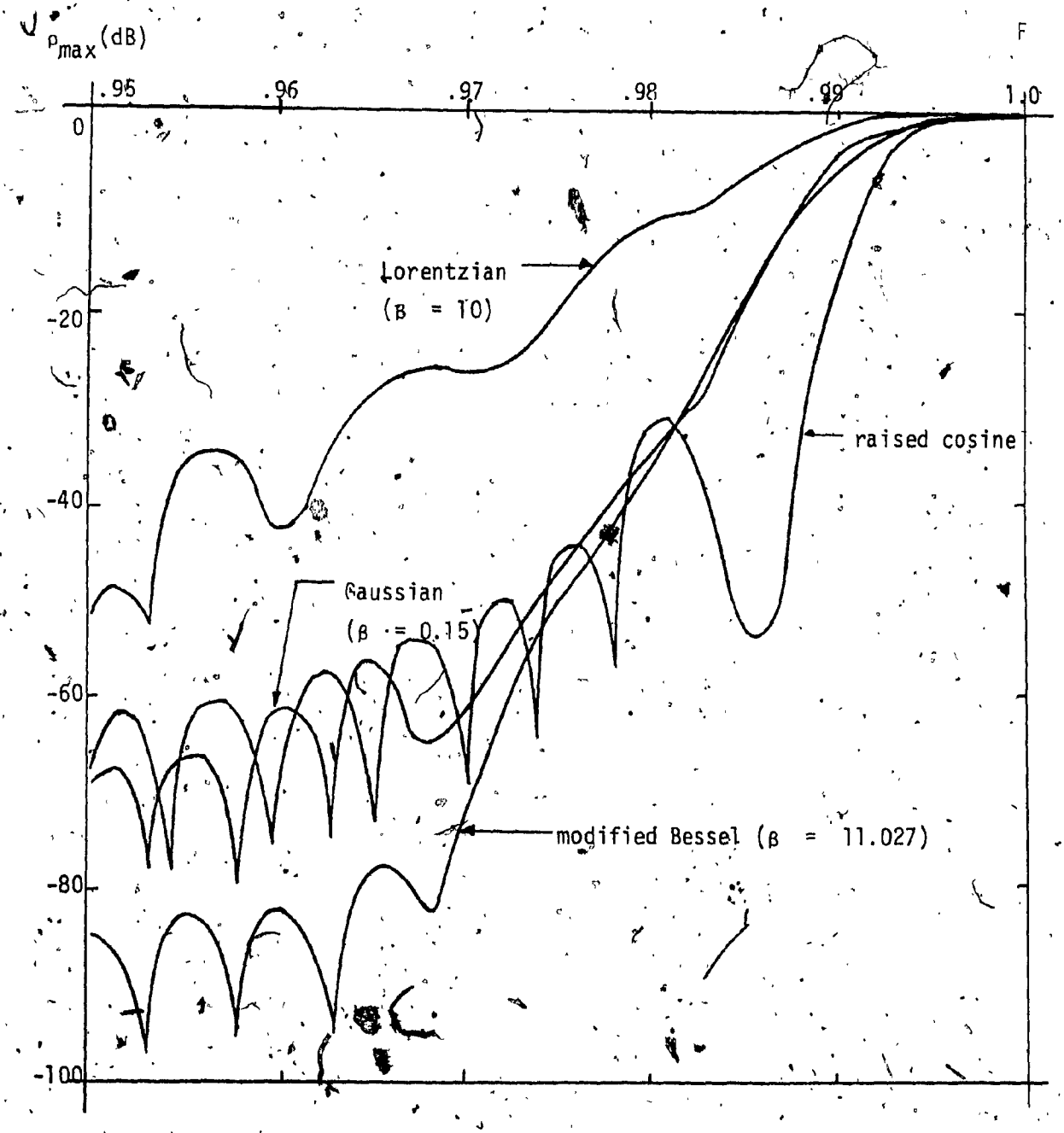

Fig. 4.6. Comparison of ρ_{max} characteristics for several taper functions. All the characteristics show symmetric figures above F = 1.

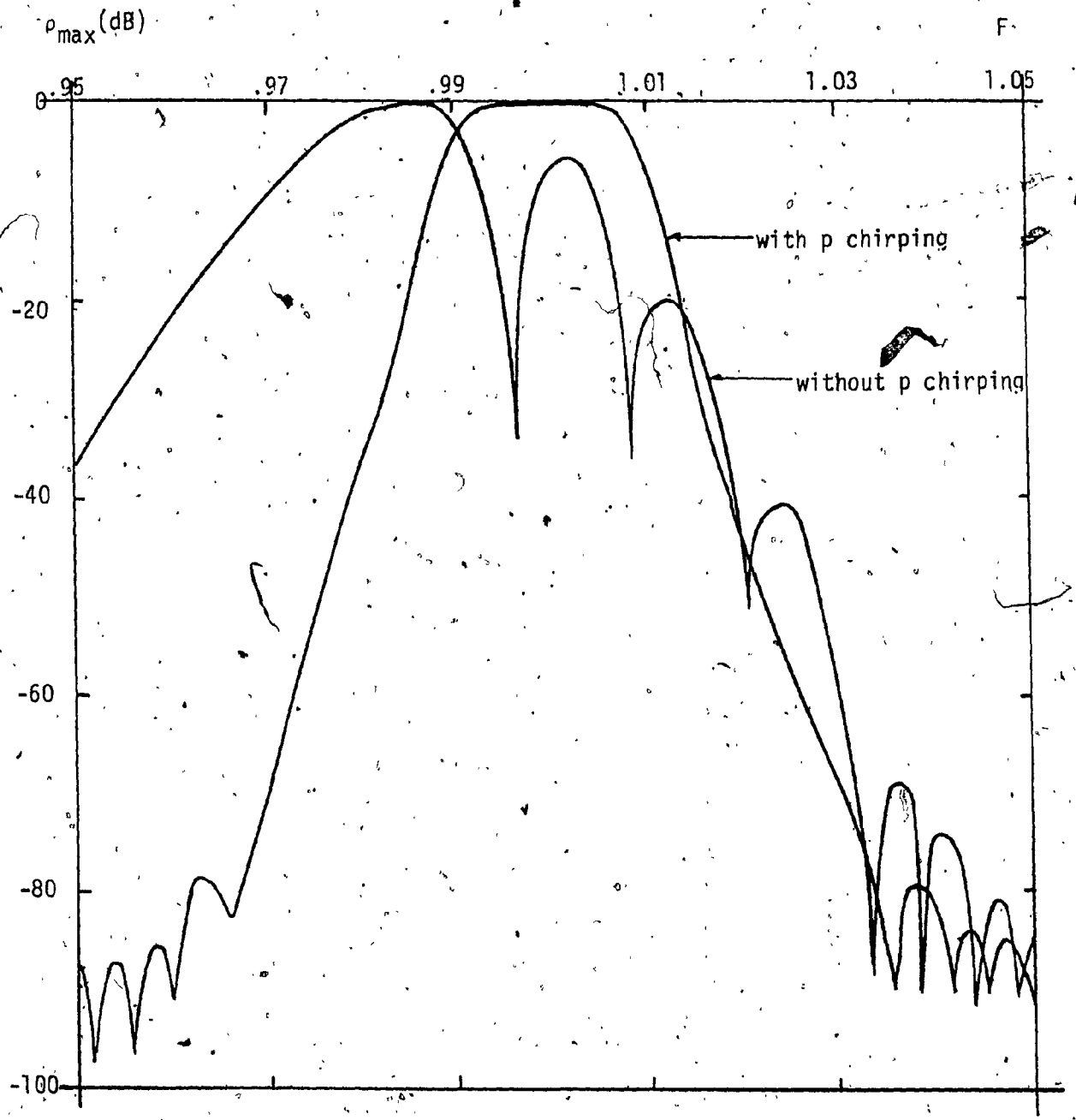

Fig. 4.7. Comparison of ρ_{max} of modified Bessel tapers with p chirping and without p chirping (y : constant)

Characteristics \ Profile function	Raised cosine	Modified Bessel	Gaussian	Lorentzian
F_R	1.	1.	1.	1.
ρ_{max}(dB)	-0.321	-0.323	-0.325	-0.533
BW	0.015	0.018	0.018	0.018
ΔF	0.004	0.008	0.010	0.021
DF	0.300	0.439	0.558	1.167
ρ_s(dB)	-34.036	-77.361	-58.441	-34.986
R_s(dB)	-34.357	-77.684	-58.766	-35.519

Table 4 . 2. Comparison of several taper functions

trating resonance shifts to downward from unity.

Recently Cross [40] published a similar analysis based on the coupled mode theory, where the performance characteristics of grating filters utilizing raised cosine, hamming, Blackman and Kaiser tapers were compared. Due to the fact that Cross does not take into consideration energy storage ($b = 0$) this result is somewhat different from those reported here, but quite similar to our results including periodicity chirping. This indicates that p chirping more or less compensates for energy storage at discontinuities.

Reflection coefficients and penetration depth characterisitcs are shown in Fig. 4.8 — 4.10 respectively for raised cosine and modified Bessel tapered gratings employing both p and y chirping.

In Table (4.3) performance characteristics and tabulated for the above tapers without chirping, with p chirping only, and with both p and y chirping respectively. The computations indicate that sidelobe suppression and roll-off steepness are inverse characteristics in the sense that if one is improved the other is degraded.

Fig. 4.8 shows that tapering and chirping increases the penetration depth at resonance. In other words the distance between the grating entrance plane and the virtual mirror at resonance is shortest for uniform gratings..

Several parameters which are dependent on the number of grooves are shown in Fig. 4.11. Note that the 3dB band width is almost constant for $N = 200$. The slight change of band width caused by variation of the numbers of grooves is probably due to a combination of effects such as discretization of the taper function into a

Variation / Function / Characteristics	h	h, p	h, p, y	
	Modified Bessel ($\beta = 11.027$)			Raised cosine
F_R	0.988	1.	1.	1.
ρ_{max}(dB)	-0.553	-0.323	-0.005	-0.056
BW	0.021	0.018	0.045	0.026
ΔF(slope)	0.017	0.008	0.013	0.008
DF	0.829	0.439	0.2889	0.308
ρ_s(dB)	-5.443	-77.361	-80.630	-56.619
R_s	-4.889	-77.037	-80.630	-56.563

Table 4.3 Comparison between modified Bessel and raised cosine tapers.

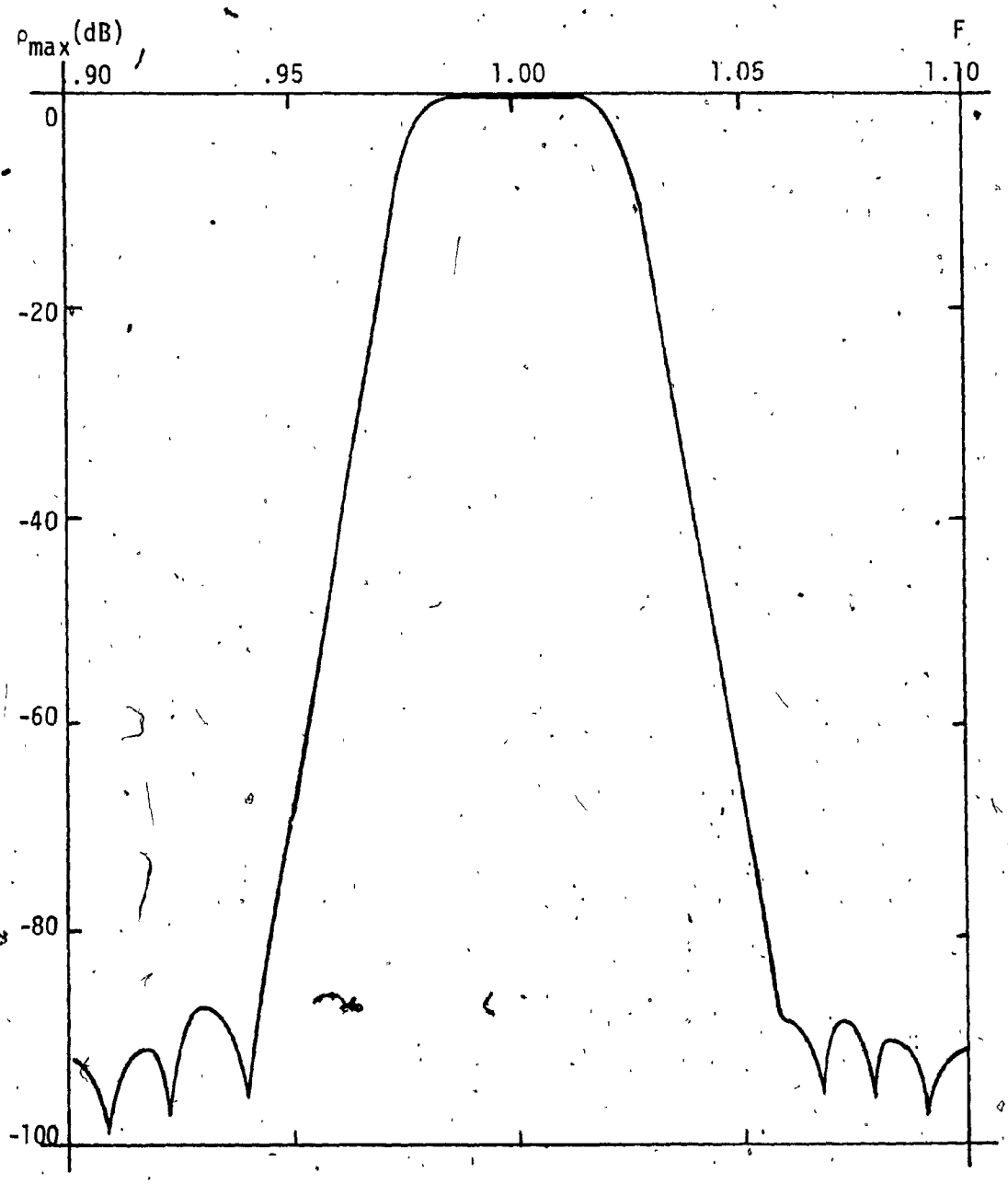

Fig. 4.8. Reflection coefficient characteristics of modified Bessel (β = 11.027) taper with p,y chirpings.

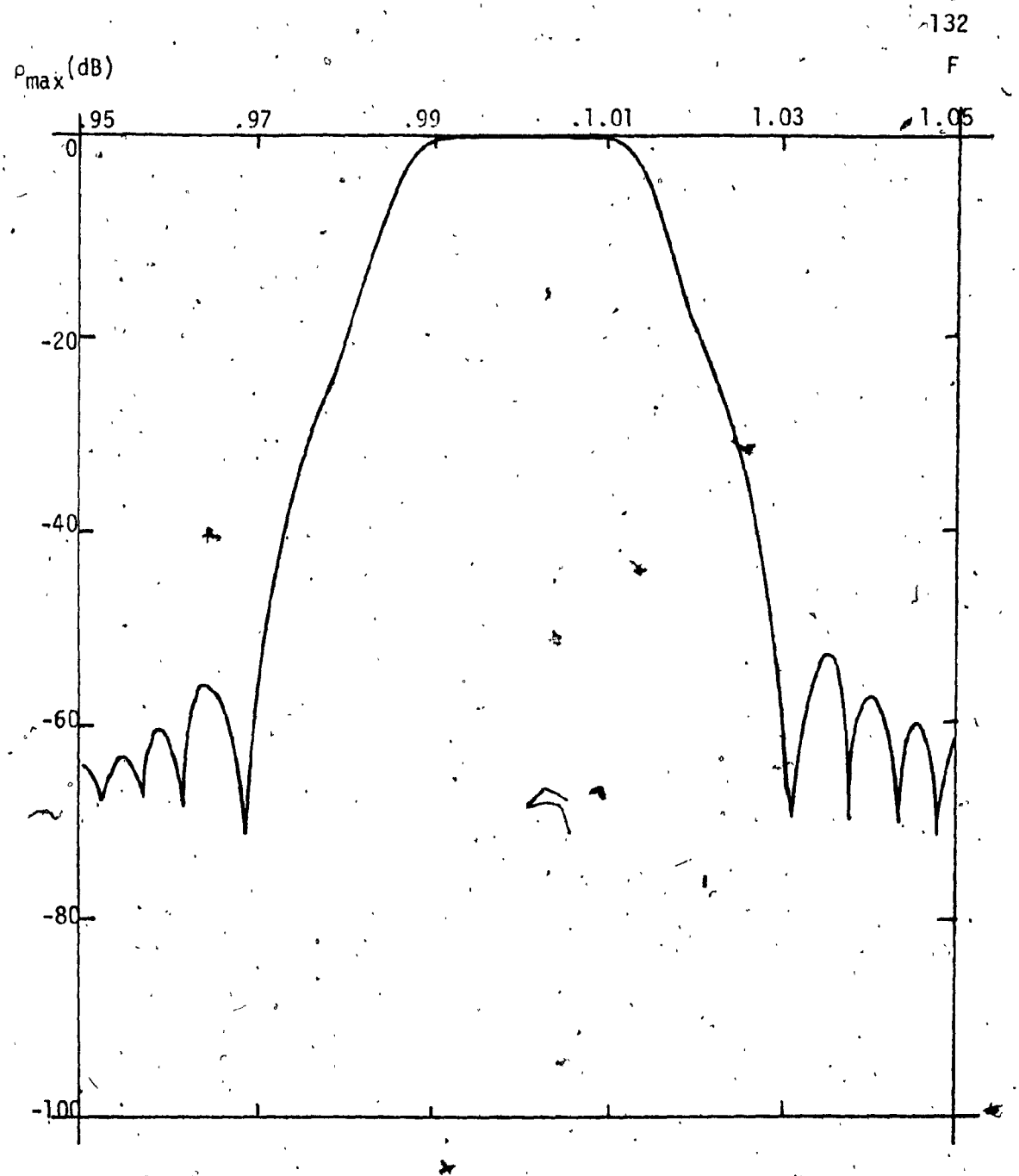

Fig. 4.9. Reflection coefficient characteristics of raised cosine taper with p,y chirpings.

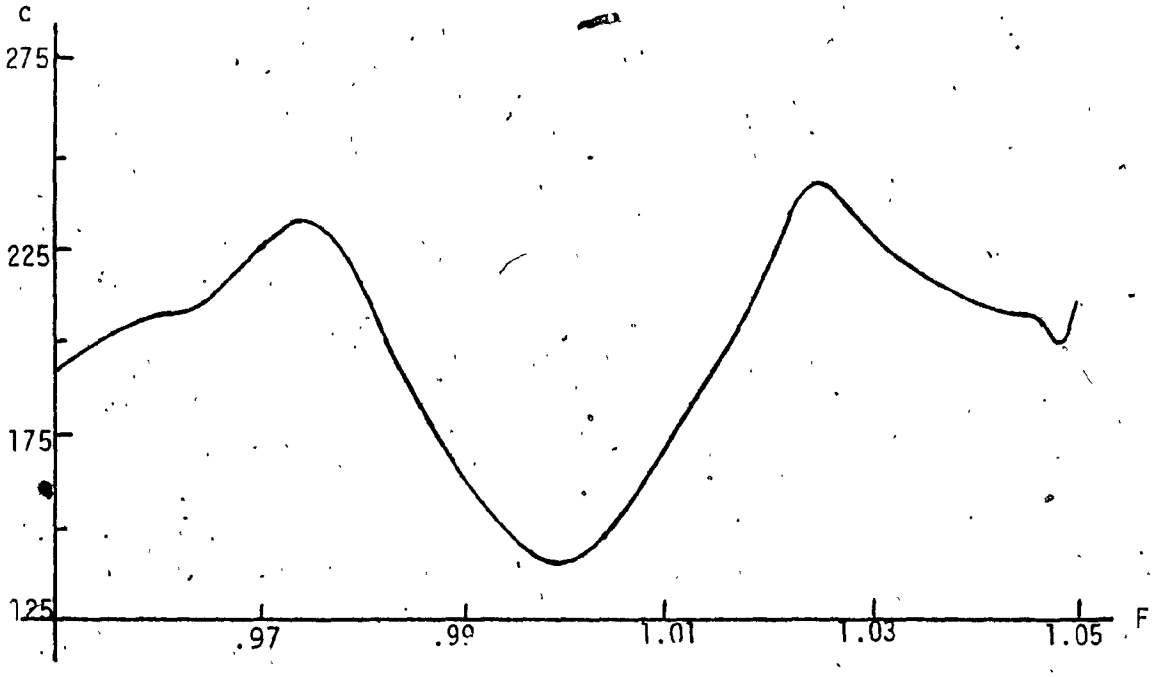

a) Modified Bessel taper

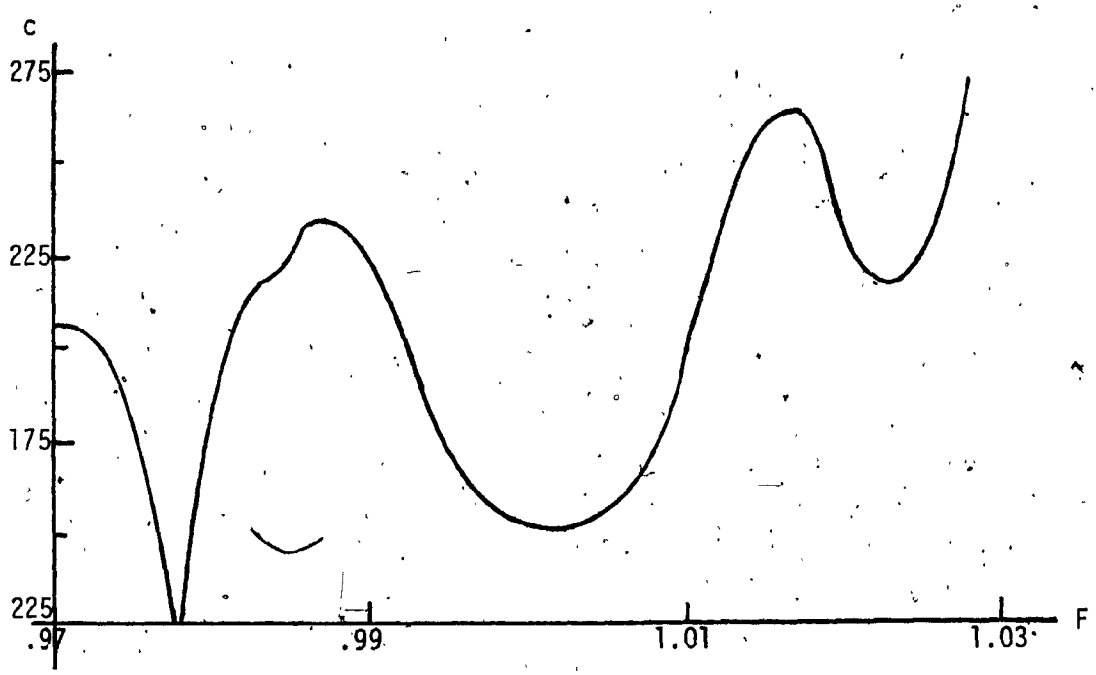

b) Raised cosine taper

Fig. 4.10 Penetration depth (c) characteristics for modified Bessel and raised cosine taper functions.

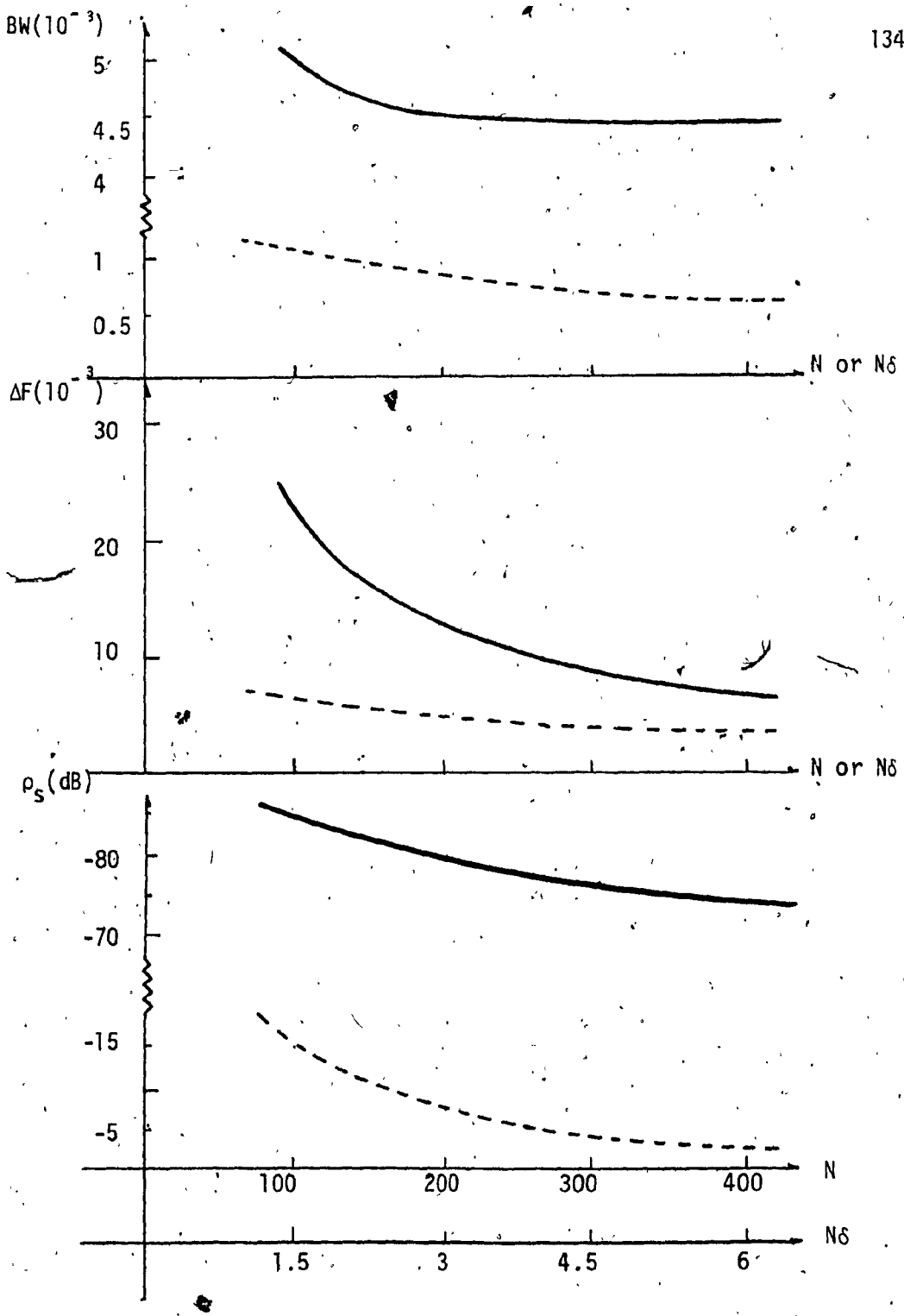

Fig. 4.11. The change of characteristics depending on the number of grooves

finite number of increments, a change in the roll-off parameter of the reflection coefficient characteristics etc. But the roll-off slope can be improved by increasing N beyond 200. The drawback of increasing N over 200 is in the rise of the sidelobe level Fig. 4.11.c. In conclusion, the modified Bessel function gives excellent sidelobe suppression and to be preferred to other methods of optimization.

4.5 Properties of Nonuniform Grating Resonators

In this section the transfer properties of grating resonator filters are examined. The filters considered are shown in Fig. (4.12). The gratings are optimized according to the principles described above and positioned with respect to each other so as to maximize the standing wave pattern in the cavity. This requires that the phase condition (3.6.2) be satisfied. For a tapered array utilizing chirping functions given in (4.4.6) and (4.4.11) respectively the phase of the reflection coefficient Γ at resonance has been computed and found to be $\phi = .88135$ rad. The corresponding phase of a tapered array featuring only a p chirping is $\phi = 0$. By substituting these values into (3.6.2) the tractional change of resonator length can be calculated. For a nominal normalized cavity length of $q = 30$. The former value results in a corrected length of $q = 30.2805$. In the latter case no correction is necessary.

The transmission characteristics of the resonator filter configured according to Fig. (3.14.b) is computed by cascading the transfer matrices of the bilaterally symmetric nonuniform gratings separated by a cavity whose physical length is. $L_c = q\,p$. The computed characteristics are illustrated in Fig. (4.12) and a comparison of the salient features of resonators fabricated with uniform and nonuniform gratings are tabulated in Table (4.4).

There are two aspects of these characteristics that depart from those of the uniform grating filter. Firstly, as a result of the increased $|\Gamma|_{max}$ indicated in Table (4.4), the unloaded Q is increased

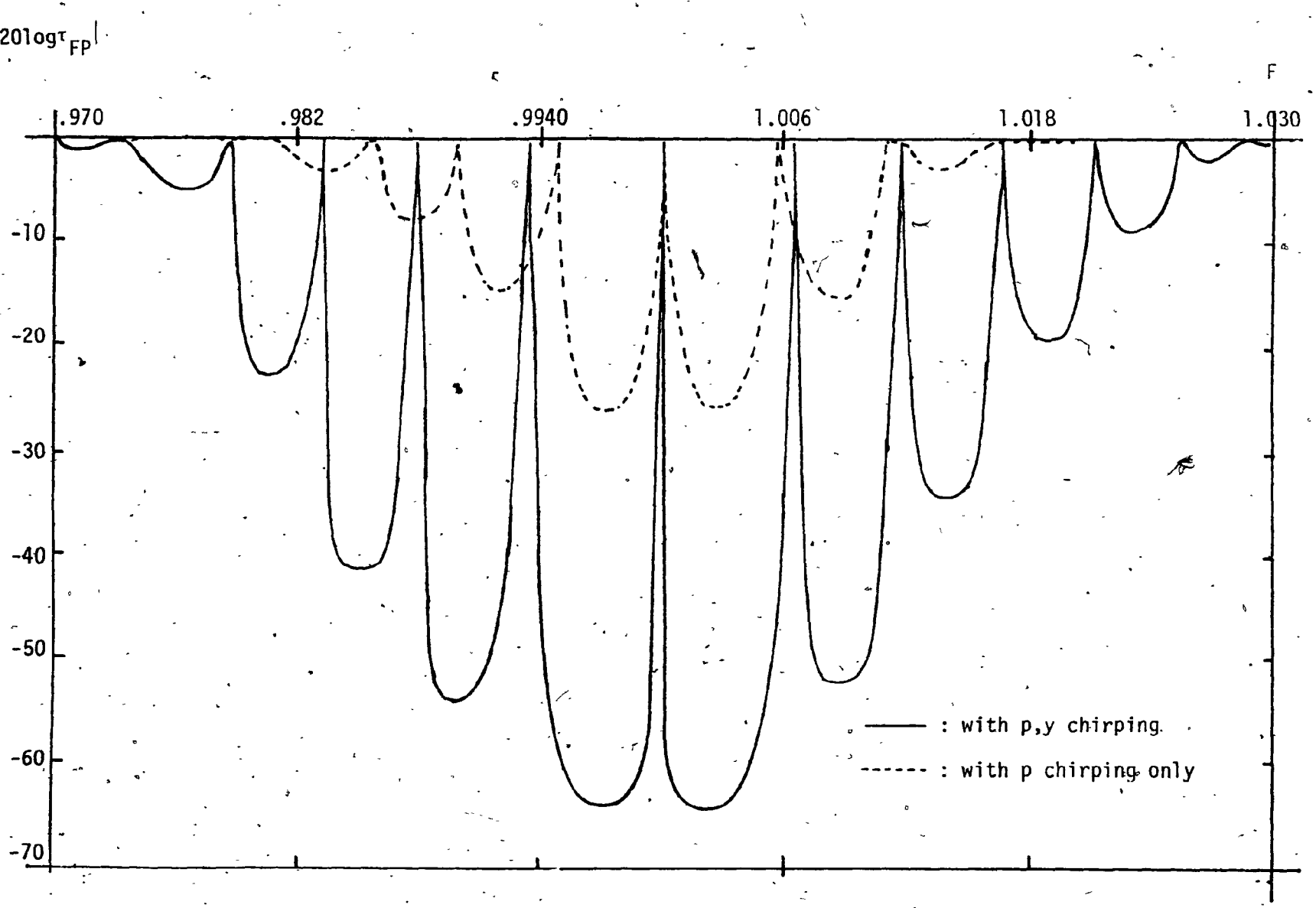

Fig. 4.12 Transmission coefficient characteristics of tapered grating-resonator without IDT

by a factor of more than 30 as indicated in Table (4.4). Secondly, as a result of several π radian phase shift excursion of the reflection coefficient Γ within the stopband, numerous axial modes appear within the stopband of the component grating.

In order to prevent spurious axial modes, resonators utilizing gratings are usually designed so that the free spectral range be equal to half the stopband width and the cavity length is chosen so that the F - P resonance coincides with the grating resonance. This ensures the F - P resonance to be at the center of the filter stopband.

Since the phase characteristics of the reflection coefficient of the nonuniform grating extends to several π radians the filter stopband likewise contains several axial modes. This explains the multitude of resonances appearing in Fig. (4.12). The free spectral range calculated from (3.6.8) using $q = 30$ and $C_R = 128$ obtained from Table (4.4) is $\Delta f_{FP}/f_o = 1/158 = 6.33 \times 10^{-3}$. This value is confirmed by Fig. (4.12).

The insertion loss characteristics of the F-P resonator including IDT's is shown in Fig. (4.13). A solid line represents the grating with p, y chirping functions while the grating with only p chirping is shown by dotted line. The offset parameter r and the resonator length are chosen to maximize the coupling to the cavity as explained in the previous chapter. Note that the filter resonant frequency is unchanged if only p chirping is applied whereas combined p and y chirping causes an offset in the resonant frequency (from 1 to .997).

Comparing Fig. (4.13) with the characteristics of the constant

	Constant grating	Tapered grating	
		h, p	h, p, ψ
F_R	0.997	1.000	1.000
ρ_{max}	0.964	0.963	0.999
BW (grating)	0.009	0.008	0.045
L_C (optimized)	$30./(1-b/\pi)$	30.000	30.280
c_R	96.000	144.000	128.000
BW (resonator)	8.5×10^{-5}	1.4×10^{-4}	2.5×10^{-6}
Q	1.19×10^{4}	6.94×10^{3}	4.0×10^{5}
Number of axial mode	1	3	10

Table 4.4. Characteristics of tapered grating and resonator.

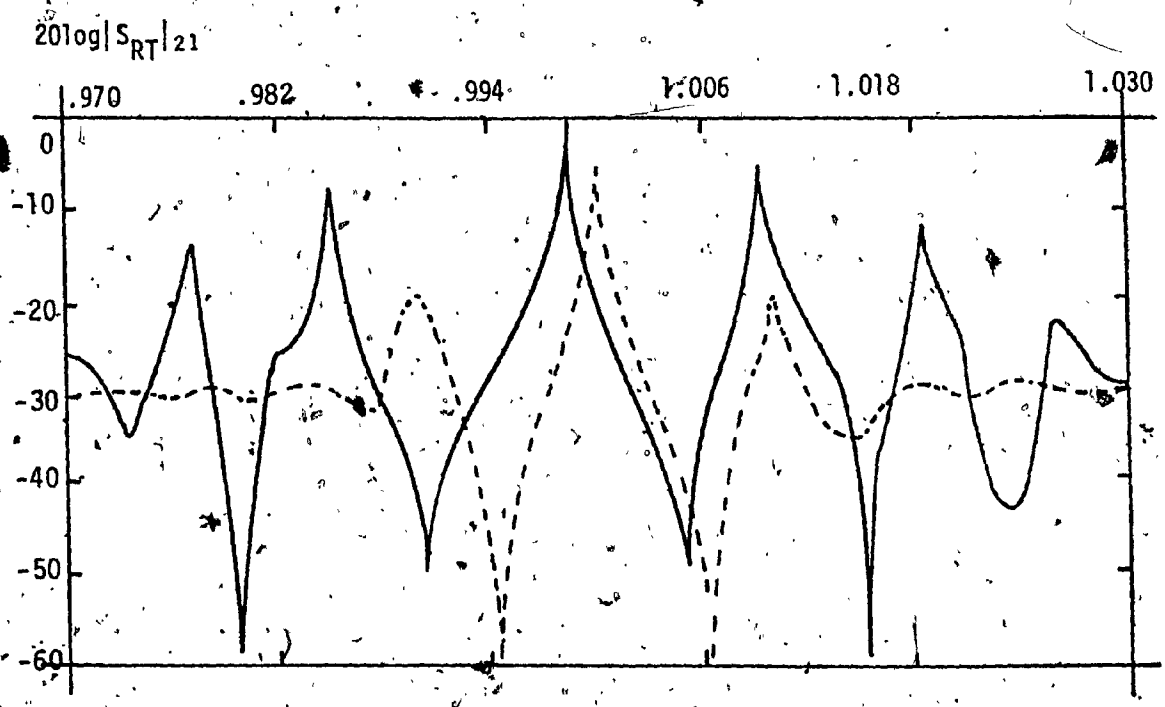

Fig. 4.13. Transmission characteristics of space coupled filter (dotted line represents the case of p chirping only)

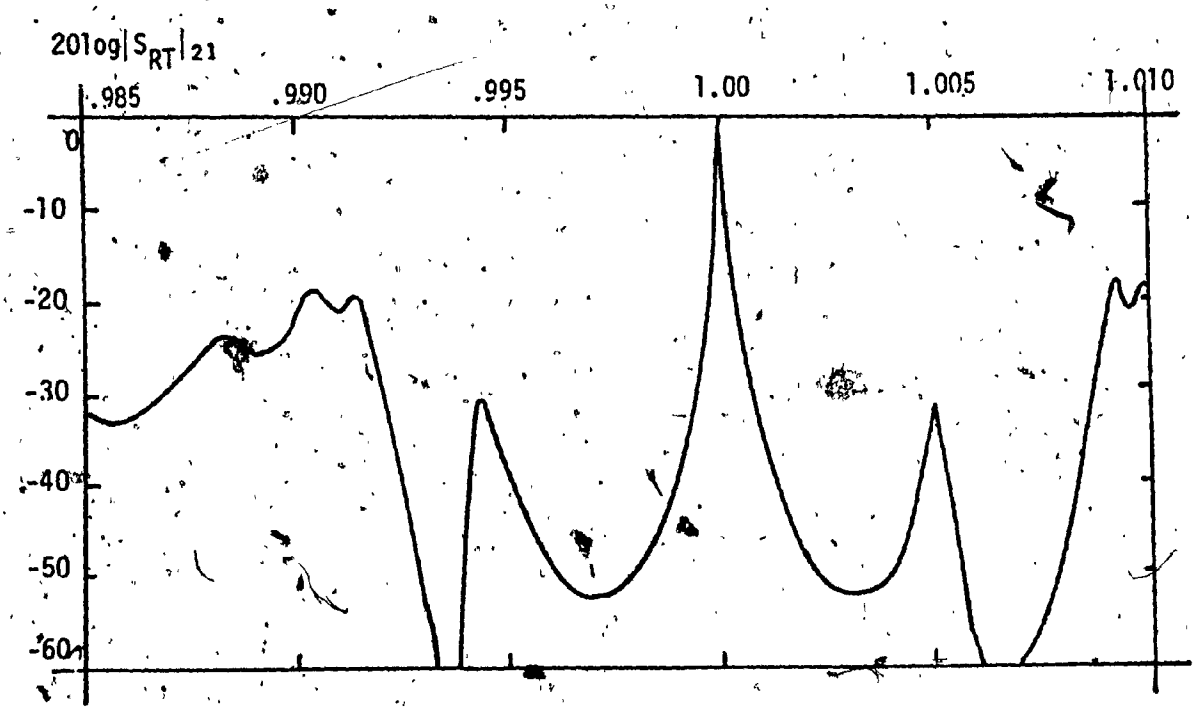

Fig. 4.14. Transmission characteristics of grating coupled filter.

grating resonator Fig. 3. 21 it is apparent that tapered grating resonators have a narrower main lobe and higher sidelobes than uniform grating resonators. The mainlobe bandwidth reduction is a result of the improvement in the Q factor. The large sidelobes are caused by the spurious axial modes which are absent in uniform grating resonators.

A p chirped grating coupled resonator filter characteristics is illustrated in Fig. (4.14). A comparison with the characteristics of the corresponding uniform case, Fig. (3.21) indicates once again a sharper mainlobe response and a degraded sidelobe suppression.

One concludes that tapering improves the filter characteristics in the immediate vicinity of resonance but the emergence of axial modes interfere with off-resonance functions. Therefore it is desirable to use this tapered F-p resonator as a comb filter in frequency multiplexing devices instead of a component of acoustically coupled F-p resonator filters.

CHAPTER V

CONCLUSION

The main objective of this thesis has been the analysis of surface Acoustic Wave (SAW) propagation in nonuniform grating arrays.

To facilitate understanding the relationship between forward and backward traveling waves in gratings, first coupled mode theory is reviewed. Next the analytic tool for the main part of this thesis, matrix analysis of periodic networks is discussed. Here three numerical methods for the multiplication of a large number of matrices were compared and results were obtained indicating the expectable relative error both within and outside the stopband. Most accurate results were obtained by direct multiplication using an IMSL subroutine.

In Chapter III uniform grating reflectors and Fabry-Perot resonators fabricated with uniform gratings have been discussed. Equivalent network models and circuit parameters have been presented which provide an accurate description of reflector characteristics. Approximations appropriate to small incremental changes of the characteristic impedance were invoked. The transmission characteristics of the grating and the resonator have been obtained in the vicinity of the fundamental (π) stopband using these approximations. Recent analytical investigations on the nature and magnitude of the energy storage parameter have been compared to experimentally observed data.

The relative bandwidth and the maximum stopband reflection has been plotted against groove depth and aspect ratio, using various loss coefficients. Based on the analytical results of Shimizu { 38 } the reflection coefficient at the second harmonic has been plotted against the so-called groove edge parameter. The last part of Chapter III has been devoted to the study of the Fabry-Perot resonator. The interdigital transducer (IDT) has been replaced with its equivalent network as described by Smith {43} . Several Fabry-Perot configurations including IDT's have been analyzed and numerical results obtained for the filter transfer characteristics. The design process includes a discussion on the correct length of the cavity and the proper positioning of the IDT. Although our method of analysis is different from that reported by Cross and Schmidt{ 34 }the numerical results here obtained are virtually identical to theirs.

In Chapter IV, nonuniform gratings have been analyzed using the circuit model approach discussed in Chapter III. The reflection coefficient peak, the bandwidth and the roll-off slope have been numerically evaluated as a function of tapering and chirping, i.e. as a function of the fractional change introduced in the groove depth, the periodicity and the aspect ratio. It has been found that for the same amount of fractional variation p-chirping has the greatest influence in shaping the transfer characteristics of the nonuniform grating.

Various taper characteristics have been investigated, amongst them the Chebyshev optimization developed by Collin {36 }, well known from microwave impedance transformer design. Our analysis shows that

SAW gratings can be treated similar to tapered waveguide sections and that the procedure of Chebyshev optimization is readily applicable to SAW grating arrays. This procedure, it has been shown, results in an increased bandwidth and a vastly improved sidelobe suppression, much like in waveguide impedance transformer. Using gratings optimized in this fashion the transmission characteristics of F-P resonators and filters are discussed and their insertion loss characteristics have been obtained. It was found that tapering and chirping greatly increases the Q of the resonator and that it causes the appearance of several axial modes within the stopband. Since the axial modes appear to have an excellent unloaded Q factor and since the level of attenuation between axial resonances is high it appears that the Fabry-Perot configuration featuring tapered grating arrays can be very useful as a comb filter.

A comparison of the grating array transfer characteristics utilizing various p chirped tapers indicates a large sensitivity of these characteristics to minuite change in taper functions. Furthermore it appears that the central and tail regions of the symmetric taper functions affect the transfer characteristics to various degree. Therefore it is suggested that further analytical and experimental work be carried out to determine the relative significance of the central and tail end geometry on the performance of the SAW grating array.

REFERENCES

1. Ash, E.A., "Surface Wave Grating Reflectors and Resonators", IEEE. Symp. MTT, New Port Beach, CA May, 1970

2. Johnson, C.C., "Field and Wave Electrodynamics", McGraw-Hill, New York, 1965, 50-57.

3. Pierce, J.R., "Coupling of Modes of Propagation", J. Appl. Phys., 25 (1954) 179 - 183

4. Kogelnik, H. and Shank, C.V., "Coupled - Wave Theory of Distributed Feedback Lasers ", J. Appl. Phys., 43(1972) 2327 - 2335

5 Marcuse, D., "Theory of Dielectric Optical Wave guides"., Academic Press, New York, 1965

6. Yariv, A., "Coupled-Mode Theory for Guided-Wave Optics", Trans. IEEE, QE-9 (1973) 919 - 933

7 Adair, J.E., "Coupled mode analysis of nonuniform coupled Transmission", Ph.D. Thesis. The University of Michigan, 1968

8. Barnes, C.W., "Conservative Coupling Between Modes of Propagation - a Tabular Summary", Proc. IEEE, 52,(1964), 64 - 73

9. Smith, R.B. "Analytic solutions for Linearly Tapered Directional Couplers", J. Opt. Soc. Am., 66(1976) 882 - 892

10. Chen, Y.S., and Ishimaru, A., "On the General Solutions of Coupled Mode Equation with Varying Coefficients , Proc. IEEE 54(1966) 1071

11 Storch, L., "The Transmission Matrix of N Alike Cascaded Networks", Trans. AIEE, 73, Part 1, (1954 - 1955), 616 - 618

12 Abramowitz, M., Stegun, I.A., eds. "Handbook of Mathematical Functions", Nat. Bur. Standards, U.S. Dept. of Commerce, 1964, Chapter 22.

13 Altman, J.L., "Microwave Circuits", D. Van Nostrand Company, Inc. New York (1964) 315

14 Matthews, H., eds.; "Surface Wave Filters", John Wiley & Sons, Inc., New York, 1977, Chapter 4

15 Li, R.C.M., Melngailis, J., "The Influence of Stored Energy at Step Discontinuities on the Behavior of Surface-Wave Gratings" Trans, IEEE, SU-22 (1975) 189-198

16 Farnell, G.W.,"Surface Wave Reflectors and Resonators", Can. Ele. Eng. J.,1, (1976), 3-13

17 Schwelb, O., "Acoustic Surface Waves in Periodic Structure", Ph D. Thesis, McGill University (1978)

18 Wu,S.D., Tuan, H-S.,"Surface Acoustic Wave Scattering from a Groove in YZ $LiNbO_3$", Proceedings, 31st Annual Symposium on Frequency Control, US Army Electronics Command, Fort Monmouth, N.J.,(1977) 271 - 274

19 Li,R.C.M.,"Analysis of Surface Wave Reflection from a Periodic Array of Grooves", 1972 Ultrasonics Symposium Proceedings, IEEE Cat. No. 72CHO708-8SU, 263-266

20. Tuan, H-S., Li,R.C.M.,"Rayleigh-wave Reflection from Groove and Step Discontinuities", J. Acoust. Soc. Am., 55,(1974), 1212 - 1217

21 Tanski, W.J.,"Developments in Resonators on Quarz", 1977 Ultrasonics Symposium Proc. IEEE Cat. N. 77CH 1264-1SU, 900-904

22 Maines, J.D. and Paige, E.S.,"Surface-Acoustic Wave Devices for Signal Processing Applications", Proc. IEEE 54(1966) 639-652

23 Bell, D.T., and Li,R.C.M.,"Surface-Acoustic-Wave Resonators" Proc. IEEE 54(1966) 711-721

24 Coldren, L.A., Rosenberg, R.L., "SAW Resonator Filter Overview: Design and Performance Trade Offs", 1978 Ultransmics Symposium Proc. IEEE Cat. 78CH1344-1SU, 422-432

25 Pease,M.C.,"Methods of Matrix Algebra", Acadmic Press, New York 1965, Chap VII

26 Li,R.C.M., Alusow, T.A. and Williamson, R.C. "Surface-Wave Resonators using grooved reflectors, "Porc. 29th Annual Frequency Control Symp. May 1975, 167-176

27 Collin,R.E., "Foundations for Microwave Engineering", McGraw-Hill New York, 1966, Chapter 4

28 Shimizu, H., Takeuchi, M., "Theoretical Studies of the Energy Storage Effects and the Second Harmonic Responses of SAW Reflection Gratings", 1979, Ultrasonic Symposium, Proceedings, IEEE, Cat. No. 79CH 1482-9179, 667-672

29 Wright, P.V., Haus, H.A., "Theoretical Analysis of Second-Order Effects in Surface-Wave Gratings", Proc. 34th Ann. Freq. Control Symp., USAERADCOM, May 1980

30 Datta, S., Hunsinger, B.I., "A Theoretical Analysis of Storage Energy in Surface Wave Gratings", 1979 Ultrasonic Symposium, Proceedings IEEE, Cat. No. 79CH1482-9179, 673-677

31 Schwelb, O. "The Transverse Resononance Method and its Application" Lecture Note

32 Yariv, A.,"Introduction to Optical Electronics", Chapter 4 Holt, Rinehart and Winston 2nd Ed. 1976

33 Mattaei, G.L., Wong, D.Y., and O Shaughnessy, B.P., "Simplifications for the Analysis of Interdigital Surface-Wave Devices", Trans. IEEE, SU-22, (1975), 105-114

34 Cross, P.S., Schmit, R.V., "Coupled Surface - Acoustic-Wave Resonators", B.S.T.J. 56 No.8 (1977), 1447-1482

35 Collin, R.E., "Theory and Design of Wide-Band Multisection Quarter-Wave Transformers", Proc. IRE, 43 Feb.(1955), 179-185

36 Collin, R.E., "The Optimum Tapered Transmission Line Matching Section", Proc. IRE, 44 April (1956) 539-548

37 Walker, L.R. and Wax, N., "Nonuniform Transmission Lines and Reflection Coefficients" J. Appl. Phys., 17 Dec. 1946 1043-1045

38 Bolinder, F., "Fourier Transforms in the Theory of Inhomogeneous Transmission Lines", Proc. IRE, 38 Nov. 1950, 1354.

39 Klopfenstein, R.W., "A Transmission Line Taper of Improved Design", Proc. IRE 44 Jan. 1956 31-35

40 P.W. Cross and H. Kogelnik, "Sidelobe Suppression in Corrugated Waveguide Filters", Optics Letters, Vol. 1 No. 1, July 1977, 43-45

41 Marshall, F.G., Newton, C.O. , and Paige, E.G.S., "Surface Acoustic Wave Multistrip Components and Their Applications, Trans. IEEE, SU-20, (1973), 134-143

42 Blφtekjaer, K. Ingebrigtwen, K.A. and Skeie, H., "Acoustic Surface Waves in Piezoelectric Materials with Periodic Metal Strips on the Surface", Trans. IEE, ED-20 (1973), 1139-1146

43 W.R. Smith, H. M. Gerade, "Analysis of Interdigital Surface Wave Transducers by Use of an Equivalent Circuit Model" IEEE, Trans. MTT-17 No. 11 Nov. (1969) 856-864

44 Smith, H.I., Melngailis. J., Williamson, R.C. and Brogan, W. T., "Ion Beam Etching of Surface Gratings", 1973 Ultrasonics Symposium Porceedings, IEEE Cat. No. 73CHO 807-8SU, 558-563

45 Sliedregt,.M. "Cylindrical waveguide cut-off wavelength", Microwave journal, May(1960).

APPENDIX

I. Derivation of Chebyshev Identity

II. Conversion Table for Matrix Representations

III. Fortran Program List "SAW7"

APPENDIX I

DERIVATION OF CHEBYSHEV IDENTITY

Let $\bar{u}_{1,2}$ be the normalized eigen vectors of a unit Q matrix with eigen values $e^{\pm j\xi}$. Then

$$\begin{bmatrix} A & B \\ C & D \end{bmatrix} \bar{u}_{1,2} = e^{\pm j\xi} \bar{u}_{1,2} \qquad (A.1.)$$

and eigen values will be given

$$e^{\pm j\xi} = (A + D)/2 \pm \{((A + D)/2)^2 - 1\}^{\frac{1}{2}} \qquad (A.2.)$$

with the corresponding eigen vectors given by

$$\bar{u}_1 = \begin{bmatrix} u_{11} \\ u_{21} \end{bmatrix} \qquad \bar{u}_2 = \begin{bmatrix} u_{12} \\ u_{22} \end{bmatrix}$$

where

$$\begin{aligned} u_{11,12} &= B\{B^2 + (e^{\pm j\xi} - A)^2\}^{-\frac{1}{2}} \\ u_{21,22} &= (e^{\pm j\xi} - A)\{B^2 + (e^{\pm j\xi} - A)^2\}^{-\frac{1}{2}} \end{aligned} \qquad (A.3.)$$

The modal matrix u and inverse of u will be

$$U = \begin{bmatrix} u_{11} & u_{12} \\ u_{21} & u_{22} \end{bmatrix}, \quad U^{-1} = (u_{11}u_{22} - u_{12}u_{21})^{-1} \begin{bmatrix} u_{22} & -u_{12} \\ -u_{21} & u_{11} \end{bmatrix} \qquad (A.4.)$$

$$\begin{bmatrix} A & B \\ C & D \end{bmatrix}^N = UD^NU^{-1} = (u_{11}u_{22} - u_{12}u_{21})^{-1} \begin{bmatrix} u_{11} & u_{12} \\ u_{21} & u_{22} \end{bmatrix} \begin{bmatrix} e^{jN} & 0 \\ 0 & e^{-jN} \end{bmatrix} \begin{bmatrix} u_{22} & -u_{12} \\ -u_{21} & u_{11} \end{bmatrix}$$

$$= (\sin\xi)^{-1} \begin{bmatrix} A\sin N\xi - \sin(N-1)\xi & B\sin N\xi \\ C\sin N\xi & D\sin\xi - \sin(N-1)\xi \end{bmatrix}$$

$$= \begin{bmatrix} AU_{N-1}(\xi) - U_{N-2}(\xi) & BU_{N-1}(\xi) \\ CU_{N-1}(\xi) & DU_{N-1}(\xi) - U_{N-2}(\xi) \end{bmatrix}$$

$$= QU_{N-1}(\xi) - IU_{N-2}(\xi) \qquad \text{(A.5.)}$$

So the Chebyshev identity is prooved.

Instead of employing diagonalization process, Sylvester's theorem was found to be very useful to derive this relation. The theorem states that if Q is a j x j matrix then any polynomial expression in powers of Q may be written as

$$p(Q) = \sum_{r=1}^{j} \{p(\lambda r) \prod_{\substack{s=1 \\ s \neq r}}^{j} (Q - \lambda_s I)/(\lambda_r - \lambda_s)\} \qquad \text{(A.6.)}$$

where I is the identity matrix, λ_r is the r'th eigenvalue of the Q matrix and $p(\lambda_r)$ is the same polynomial as p(Q). So in our case j = 2 and $p(Q) = Q^N$. Therefore from (A.1.)

$$\lambda_1 = e^{j\xi}, \qquad \lambda_2 = e^{-j\xi}$$

Substitution of these eigen values into (A.6.) results in

$$Q^N = \lambda_1^N(Q - \lambda_2 I)/(\lambda_1 - \lambda_2) + \lambda_2^N(Q - \lambda_1 I)/(\lambda_2 - \lambda_1)$$

$$= Q(\lambda_1^N - \lambda_2^N)/(\lambda_1 - \lambda_2) + I(\lambda_1\lambda_2^N - \lambda_2\lambda_1^N)/(\lambda_1 - \lambda_2)$$

$$= Q\sin N\xi/\sin\xi + I\sin(N - 1)\xi/\sin\xi$$

$$= QU_{N-1}(\xi) + IU_{N-2}(\xi) \qquad (A.7.)$$

APPENDIX II

Two Port Network Conversion Table

Variables	Relation	Matrix	Losslessness	Reciprocity	Symmetry
$\bar{V} = \begin{bmatrix} V_1 \\ V_2 \end{bmatrix}$	$\bar{V} = Z\,\bar{I}$	$Z = \begin{bmatrix} Z_{11} & Z_{12} \\ Z_{21} & Z_{22} \end{bmatrix}$	$Z + Z^{\dagger} = 0$	$Z_{12} = Z_{21}$	$Z_{11} = Z_{22}$
$\bar{I} = \begin{bmatrix} I_1 \\ I_2 \end{bmatrix}$	$\bar{I} = Y\bar{V}$	$Y = \begin{bmatrix} Y_{11} & Y_{12} \\ Y_{21} & Y_{22} \end{bmatrix}$	$Y + Y^{\dagger} = 0$	$Y_{12} = Y_{21}$	$Y_{11} = Y_{22}$
$\bar{E}_1 = \begin{bmatrix} V_1 \\ I_1 \end{bmatrix}$ $\bar{E}_2 = \begin{bmatrix} V_2 \\ -I_2 \end{bmatrix}$	$\bar{E}_2 = Q\bar{E}_1$	$Q = \begin{bmatrix} A & B \\ C & D \end{bmatrix}$	$Q^{-1} = \sigma_1 Q^{\dagger} \sigma_1$	$\Delta Q = 1$	$A = D$
			A, D : Real, B, C : Imaginary		
$\bar{A} = \begin{bmatrix} a_1 \\ a_2 \end{bmatrix}$ $\bar{B} = \begin{bmatrix} b_1 \\ b_2 \end{bmatrix}$	$\bar{B} = S\bar{A}$	$S = \begin{bmatrix} S_{11} & S_{12} \\ S_{21} & S_{22} \end{bmatrix}$	$SS^{\dagger} = I$	$S_{12} = S_{21}$	$S_{11} = S_{22}$
$\bar{A}_1 = \begin{bmatrix} a_1 \\ b_1 \end{bmatrix}$ $\bar{A}_2 = \begin{bmatrix} b_2 \\ a_2 \end{bmatrix}$	$\bar{A}_2 = A\bar{A}_1$	$A = \begin{bmatrix} a_{11} & a_{12} \\ a_{21} & a_{22} \end{bmatrix}$	$A^{-1} = \sigma_3 A^{\dagger} \sigma_3$	$\Delta A = 1$	$A_{12} = A_{21}$
			$A_{11} = A_{22}^{*}$, $A_{12} = A_{21}^{*}$		

Table A. 1. Several matrices representation of two ports network

	Z	Y	S	Q	A
Z	$\frac{Z}{Z_0} = \frac{I+S}{I-S}$	$\Delta Z = \Delta Y^{-1}$	$L = 1 - S_{11} - S_{22} + \Delta S$	$\Delta Z = \frac{B}{C}$	$L = A_{11} + A_{12} - A_{21} - A_{22}$
Y	$\Delta Y = \Delta Z^{-1}$	$\frac{Y}{Y_0} = \frac{I-S}{I+S}$	$L = 1 + S_{11} + S_{22} + \Delta S$	$\Delta Y = \frac{C}{B}$	$L = A_{21} - A_{11} + A_{12} - A_{22}$
S	$L = \frac{\Delta Z}{Z_{11}Z_{22}} + 1 + \frac{Z_{11}}{Z_{22}} + \frac{Z_{22}}{Z_{11}}$	$L = \frac{\Delta Y}{Y_{11}Y_{22}} + 1 + \frac{Y_{11}}{Y_{22}} + \frac{Y_{22}}{Y_{11}}$	$S = \frac{Z-I}{Z+I} = \frac{I-Y}{I+Y}$	$L = \bar{A} + \bar{B} + \bar{C} + \bar{D}$	$\Delta S = -\frac{A_{22}}{A_{11}}$
Q	$\Delta Q = \frac{Z_{12}}{Z_{11}}$	$\Delta Q = \frac{Y_{12}}{Y_{11}}$	$\Delta Q = \frac{S_{12}}{S_{11}}$	$\bar{A} = A\sqrt{\frac{Z_{22}}{Z_{11}}}$ $\quad \bar{B} = \frac{B}{\sqrt{Z_{11}Z_{22}}}$ $\quad \bar{C} = C\sqrt{Z_{11}Z_{22}}$ $\quad \bar{D} = D\sqrt{\frac{Z_{11}}{Z_{22}}}$	$\Delta Q = \Delta A$
A	$\Delta A = \frac{Z_{21}}{Z_{11}}$	$\Delta A = \frac{Y_{21}}{Y_{11}}$	$\Delta A = \frac{S_{21}}{S_{11}}$	$\frac{\bar{A}+\bar{B}+\bar{C}+\bar{D}}{2}$ $\quad \frac{\bar{A}-\bar{B}+\bar{C}-\bar{D}}{2}$ $\quad \frac{\bar{A}+\bar{B}-\bar{C}-\bar{D}}{2}$ $\quad \frac{\bar{A}-\bar{B}-\bar{C}+\bar{D}}{2}$	

Table A.2. A conversion table for two ports matrix representation

APPENDIX III

NON UNIFORM GRATINGS, FABRY-PEROT RESONATOR, AND FILTER TRANSMISSION CHARACTERISTICS

Source program filename	SOSAW7
Object program filename	OBSAW7
Date	Dec. 10, 1980
Required field length	63500
Language	Fortran Version 4.4
System	NOS 1.4
Compilation time	3.5 CP seconds
Execution time	30 - 95 seconds depending on commends
Program name	SAW7
Libraries used	Fortran; IMSL { VMULFF, USPLT, MMRSI1 }

SAW7 computes the transmission characteristics of uniform and nonuniform cascaded two ports network and Fabry - Perot resonator filters with or without IDTs.

SAW7 consists of a main program and subroutines called:

ARRAY	REFLEX	TIMED
TRANS	FABRY	CONVRT
DELAY	COUPLE	FILTER

The main program is used to read in data via four input data arrays i.e. LM(3), LN(7), VV(8), and UV(10) to set up the output requirement and feed in independent parameters.

The most important subroutine, ARRAY does all the computations pertaining to the reflective array. Thus firstly it computes a number of parameters which describe the unit cell of which the array consists, from these it obtains the A, B , C, D parameters of the unit cell, it then proceeds to call IMSL subroutine VMULFF as many as required to cascade the unit cells and results in the Q matrix of entire gratings. In the last part of ARRAY reciprocity and Bilaterality are demanded and checked according to predetermined input value REC. The functions of the other subroutines are described below.

REFLEX computes and return the value of reflection coefficient in absolute and dB scale with its phase and input impedance Z_I standing wave ratio (SWR) from the computed

elements of entire Q matrix of gratings.

TIMED calculates the relative penetration depth c from the input parameter which is the phase of reflection coefficient (Γ). The derivative of ϕ is calculated by using central difference formular which are accurate to the second order of the step size. TRANS obtains the magnitude and phase of the transmission coefficient of one array from the element of S matrix of gratings.

FABRY combines two resulting Q matrices of an array and one array - transmission line (F-P resonator length) combination and after transforming it into S matrix of resonator returns the magnitude and phase of transmission coefficient of the resonator. CONVRT performs the transformation of the computed Q matrix to scattering matrix (S).

DELAY post - multiplies the Q matrix of a two port with that of a delay line (transmission line) of given length DN and results in the matrix of the transmission line grating combination. COUPLE obtains entire Q matrix of the F-P resonator with input and output IDTs and transforms it into S matrix.

FILTER obtains the Q matrix of the grating coupler and returns the characteristics of the entire resonator filter coupled by the grating coupler. If the coupler is identical to the grating of the resonator the calculation for the grating coupler is omitted. Consequently computer execution time is saved comprehensably.

The description of input arrays provided by user is the the following:

LM array (Integer 3 elements)

LM(1)
1. Reflection coefficient (Γ) of a grating
2. Transmission coefficient (T) of a grating
3. F-P resonator insertion loss without IDTs
4. F-P resonator insertion loss with IDTs
5. Grating coupled F-P resonator filter characteristics.

LM(2)
1. All output discrete values are printed and tapering, chirping functions if necessary, are plotted.
2. Priting of putput values is suppresed.
3. Only characteristic curves are plotted.

LM(3)
1. Resonator length is optimized.
3. Resonator length is not optimized

LN Array (Integer 7 elements)

LN(1)
1. No tapering and chirping
2. Tapering only
3. P chirping only
4. y chirping only
5. Tapering and p chirping
6. Tapering and y chirping
7. p and y chirping
8. Tapering and p,y chirping
9. For several plotting in (1)

LN(2) : Tapering function

0 : Default

1 : Harmonic variation (1 + cosωt)

2 : Linear variation

3 : Quadratic variation

4 : Modified Bessel

5 : Raised cosine

6 : Lorentzian

7 : Gaussian

LN(3) : p - chirping function

0 : Default

1 : Harmonic variation

2 : Linear variation

3 : Quadratic variation

4 : Optimized variation

LN(4) : y chirping function

0 : Default

1 : Harmonic variation

2 : Linear variation

3 : Quadratic variation

4 : Optimized variation

LN(5) : Constant grating characteristics

0 : Default

1 : h

2 : Γ - y characteristics

3 : y

LN(6) : Number of grooves in the grating coupler

LN(7) : Number of grooves in the array coupler

VV Array (Real, 8 elements)

VV(1) : The value of h

VV(2) : Resonator length devided by p

VV(3) : b_i

VV(4) : y

VV(5) : Parameter β in the tapered function

VV(6) : Parameter β in the p chirping function

VV(7) : Parameter β in the y chirping function

VV(8) : Tolerance of reciprocity

UV Array (Real, 10 elements)

UV(1) : C_1

UV(2) : C_2

UV(3) : Initial value of relative frequency F

UV(4) : Increment of frequency F

UV(5) : Minimum value of vertical axis in the plotting in dB scale

UV(6) : Minimum penetration depth of the vertical axis for plotting

UV(7) : Maximum penetration depth of the vertical axis for plotting

UV(8) : b_T

UV(9) : τ

UV(10) : Offset parameter r

```
SAW7        74/835  OPT=1                          FTN 4.8+528        81/
      PROGRAM SAW7(INPUT,OUTPUT)
      EXTERNAL VMULFF,USPLT,CONVRT,MMBSIL,DELAY,FABRY
      COMMON/BLOCK1/PHI,FI,BRB/BLOCK2/LN,VV,UV,YI
      DIMENSION II(144),IC(10),A(4),AP(4),AD(4),BB(4),IMAG(5,5),F(101)
     C,RHO(101),FAI5(101),ORHO(101),TAU(101),DTAU(101),FAI7(101),
     CPO(101),TEP(101),FAI8(101),TCP(101),FAI9(101),VA(2),ARHO(101,
     C2),  ADRHO(101,2),YA(101),YR(101,2),LM(3),LN(7),VV(8),UV(10)
      COMPLEX CON(2,2),CRN(2,2),DON(2,2),Z,BW
      DATA II,IC,BB/154*1H ,0.2,0.8,0.,1./
      PHI=4.*ATAN(1.)
      IFLAG=1
      READ*,LM,LN
      READ*,VV
      READ*,UV
      PRINT 101,LM,LN,VV,UV
      FINT=UV(3) $ DF=UV(4)   $ FFL=FINT+100.*DF
      A(1)=FINT   $ A(2)=FFL   $ A(3)=UV(5) $ A(4)=0.
      AP(1)=A(1)  $ AP(2)=A(2) $ AP(3)=-PHI $ AP(4)=PHI
      AD(1)=A(1)  $ AD(2)=A(2) $ AD(3)=UV(6)$ AD(4)=UV(7)
      NN=LN(7)    $ N=LN(6)    $ REC=VV(8)  $ SL=VV(2)
      RT=UV(8)    $ TO=UV(9)   $ BRB=1.-UV(2)*VV(1)**2/PHI
      IF(LM(3).EQ.1) BRB=1.
      IF(LN(1).NE.9) GO TO 4
      DO 201 II=1,2
      IF(LN(5)-2) 203,203,205
  203 VA(II)=VV(1)+0.005*FLOAT(II-1)
      VV(1)=VA(II)
      IF(LN(5).EQ.2) GO TO 160
      GO TO 220
  205 VA(II)=VV(4)+0.2*FLOAT(II-1)
      VV(4)=VA(II)
  220 DO 210 IJ=1,101
      F(IJ)=FINT+DF*FLOAT(IJ-1)
      FI=F(IJ)   $  N=IJ
      CALL ARRAY(NN,N,CON,IFLAG,REC,IFLAG)
      IF(IFLAG-2) 215,12,12
  215 CALL CONVRT(CON,CRN)
      CALL REFLEX(CRN,R,DR,FS,Z,ZIN,F6,S)
      ARHO(IJ,II)=R   $  ADRHO(IJ,II)=DR
  210 CONTINUE
      GO TO 201
  160 YINT=0.2
      DO 260 IK=1,101
      YA(IK)=YINT+0.006*FLOAT(IK-1)
      YI=YA(IK)   $  N=IK
      CALL ARRAY(NN,N,CON,IFLAG,REC,IFLAG)
      IF(IFLAG-2) 165,12,12
  165 CALL CONVRT(CON,CRN)
      YR(IK,II)=CABS(CRN(1,1))
  260 CONTINUE
  201 CONTINUE
      GO TO 224
    4 DO 10 I=1,101
      F(I)=FINT+DF*FLOAT(I-1)
      FI=F(I)   $  N=I
      CALL ARRAY(NN,N,CON,IFLAG,REC,IFLAG)
      IF(N.EQ.1) IK=IFLAG
```

```
SAW7        74/835  OPT=1                                FTN 4.8+528          81/(

      IF(IFLAG-2) 11,12,12
   11 BW=(CON(1,1)+CON(2,2))/2.
      ABW=REAL(BW)
      IF(LM(1).EQ.3) GO TO 50
      CALL CONVRT(CON,CRN)
      IF(LM(1).EQ.2) GO TO 40
      CALL REFLEX(CRN,R,DR,F5,Z,ZIN,F6,S)
      IF(LM(1).GE.4) GO TO 50
      RHO(I)=R  $  DRHO(I)=DR  $  FAI5(I)=F5.
      CALL TIMED(N,DF,FAI5,PD)
      IF(IABS(I-1).GT.1.E-6) GO TO 29
      RHOR=RHO(I)$FR=F(I)
      GO TO 30
   29 IF(RHOR.GE.RHO(I)) GO TO 30
      RHOR=RHO(I)$FR=F(I)
   30 CONTINUE
      IF(LM(2).NE.1) GO TO 10
      IF(I.EQ.1) PRINT 110
      PRINT 111,F(I),RHO(I),DRHO(I),FAI5(I),ZIN,F6,S,PD(I),ABW
      GO TO 10
   40 CALL TRANS(CRN,T,DT,F7)
      TAU(I)=T$DTAU(I)=DT$FAI7(I)=F7
      IF(LM(2).NE.1) GO TO 10
      IF(I.EQ.1) PRINT 115
      PRINT 116 ,F(I),TAU(I),DTAU(I),FAI7(I)
      GO TO 10
   50 OND=SL/BRB
      IF(LM(1).GE.4) GO TO 60
      CALL DELAY(FI,OND,CON,DON)
      CALL FABRY(CON,DON,AFP,FP,F8)
      TP=AFP$TFP(I)=FP$FAI8(I)=F8
      IF(LM(2).NE.1) GO TO 10
      IF(I.EQ.1) PRINT 125
      PRINT 125,F(I),TP,TFP(I),FAI8(I)
      GO TO 10
   60 RPI=UV(10)/BRB
      IF(LM(1).EQ.5) GO TO 70
      CALL COUPLE(Z,OND,RPI,BT,TD,ACP,CP,F9)
      TCP(I)=CP  $  FAI9(I)=F9
      IF(LM(2).NE.1) GO TO 10
      IF(I.EQ.1) PRINT 124
      PRINT 126,F(I),ACP,TCP(I),FAI9(I)
      GO TO 10
   70 CALL FILTER(Z,CON,N,OND,RPI,BT,TD,ACP,CP,F9,IIK)
      IF(IIK-2) 71,13,13
   71 TCP(I)=CP  $  FAI9(I)=F9
      IF(LM(2).NE.1) GO TO 10
      IF(I.EQ.1) PRINT 123
      PRINT 126,F(I),ACP,TCP(I),FAI9(I)
   10 CONTINUE
      IF(IK-2) 15,15,16
   15 IF(LM(1).EQ.1) PRINT 121,FP,RHOR
      GO TO 17
   16 PRINT 122,FR,RHOR
   17 NR=LM(1)
      GO TO (61,62,63,64,64) NR
   61 CALL USPLT(F,DRHO,101,101,1,1,TT,A,IC,1,IMAG4,IER)
```

```
SAW7        74/835  OPT=1                    FTN 4.8+528        81/0

      IF(LM(2).EQ.3)  GO TO 222
      CALL USPLTIF,PD,101,101,1,1,TT,AD,IC,1,IMAG4,IER)
      GO TO 222
   62 CALL USPLTIF,QTAU,101,101,1,1,TT,A,IC,1,IMAG4,IER)
      CALL USPLTIF,FAZ7,101,101,1,1,TT,AP,IC,1,IMAG4,IER)
      GO TO 222
   63 CALL USPLTIF,TFP ,101,101,1,1,TT,A,IC,1,IMAG4,IER)
      CALL USPLTIF,FAI8,101,101,1,1,TT,AP,IC,1,IMAG4,IER)
      GO TO 222
   64 CALL USPLTIF,TCP ,101,101,1,1,TT,A,IC,1,IMAG4,IER)
      CALL USPLTIF,FAI9,101,101,1,1,TT,AP,IC,1,IMAG4,IER)
      GO TO 222
  224 IF(LN(5).EQ.2) GO TO 230
      IF(LM(2).EQ.2) GO TO 280
      PRINT 310
      PRINT 311,(F(I),(ARHO(I,J),ADRHO(I,J),J=1,2),I=1,101)
      GO TO 280
  230 IF(LM(2).EQ.2) GO TO 237
      PRINT 235
      PRINT 236,(YA(K),(YR(K,J),J=1,2),K=1,101)
  237 CALL USPLTIYA,YR,101,101,2,1,TT,BB,IC,1,IMAG4,IER)
      GO TO 222
  280 CALL USPLTIF,ADRHO,101,101,2,1,TT,A,IC,1,IMAG4,IER)
      GO TO 222
   12 PRINT 150
      GO TO 222
   13 PRINT 151
  222 STOP
  101 FORMAT(1H1,//,40X,*INPUT    DATA*,//,15X,3(I2,9X),7(I3,8X),
     C//,13X,8(F8.4,6X),//,10X,10(F10.5,2X))
  110 FORMAT(1H1,//,10X,*F*,13X,*RHO*,11X,*RHO(DB)*,11X,*PHASE*,10X,*Z*,
     C7X,*PHASE*,7X,*S.W.R*,8X,*P.D*,7X,*AN(REAL)*,//)
  111 FORMAT(7X,F6.4,6X,F12.10,4X,F12.7,6X,F8.5,4X,F9.6,4X,F8.5,2X,
     .CF9.4,4X,F7.2,3X,F12.8)
  115 FORMAT(1H1,//,15X,*F*,23X,*TAU*,20X,*TAU(DB)*,22X,*PHASE*,30X,//)
  116 FORMAT(13X,F6.4,15X,F12.10,10X,F12.8,20X,F10.6,20X)
  121 FORMAT(1X,//,10X,*R. FREQ.= *,F6.4,10X,*MAX RHO= *,F12.10,
     C10X,*BILATERAL*)
  122 FORMAT(1X,//,10X,*R. FREQ.= *,F6.4,10X,*MAX RHO= *,F12.10,
     C10X,*NON BILATERAL*)
  123 FORMAT(1H1,//,15X,*F*,18X,*TAU(GRATING)*,9X,*TAU(DB)*,19X,*PHASE*
     C,//)
  124 FORMAT(1H1,//,15X,*F*,18X,*TAU(COUPLED)*,9X,*TAU(DB)*,19X,*PHASE*
     C,//)
  125 FORMAT(1H1,//,15X,*F*,20X,*TAU(R)*,15X,*TAU(DB)*,18X,*PHASE*,//)
  126 FORMAT(13X,F6.4,14X,F12.10,8X,F12.8,15X,F8.5)
  150 FORMAT(1H0,20X,*NON  RECIPROCAL  *)
  151 FORMAT(1H0,20X,*GRATING COUPLER IS NOT BILATERALLY SYMMETRIC*)
  235 FORMAT(1H1,//,20X,*Y*,40X,*RHO*,//)
  236 FORMAT(18X,F6.3,20X,2(F12.10,10X))
  310 FORMAT(1H1,//,12X,*F*,22X,2(*RHO*,8X,*RHO(DB)*,10X),//)
  311 FORMAT((10X,F6.4,20X,2(E12.10,5X,F12.7,10X)))
      END
```

```
      SUBROUTINE ARRAY(LL,N,CON,I,LAG,REC,IBIS)
      COMMON/BLOCK1/PHI,FI,BR8/BLOCK2/LN,VV,UV,YI
      DIMENSION Q(4,4),P(4,4),R(4,4),E(4,4),QNO(4,4),TT(144),IC(10)
     C,BB(4),IMAG4(5,5),1,AIY(201),AX(201),AT(201),AS(201),LN(7),
     *VV(8),UV(10)
      REAL MMBS(1)
      COMPLEX CON(2,2),CDON,CMON
      DATA TT,IC,BB/154*1H ,0.,1.,0.,0./
      VDZ=UV(1)*VV(1)  $  VOV=0.
      BR=UV(2)*VV(1)**2  $  BI=VV(3)  $  Y=VV(4)
      IBIS=1  $  AX(1)=0.
      Z=1.+VDZ$V=1.+VDV
      T=1.$S=1.
      DO 20 I=1,LL
      IF(LN(1).EQ.9) GO TO 25
      X=FLOAT(I)/FLOAT(LL)
      IF(LL.EQ.200) AX(I+1)=X
      NL=LN(1)
      NH=LN(2)
      GO TO (25,12,11,16,12,16,16,16,25) NL
   12 GO TO (77,76,21,23,22,24,75) NH
   77 T=1.+VV(5)*SIN(10.*PHI*X)
      GO TO 25
   76 T=1.+VV(5)*(X-0.5)
      GO TO 25
   21 T=-VV(5)*X*(X-1.)
      GO TO 25
   23 U=VV(5)*SQRT(1.-(2.*X-1.)**2)
      IF(I.EQ.LL) GO TO 36
      W=MMBS(1(1,U,IER)/U
      T=VV(5)**2*2./(EXP(VV(5))+EXP(-VV(5)))*W
      GO TO 25
   36 T=0.0009
      GO TO 25
   22 T=1.+COS(2.*PHI*X+PHI)
      GO TO 25
   24 T=VV(5)/(PHI*(1.+(VV(5)*(X-0.5))**2))
      GO TO 25
   75 T=EXP(-.5*((X-.5)/VV(5))**2)/(VV(5)*SQRT(2.*PHI))
      GO TO 25
   13 NP=LN(3)
      GO TO (31,26,28,27) NP
   31 S=1.+VV(6)*SIN(10.*PHI*X)
      GO TO 33
   26 S=1.+VV(6)*(X-.5)
      GO TO 33
   28 S=1.-VV(6)*(X-.5)**2
      GO TO 33
   27 S=1.-UV(2)*(VV(1)*T)**2/PHI
      GO TO 33
   16 IF(LN(4)-2) 79,80,81
   79 TY=1.+VV(7)*SIN(10.*PHI*X)
      Y=VV(4)*TY
      IF((LN(1).EQ.6) .OR.(LN(1).EQ.8)) GO TO 12
      IF(LN(1).EQ.7) GO TO 13
      GO TO 25
   80 TY=1.+VV(7)*(X-0.5)
      Y=VV(4)*TY
      IF((LN(1).EQ.6) .OR.(LN(1).EQ.8)) GO TO 12
      IF(LN(1).EQ.7) GO TO 13
      GO TO 25
   81 TY=1.-VV(7)*(X-0.5)**2
      Y=VV(4)*TY
      IF((LN(1).EQ.6) .OR.(LN(1).EQ.8)) GO TO 12
      IF(LN(1).EQ.7) GO TO 13
   25 VDZ=UV(1)*VV(1)*T
      BR=UV(2)*(VV(1)*T)**2
      Z=1.+VDZ$V=1.+VDV
      IF(IN.EQ.1).AND.(I.EQ.200)) AT(I+1)=T
      IF((LN(1).EQ.5).OR.(LN(1).EQ.8)) GO TO 19
      IF(LN(5).EQ.2) GO TO 55
      THM=PHI*FI*Y/V
      THS=PHI*FI*(1.-Y)
      GO TO 44
   55 FY=1.-BR/PHI
      THM=PHI*FY*Y)/V
      THS=PHI*FY*(1.-Y)
```

```
      GO TO 44
   32 AFI=FI*S
      AA=UV(2)*T+VV(1)   S   C1=UV(1)
      IF((N.EQ.1).AND.(LL.EQ.200))  AS(I+1)=S
      THM=PHI*AFI*Y/V
      THS=PHI*AFI*(1.-Y)
   44 CONTINUE
      IF((N.EQ.1).AND.(LL.EQ.200)) ATY(I+1)=Y
      A=COS(THM)*COS(THS)$B=COS(THM)*SIN(THS)
      C=SIN(THM)*COS(THS)$D=SIN(THM)*SIN(THS)
      Q(1,1)=A-BR*Z*C-Z*D$Q(2,1)=BI*(2.*A-Z*D)-2.*BI*BR*Z*C
      Q(1,2)=-BI*Z*C$Q(2,2)=A-BR*(Z*C+2.*BI*(BR**2-BI**2)*Z*D-1./Z*D
      Q(3,1)=Z*BI*C$Q(4,1)=BR*(2.*A-Z*D)-(BR**2-BI**2)*Z*C+1./Z*C+B
      Q(3,2)=B+Z*C-BR*Z*D$Q(4,2)=BI*(Z*C+2.*B)-2.*BR*BI*Z*D
      Q(1,3)=-Q(3,1)$Q(1,4)=-Q(3,2)$Q(2,3)=-Q(4,1)$Q(2,4)=-Q(4,2)
      Q(3,3)=Q(1,1)$Q(3,4)=Q(1,2)$Q(4,3)=Q(2,1)$Q(4,4)=Q(2,2)
      IF(I.GE.LL) GO TO 20
      IF(IABS(I-1).GT.1.E-6) GO TO 7
      DO 3 L=1,4
      DO 3 K=1,4
    3 P(L,K)=Q(L,K)
      JFLAG=2
      IF(LN(1).EQ.9) GO TO 7
      GO TO 20
    7 CALL VMULFF(P,Q,4,4,4,4,4,R,4,IER)
      IF(LN(1).EQ.9) JFLAG=JFLAG+1
      DO 5 LK=1,4
      DO 5 KK=1,4
    5 P(LK,KK)=R(LK,KK)
      IF(JFLAG.GE.LL) GO TO 29
      IF(JFLAG.NE.2) GO TO 7
   20 CONTINUE
   29 CONTINUE
      E(1,1)=COS(THM)-Z*BR*SIN(THM)
      E(1,2)=0.$E(2,1)=2.*BI*(COS(THM)-Z*BR*SIN(THM))
      E(2,2)=COS(THM)-BR*Z*SIN(THM)
      E(4,1)=2.*BR*COS(THM)-(BR**2-BI**2)*Z*SIN(THM)+SIN(THM)/Z
      E(4,2)=BI*Z*SIN(THM)
      E(3,1)=BI*Z*SIN(THM)$E(3,2)=Z*SIN(THM)
      E(1,3)=-E(3,1)$E(1,4)=-E(3,2)$E(2,3)=-E(4,1)$E(2,4)=-E(4,2)
      E(3,3)=E(1,1)$E(3,4)=E(1,2)$E(4,3)=E(2,1)$E(4,4)=E(2,2)
      CALL VMULFF(R,E,4,4,4,4,4,QNO,4,IER)
      CON(1,1)=(1.,0.)*QNO(1,1)+(0.,1.)*QNO(3,1)
      CON(1,2)=(1.,0.)*QNO(1,2)+(0.,1.)*QNO(3,2)
      CON(2,1)=(1.,0.)*QNO(2,1)+(0.,1.)*QNO(4,1)
      CON(2,2)=(1.,0.)*QNO(2,2)+(0.,1.)*QNO(4,2)
      CDON=CON(1,1)*CON(2,2)-CON(1,2)*CON(2,1)
      CMON=CON(1,1)-CON(2,2)
      DCN=CABS(CDON)$RON=CABS(CMON)
      IF(ABS(DON-1.).GE.REC) GO TO 10
      IF((N.EQ.1).AND.(RON.GE.1.E-6))IBS=3
      IF(LL.NE.200) RETURN
      IF((LN(1).EQ.1).OR.(LN(1).EQ.9)) RETURN
      IF(N.NE.1) RETURN
      AT(1)=0. $ AS(1)=AS(2) $ ATY(1)=ATY(2)
      IF(LN(1)-3) 51,52,57
   51 CALL USPLT(AX,AT,201,201,1,2,TT,BB,IC,1,IMAG4,IER)
      IF((LN(1).EQ.5).OR.(LN(1).EQ.8)) GO TO 52
      RETURN
   52 CALL USPLT(AX,AS,201,201,1,2,TT,BB,IC,1,IMAG4,IER)
      RETURN
   57 IF(LN(1).EQ.5) GO TO 51
      CALL USPLT(AX,ATY,201,201,1,2,TT,BB,IC,1,IMAG4,IER)
      IF(LN(1).EQ.4) GO TO 59
      IF(LN(1)-7) 51,52,51
   59 RETURN
   10 IFLAG=2
      RETURN
      END
```

```
      SUBROUTINE DELAY(F,DN,CRN,DQN)
      COMPLEX CRN(2,2),DQN(2,2)
      PHI=4.*ATAN(1.)
      THETA=PHI*DN*F
      DQN(1,1)=COS(THETA)*CRN(1,1)+(0.,1.)*SIN(THETA)*CRN(1,2)
      DQN(1,2)=COS(THETA)*CRN(1,2)+(0.,1.)*SIN(THETA)*CRN(1,1)
      DQN(2,1)=COS(THETA)*CRN(2,1)+(0.,1.)*SIN(THETA)*CRN(2,2)
      DQN(2,2)=COS(THETA)*CRN(2,2)+(0.,1.)*SIN(THETA)*CRN(2,1)
      RETURN
      END
```

```
ROUTINE TRANS      74/835  OPT=1                    FTN 4.8+528

      SUBROUTINE TRANS(CRN,T,DT,F7)
      COMMON/BLOCK1/PHI,FI ,BRB
      COMPLEX CRN(2,2)
      T=CABS(CRN(2,1))
      DT=20.*ALOG10(T)
      A5=AIMAG(CRN(2,1))$A6=REAL(CRN(2,1))
      F7=ATAN2(A5,A6)
      RETURN
      END
```

```
ROUTINE CONVRT     74/835  OPT=1                    FTN 4.8+528

      SUBROUTINE CONVRT(CON,CRN)
      COMPLEX CON(2,2),CRN(2,2),DEN
      DEN=CON(1,1)+CON(1,2)+CON(2,1)+CON(2,2)
      CRN(1,1)=(CON(1,1)+CON(1,2)-CON(2,1)-CON(2,2))/DEN
      CRN(1,2)=2./DEN$CRN(2,1)=2./DEN
      CRN(2,2)=(-CON(1,1)+CON(1,2)-CON(2,1)+CON(2,2))/DEN
      RETURN
      END
```

```
ROUTINE FARRY      74/835  OPT=1                    FTN 4.8+528

      SUBROUTINE FARRY(CRN,DON,AFP,FP,F5)
      COMMON/BLOCK1/PHI,FI ,BRB
      COMPLEX CRN(2,2),DON(2,2),FPR(2,2),FPTN(2,2)
      FPR(1,1)=DON(1,1)*CRN(2,2)+DON(1,2)*CRN(2,1)
      FPR(1,2)=DON(1,1)*CRN(1,2)+DON(1,2)*CRN(1,1)
      FPR(2,1)=DON(2,1)*CRN(2,2)+DON(2,2)*CRN(2,1)
      FPR(2,2)=DON(2,1)*CRN(1,2)+DON(2,2)*CRN(1,1)
      CALL CONVRT(FPR,FPTN)
      AFP=CABS(FPTN(2,1))
      FP=20.*ALOG10(CABS(FPTN(2,1)))
      A1=AIMAG(FPTN(2,1))$A2=REAL(FPTN(2,1))
      F5=ATAN2(A1,A2)
      RETURN
      END
```

```
      SUBROUTINE CODE(Z,Q,R,B,T,ACP,CP,F9)
      COMMON/BLOCK1/PHI,FI,BRB
      COMPLEX QTN(2,2),QDN(2,2),YAD,Z
      RP=R
      THETA=0.5*PHI*FI*(Q-RP)
      YAD=(1./Z+(0.,1.)*TAN(THETA))/(1.+(0.,1.)*TAN(THETA)/Z)
      QTN(1,1)=(0.,1.)*YAD/B
      QTN(1,2)=(0.,1.)/B
      QTN(2,1)=(0.,1.)*B-T*YAD/B
      QTN(2,2)=-T/B
      CALL DELAY(FI,PP,QTN,QDN)
      CALL FARRY(QTN,QDN,ACP,CP,F9)
      RETURN
      END
```